particles

MDPI

Review

Status and Perspectives of 2ϵ, $\epsilon\beta^+$ and $2\beta^+$ Decays

Pierluigi Belli [1,2,*,†], Rita Bernabei [1,2,*,†] and Vincenzo Caracciolo [1,2,3,*,†]

1 Istituto Nazionale di Fisica Nucleare (INFN), sezione di Roma "Tor Vergata", I-00133 Rome, Italy
2 Dipartimento di Fisica, Università di Roma "Tor Vergata", I-00133 Rome, Italy
3 INFN, Laboratori Nazionali del Gran Sasso, I-67100 Assergi, Italy
* Correspondence: pierluigi.belli@roma2.infn.it (P.B.); rita.bernabei@roma2.infn.it (R.B.); vincenzo.caracciolo@roma2.infn.it (V.C.)
† These authors contributed equally to this work.

Abstract: This paper reviews the main experimental techniques and the most significant results in the searches for the 2ϵ, $\epsilon\beta^+$ and $2\beta^+$ decay modes. Efforts related to the study of these decay modes are important, since they can potentially offer complementary information with respect to the cases of $2\beta^-$ decays, which allow a better constraint of models for the nuclear structure calculations. Some positive results that have been claimed will be mentioned, and some new perspectives will be addressed shortly.

Keywords: positive double beta decay; double electron capture; resonant effect; rare events; neutrino

check for updates

Citation: Belli, P.; Bernabei, R.; Caracciolo, V. Status and Perspectives of 2ϵ, $\epsilon\beta^+$ and $2\beta^+$ Decays. *Particles* **2021**, *4*, 241–274. https://doi.org/10.3390/particles4020023

Academic Editor: Armen Sedrakian

Received: 14 April 2021
Accepted: 27 May 2021
Published: 2 June 2021

1. Introduction

The double beta decay (DBD) is a powerful tool for studying the nuclear instability, the electroweak interaction, the nature of the neutrinos, and physics beyond the Standard Model (SM) of Particle Physics. The theoretical interpretations of the double beta decay with the emission of two neutrinos is well described in the SM; the process is characterized by a nuclear transition changing the atomic number Z of two units while leaving the atomic mass number A unchanged. According to the Weizsäcker mass formula [1], the double beta decay can proceed between two even-even nuclei. Reference [2] initially discussed the theoretical description of the double beta decay; four kinds of DBD decay modes are possible. In particular, the DBDs predicted from the SM are:

$$\begin{array}{rrcl} 2\nu2\beta^- : & (A,Z) & \longrightarrow & (A,Z+2)+2e^-+2\bar{\nu} \\ 2\nu2\beta^+ : & (A,Z) & \longrightarrow & (A,Z-2)+2e^++2\nu \\ 2\nu\varepsilon\beta^+ : & (A,Z)+e^- & \longrightarrow & (A,Z-2)+e^++2\nu \\ 2\nu2\varepsilon : & (A,Z)+2e^- & \longrightarrow & (A,Z-2)+2\nu \end{array}$$

In the case of a DBD decay with the emission of two neutrinos, the half-life ($T_{1/2}$) is given by the formula (see e.g., Reference [3]):

$$\frac{1}{T^{2\nu}_{1/2}} = G^{2\nu}(E_0,Z)\left|M^{2\nu}_{GT} - \frac{g_V^2}{g_A^2}M^{2\nu}_F\right|^2, \quad (1)$$

where: (i) the function $G^{2\nu}(E_0,Z)$ is the result of the integration in the phase space of the leptons; (ii) E_0 is the energy difference between the initial and final states; (iii) the matrix elements $M^{2\nu}_{GT}$ and $M^{2\nu}_F$ contain the nuclear structure information for Gamow–Teller and Fermi transitions; and, (iv) g_V and g_A are the vector and axial-vector weak interaction effective coupling constants.

On the other hand, DBD modes without the presence of neutrinos are possible beyond the SM and, if observed, they will open windows on new physics [4–10]. The half-life

of a neutrinoless DBD can parameterised by the following formula (using the formalism presented in Reference [11]):

$$\frac{1}{T_{1/2}^{0\nu}} = G^{0\nu}(E_0, Z)\left|M_{GT}^{0\nu} - \frac{g_V^2}{g_A^2} M_F^{0\nu}\right|^2 \langle m_\nu \rangle^2 \,, \tag{2}$$

where: (i) the function $G^{0\nu}(E_0, Z)$ is the result of two-electron phase space integration; (ii) the nuclear matrix elements $M_{GT}^{0\nu}$ and $M_F^{0\nu}$ contain the nuclear structure information for Gamow–Teller and Fermi transitions for the case of neutrinoless emission; and, (iii) $\langle m_\nu \rangle$ is the Majorana effective mass definition for the electronic neutrino:

$$\langle m_\nu \rangle \quad = \quad \left| e^{i\alpha_1} \left| U_{e,1}^2 \right| m_1 + e^{i\alpha_2} \left| U_{e,2}^2 \right| m_2 + \left| U_{e,3}^2 \right| m_3 \right| \,,$$

where m_i are the masses of the neutrino eigenstates; α_1, α_2 are the Majorana phases; and, $U_{e,i}$ are the electronic neutrino elements of the PMNS mixing matrix [12].

Among the many theoretical frameworks, an interesting one is the case of weak interactions with the right-handed lepton current. In this case, while assuming λ, η, and κ as three new coupling constants, the effective general Hamiltonian is [11]:

$$H_{LR} \quad = \quad \frac{G_F}{\sqrt{2}} \left[J_L^\mu \left(M_{L\mu}^\dagger + k M_{R\mu}^\dagger \right) + J_R^\mu \left(\eta M_{L\mu}^\dagger + \lambda M_{R\mu}^\dagger \right) \right] + \text{h.c.},$$

where $J_{L(R)}$ and $M_{L(R)}$ are the lepton and quark left- (right-) handed currents, respectively, and G_F is the Fermi constant. Thus, combining the contributions from the mass and the right-handed current terms, we have a general formula that has the form [11]:

$$\frac{1}{T_{1/2}^{0\nu}} \quad = \quad C_1 \left(\frac{\langle m_\nu \rangle}{m_e} \right)^2 + C_2 \langle \eta \rangle^2 + C_3 \langle \lambda \rangle^2 + C_4 \frac{\langle m_\nu \rangle}{m_e} \langle \eta \rangle + C_5 \frac{\langle m_\nu \rangle}{m_e} \langle \lambda \rangle + C_6 \langle \eta \rangle \langle \lambda \rangle .$$

The functions C_n contain the nuclear matrix elements and phase space integrals (all of the C_n definitions are in Reference [11]); for example, the C_1 term is derivable from Equation (2) [11,13]:

$$C_1 = G^{0\nu}(E_0, Z)\left|M_{GT}^{0\nu} - \frac{g_V^2}{g_A^2} M_F^{0\nu}\right|^2 m_e^2 .$$

Instead, $\langle \lambda \rangle$ and $\langle \eta \rangle$ are the effective values of λ and η over the mixing matrix for left- and right-handed neutrinos (see Reference [11] for their explicit definitions). We emphasize that $\langle \lambda \rangle$, $\langle \eta \rangle$, and $\langle m_\nu \rangle$ are quantities that can be evaluated by the analysis of neutrinoless double beta decay experiments.

The nuclear matrix elements contain the wave function of the initial and final even-even nuclear states, but—especially for the calculation of the 2ν mode (in the 0ν mode the virtual neutrinos have relatively high energy with respect to the average energy transition among the initial and final states and the intermediate states, known as the "closure approximation". Thus, in the "closure approximation", only the wave functions of the initial and final states are required. Moreover, the nuclear matrix elements for both 2ν and 0ν modes are the same)—a sum of all the matrix elements of the intermediate odd-odd nuclear states is also required. Ideally, in order to determine the matrix elements, it is necessary to solve a many-body problem assuming a relativistic nucleon–nucleon interaction and, thus, infer the total wave function. Unfortunately, such a procedure is not practically feasible, and several assumptions and approximations on the nuclear structure and interactions are needed, which affect the evaluation of the matrix elements and the vector and axial-vector form factors. Moreover, some approximations are more efficient for light nuclei than heavy ones, or vice-versa.

Focusing on the Feynman diagrams (see Figure 1), the $2\beta^+$ are topologically equal to the $2\beta^-$ decays; therefore, the differences in the decay rates are dominated by the phase space terms and the mass difference between the parent and daughter nuclei ($Q_{\beta\beta}$). However, the positrons emission allows for implementing a mighty signature, especially when coincidence logic is adopted. In perturbation theory, the nuclear matrix elements of the $\epsilon\beta^+$ and the 2ϵ decays are of the same order as the $2\beta^+$ decay, but, generally, the phase space is higher (the kinetic energy that is available for each DBD+, where M(A,Z) is the atomic mass of the isotope with mass number A and atomic number Z, is: $K_{2\beta^+} = M(A,Z) - M(A,Z-2) - 4m_e$, $K_{\epsilon\beta^+} = M(A,Z) - M(A,Z-2) - 2m_e - E_a$, and $K_{2\epsilon} = M(A,Z) - M(A,Z-2) - 2E_a$, where E_a is the excitation energy of the atomic shell of the daughter); thus, the corresponding $T_{1/2}$ is lower. Reference [14] lists the 35 isotopes, which can decay through the $2\beta^-$ mode (DBD-) with forbidden or suppressed β^- decay. Typically, they have a larger Q-value with respect to the DBD in positive channels (DBD+) and, thus, a lower half-life.

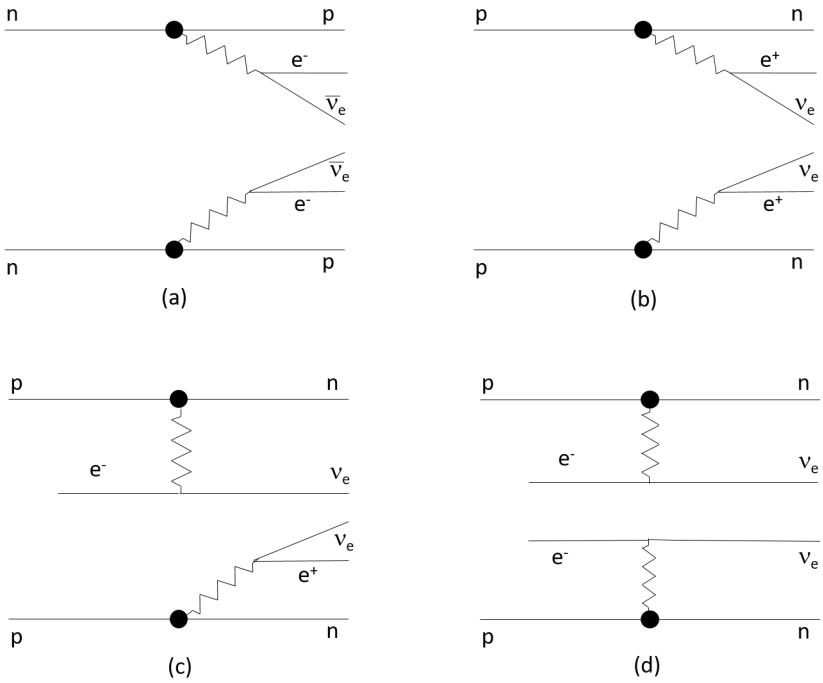

Figure 1. Leading-order schematic Feynman diagrams for the $2\nu2\beta^-$ (**a**), $2\nu2\beta^+$ (**b**), $2\nu\epsilon\beta^+$ (**c**), and $2\nu2\epsilon$ (**d**) decay modes.

However, the 34 DBD+ emitters (as listed in the following Sections and Tables therein) allow us to study the DBD for other nuclei and, thus, test the calculations of a different nucleus shape and decay modes that involve the vector and axial-vector weak effective coupling constants, etc. (see the next Sections). This expands the possibilities of the experimental tests for the achievement of important complementary information. Instead, the case of the 0ν mode involves the neutrino mass and new specific theoretical scenarios; but, in some model cases, one can consider the 2ν nuclear matrix element as a test case for the 0ν modes.

Moreover, several new features arise while assuming either a non-vanishing neutrino mass or lepton number violating ($\Delta L \neq 2$) processes. The possible "resonant effect" on the $0\nu2\epsilon$ mode when the initial and final states are energetically degenerate is a remarkable example. In this case, the process can profit from an increased counting rate of several orders of magnitude and, in some cases, the sensitivity can approach that of the DBD- (e.g., the case of the resonant transition of ^{152}Gd $\rightarrow$ ^{152}Sm $\sim 10^{27}$ yr) [15] . Actually, the counting rate can increase by a factor 10^6 if the energetic degeneration between the initial and final states is about 10 keV [16–22]. Another relevant aspect, with regards to

the 0ν modes, is that the mutual information from the simultaneous study of positive and negative DBD can constrain the theoretical parameters with very high confidence (see, e.g., Reference [23]).

Furthermore, the DBD without neutrinos emission also breaks the $(B - L)$ SM accidental symmetry [24]. In theory, where such a global symmetry is spontaneously broken, Goldstone bosons, known as Majorons, can appear. In 0νDBD, three kinds of Majoron models have been proposed: singlet, doublet, and triplet Majoron field. The emission of Majorons can be experimentally inferred by studying the energy spectrum of the SM particles that are emitted during the DBD.

In the case of 0νDBD, adopting a model-dependent framework and assuming the experimental results from the neutrino oscillation experiments, a range of values of effective-DBD-neutrino mass ($\langle m_\nu \rangle$ [25]) can be obtained as a function of the lightest neutrino mass (see Figure 2). Thus, the experimental limits on the half-lives and, consequently, the limits on $\langle m_\nu \rangle$, can be compared with the present theoretical expectations.

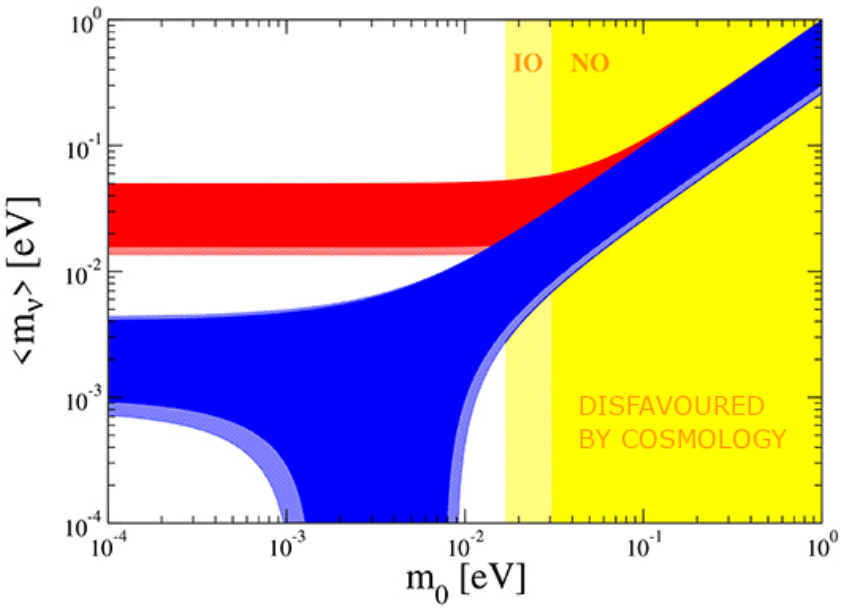

Figure 2. Predictions on the $\langle m_\nu \rangle$ from neutrino oscillations versus the lightest neutrino mass, m_0, in the two cases of the normal (NO, the on-line blue region) and inverted (IO, the on-line red region) hierarchy of the neutrinos' masses. The 2σ and 3σ values of neutrino oscillation parameters are considered. The m_0 region that is disfavored by cosmological data ($\Sigma m_\nu < 0.12$ eV) is presented in (on-line) yellow (>30 meV for the NO and >16 meV for the IO). Reprinted from Reference [25]. The upper limits on $\langle m_\nu \rangle$ inferred by some DBD experiments are: (61–165) meV (KamLAND-Zen, ^{136}Xe) [26], (75–350) meV (CUORE, ^{130}Te) [27], (79–180) meV (GERDA, ^{76}Ge) [28], (0.33–0.62) eV (NEMO-3, ^{100}Mo) [29], and (1.0–1.7) eV (AURORA, ^{116}Cd) [30,31].

For all of these arguments, it is very important to evaluate the calculations (matrix elements, coupling constant, CP-phases [32,33], etc.) and the assumptions that are considered in a model via experimental verifications. In addition, having assumed a nuclear model, the nuclear matrix element for the two-neutrino mode differs from the neutrinoless mode, but they are related to each other through relevant parameters. For instance, the g_A and the strength of the particle–particle interaction in the quasi-particle random-phase approximation model (that is often known by the acronym QRPA) are obtained from the β-decay and 2ν-DBD measurements [34,35]. Moreover, in the free nucleon interaction, the g_A value is 1.2701 [36], but, when considering a nuclear decay, there are indications that the phenomenological axial-vector coupling value is reduced at $g_A < 1$ [37–39], more precisely: $g_A \sim 1.269A^{-0.18}$ or $g_A \sim 1.269A^{-0.12}$, depending on the nuclear model adopted to infer the g_A value [39–41]. Thus, DBD investigation with various nuclei would shed new light

on constraining these and other important parameters. On the other hand, from an experimental point of view, important developments, in terms of radio-purification, isotopes enrichment, and new detectors, are needed for broadening the study of the DBD, including more potential nuclei.

To this purpose, there are different experimental approaches, such as those that are capable of distinguishing—while properly accounting for the energy resolution—the beta spectrum of the 0ν and 2ν modes or those that are able to detect the gamma emitted from the excited final states (see also, e.g., Reference [42] for DBDs in excited states and Reference [19] for 2ϵ decay modes).

2. Experimental Techniques to Study the Double Beta Decay in Positive Modes

Three main experimental methods exist for investigating the DBD: geochemical, radiochemical, and direct. The geochemical experiments use double-beta emitters in geological ores and have an advantage in the long geological times during which the daughter nuclei have been accumulated. The DBD parent is usually part of an ore sample from which the atom of a daughter isotope is chemically extracted and analyzed by mass spectroscopy. Such an approach has different possible sources of errors to be carefully considered: the estimation of the ore sample age, possible release of gas in the ore sample, fission or neutron-capture processes, an initial high concentration of daughter nucleus, etc. Moreover, this type of measurement does not allow the separation of the 2ν and 0ν modes; therefore, the measured decay rate is a global rate that considers all of the possible decay modes and transitions. Historically, the method was initially applied when the daughter was a rare gas, as ^{82}Se $\rightarrow^{82}$Kr, ^{130}Te $\rightarrow^{130}$Xe; recently, the technique has also been extended to the case of ^{130}Ba $\rightarrow^{130}$Xe, ^{132}Ba $\rightarrow^{132}$Xe.

The radiochemical method uses double-beta emitters, having the daughter nuclei with a shorter decay time than the geochemical experiments. The basic idea utilized in the radiochemical experiments is picking out the produced atoms in the final state (that are radioactive) from a vast amount of target material, concentrating and purifying them, and then finally counting their number through their decay. However, differently from geochemical experiments, some uncertainties—such as estimating the ore sample age, the defection on the retention of the gas in the ore sample, etc.—are less problematic. Nevertheless, as in the previous method, the measured decay rate is a global rate over all the possible decay modes and transitions.

The direct experimental approach allows for the study of the energy spectrum due to the emitted particles in the DBD processes. In this approach, the specific DBD transition can be pointed out. We have two main methods in this contest: one in which the source of the DBD is external to the detector ("source $\neq$ detector") and the second one in which the "source = detector". The first one is commonly used to study the gammas that are emitted from a pure sample containing the isotope of interest and/or, in a few cases, the emitted positrons/electrons. Instead, the second one guarantees a very high detection efficiency and the possible exploitation of coincidence techniques among the emitted positrons/electrons and gammas.

We briefly summarize the advantages and problems to be overcome in order to profit from the direct detection approach—besides the theoretical features, which are basically addressed in the previous section—that marks the experimental efforts.

The DBD is an extremely rare phenomenon; thus, a very low background counting rate in the energy of interest is mandatory. The increase of the signal-to-background ratio is of crucial importance. In fact, the experimental half-life in the case of a positive signal is given by:

$$T_{1/2} = \ln(2)\,\mathrm{T}\,\epsilon\,\frac{N}{S}$$

where T is the measuring time, ϵ is the detection efficiency, N is the number of double-beta decaying nuclei, and S is the number of counts attributed to the signal searched for.

If no signal is detected, then the sensitivity of an experiment is usually defined as the minimum half-life compatible with the background fluctuations at a certain C.L. corresponding to a number of sigma, m_σ. While assuming that the background counts scale linearly with the mass of the detector, the sensitivity can be written:

$$T_{1/2,\mathrm{lim}} = \ln(2)\,\frac{1}{m_\sigma}\epsilon\,\frac{\delta\,\eta\,N_A}{M_A}\sqrt{\frac{\mathrm{T}\,M}{B\,\Delta_E}}$$

where δ is the isotopic abundance of the double-beta candidate, η is the stoichiometric multiplicity of the element containing the DBD candidate, N_A is the Avogadro number, B is the background rate per unit mass and energy, Δ_E is the FWHM energy resolution (the region where conventionally B is integrated assuming that the signal shape is a peak), and M_A is the compound molecular mass. Thus, there are some crucial key experimental parameters for improving the experimental sensitivity. In addition, when considering the arguments drafted in Section 1, isotopes with high Q-values and large nuclear matrix elements are favored.

In the energy of interest, the main sources of background (that have to be mitigated in all of the experiments concerning rare event investigations; even though, an irreducible background can be present due to the solar neutrino interaction with the detector materials [41,43]) come from:

- cosmic rays: this implies installing the experiment deep underground;
- neutrons that are induced by muons and neutrinos in the rock or by (α,n) reactions: a suitable dedicated shield has to be implemented when necessary;
- natural radioactivity due to the U/Th chains, ^{40}K isotope, ^{210}Pb, etc.;
- anthropogenic activities, in particular for ^{137}Cs;
- cosmogenic activation: radio-isotopes that are induced by spallation in the material during their storage at sea level or during transportation; and,
- radio-isotopic activation that is induced by neutron calibration procedures when applied.

Choosing a suitable Deep Underground Laboratory (DUL) is the first condition in achieving the highest sensitivity in ultra-low level detection. The main advantage of a DUL is to reduce the cosmic ray muons flux. Currently, fourteen DULs are operating and three new ones are in construction. The first ones are: Boulby Underground Laboratory (BUL) in UK; Baksan Neutrino Observatory (Baksan) in Russia; Callio Laboratory (CLAB) in Finland; China Jinping Underground Laboratory (CJPL) in China; India-based Neutrino Observatory (INO) in India; Kamioka in Japan; Gran Sasso Underground Laboratories (LNGS) in Italy; Canfranc Underground Laboratory (LSC) in Spain; Modane Underground Laboratory (LSM) in France; Sudbury Neutrino Observatory (SNOlab) in CANADA; Sanford Underground Research Facility (SURF) in USA; Soudan Underground Laboratory (Soudan) in USA; Waste Isolation Pilot Plant (WIPP) in USA; and, Laboratories at the Yangyang pumped storage power plant (Y2L) in South Korea. The DULs under construction are: Agua Negra Deep Experiment Site(ANDES) between Chile and Argentina; Astroparticle Research Laboratory (ARF) in South Korea; and, Stawell Underground Physics Laboratory (SUPL) in Australia. The cosmic ray muons flux in the DULs is shown in Figure 3. The depth, the nature, and the quality of the rock, in terms, for example, of radioactivity, play an important role.

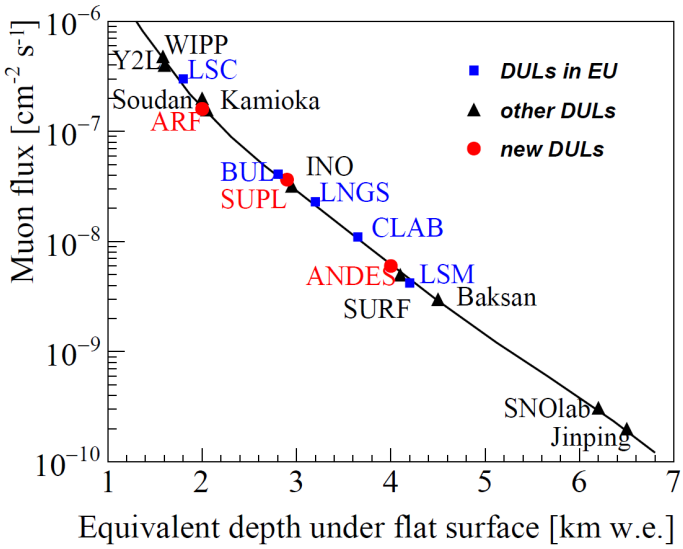

Figure 3. Cosmic ray muon flux as a function of the overburden of rock in kilometers water equivalent (km w.e.). The DULs are indicated. In particular the DULs operating in Europe are indicated with blue square marker; the DULs operating in the others continents are indicated with black triangles and the DULs under construction are indicated with red circles. Reprinted from Reference [44].

Indeed, exposure of powders, materials, and compounds to the cosmic rays can produce possible non-standard cosmogenic contaminants. In fact, during the powders storage, the crystal growing, or the handling at sea level, radioactive isotopes can be generated by cosmic rays' interactions. The same is for the shielding compounds or for the materials that are used to build the experimental infrastructure. In general, it is good practice to wait for the decay of the short-life cosmogenic isotopes before starting the measurements. Figure 4 shows an example of the activation processes at sea level and the subsequent decay in underground site.

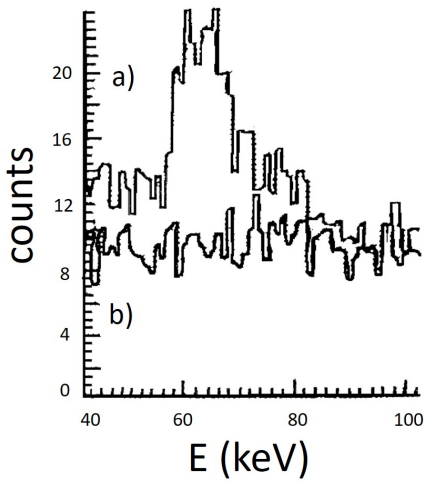

Figure 4. An example of activation at sea level: the energy spectrum collected at LNGS with a NaI(Tl) detector just stored underground (**a**) and eight months later (**b**). The role of ≃65 keV peak due to ^{125}I ($T_{1/2}$ = 59.4 days) activation at sea level is evident. Reprinted from Reference [45].

From the muons surviving the coverage of an underground laboratory—typically the flux is of a few μ's m^{-2} h^{-1} at ∼3000 m water equivalent depth—either can have direct interactions in the experimental set-up or can produce in the surroundings and/or inside the set-up secondary particles, such as fast neutrons, γ's, electrons, spallation nuclei, etc.

Such direct or indirect events are a potential background for low counting rate experiments, such as those in DBD investigation. Thus, in order to moderate the surviving muons in the DBD experiments, a good strategy is to use a multi-detector set-up to identify their passage by topological methods. In some cases, a muon veto could be used, especially if the detector area is very wide or the underground laboratory's depth is not enough. Instead, the background event due to the neutrons emerging from the surrounding rock can be mitigated by a moderation material (rich in nuclei with light atomic mass) plus a shielding material with a high cross-section for thermal neutron capture, such as, e.g., cadmium, gadolinium, boron, etc. Typically, the overall neutron flux in underground laboratories is of the order of 10^{-6} cm^{-2} s^{-1} [46].

A significant background contribution would come from radio-isotopes into the detector itself. Figure 5 shows an example of such a background; in particular, the energy spectrum of α events due to the radio-nuclides of the U/Th chains inside a $CdWO_4$ detector is shown [47]. The authors report how the radioactive contamination of a sample of $^{116}CdWO_4$ crystal scintillator by thorium was reduced by a factor ∼10, down at the level of 0.01 mBq/kg (^{228}Th), and the total α activity of uranium and thorium daughters was reduced by a factor ∼3, down to 1.6 mBq/kg, by exploiting a re-crystallization procedure. The application of chemical/physical purification procedures is another important aspect for reducing the internal contamination in both a sample and detector. These techniques are in continuous development. In particular, the initial material—often obtained from a commercial site—is purified or further purified by exploiting different techniques (depending on the compound in use) as electron-beam melting, chemical separation, micro-distillation, and many others. Some examples, among these techniques, are discussed in [30,31,48–62] and the references therein. Moreover, the neutron calibrations—if any—can activate new radioactive isotopes, e.g., by neutron-capture or spallation processes with the material of the detectors and its frame/structure. Such a type of calibration is strongly disfavored in the DBD set-up.

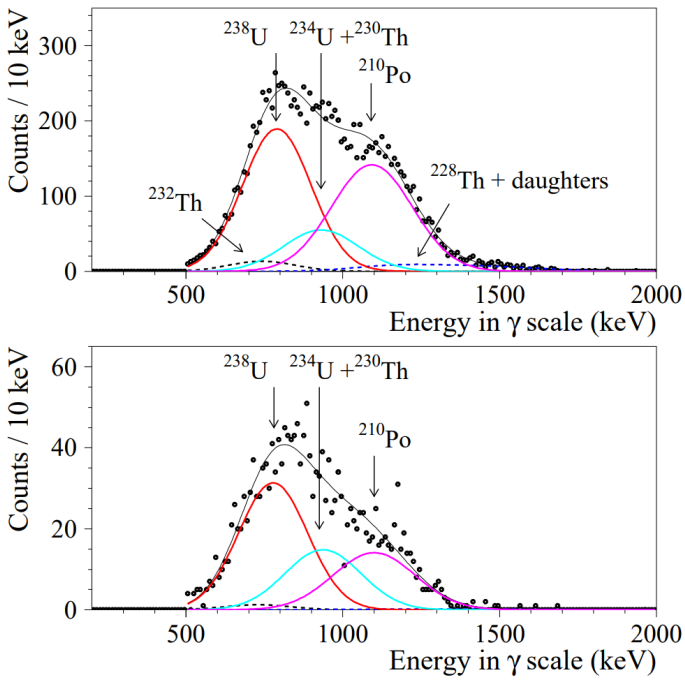

Figure 5. An example of the effect of the re-crystallization procedure in order to reduce the radioactive contamination of a detector to improve a double beta decay experiment's sensitivity. In particular, (color on-line) the energy spectra of α events that were selected by the pulse-shape discrimination from the data that accumulated in the low-background set-up with a $^{116}CdWO_4$ crystal scintillator before (**top**) and after the re-crystallization (**bottom**) are shown. Reprinted from Reference [47].

The most commonly considered detectors in DBD experiments are: (i) semiconductor detectors, (ii) scintillation detectors, (iii) ionization chambers, (iv) bolometric detectors, and their possible combinations (in addition, passive experiments, also utilizing the kinds of detectors listed above, are built as tracking detectors. It is the case, e.g., of SuperNEMO [63] or ELEGANT [64] that, nevertheless, are focusing on the DBD-). In many applications, solid detector medium is of great advantage, thanks to the high-density with respect to gaseous and liquid media. These are the cases of semiconductor, crystal scintillation, and bolometric detectors. In particular, semiconductor detectors offer high energy resolution, and germanium diodes are widely used in the DBD experiments. This detector type provides the possibility to study the DBD of $2\beta^-$ process in ^{76}Ge, where the source and detector are the same. Nevertheless, germanium-diodes are widely used as a gamma spectrometer in DBD experiments to excite levels of daughter nuclei and in a more general manner in the case of DBD+. In the former case and when considering a ground-state transition, only the two electrons' sum energy is measured. In the second case, instead, the X-rays and/or γ-rays coming out of the DBD+ and the γ quanta that are emitted from the positron annihilation can be measured. In the latter case, the thickness of dead layer can play a crucial role in the energy threshold: the crossed dead layer strongly suppresses the γ- or X-rays flux at low energy and, thus, the detection efficiency is poor. At the moment, the most used type of germanium detectors is the high pure germanium diode (HP-Ge) operating at cryogenic temperature. Other attempts to perform semiconductor experiments concern the use of CdTe or CdZnTe detectors that allow for the operation at room temperature [65,66]. In this case, there are seven possible DBD emitters, but, at present, the technology seems to not yet be mature.

Many other DBD emitters can be used in solid (or liquid) scintillator detectors (also taking advantage of the possible "source = detector" approach). Typically, the energy resolution (especially for liquids) is worse than in the ionization detectors; however, the technique offers several other advantages: the availability of many nuclei to be used as target, the possibility to operate at room temperature, a high duty cycle, high operation stability, often no environmental impact, etc. In addition, there is also great interest in many other different applications. For example, the NaI(Tl) scintillator is being used to the search for solar axions, possible charge non-conservation processes, matter stability, rare nuclear decay modes, exotics in cosmic rays, DM, and others [67–77]. Moreover, low background crystal scintillators are being used for a long time in rare α and β decays (see e.g., [78]). Hoverer, a very wide choice of scintillators is available for DBD experiments, such as $CdWO_4$ (due to ^{106}Cd, ^{108}Cd, ^{114}Cd, ^{116}Cd, ^{180}W, ^{186}W), $CaMoO_4$ (due to ^{100}Mo), and their enrichments (such as ^{106}Cd, ^{116}Cd and ^{100}Mo) [31,79–84]. Meanwhile, new developments on scintillation materials, like $CeCl_3$, CeF_3, and SrI_2(Eu), gave encouraging results [85–90]. Efforts are also in progress regarding further improvements of BaF_2, $BaWO_4$, $ZnWO_4$, $CaWO_4$, $CaMoO_4$, $CdWO_4$, CaF_2, BGO, LiF, $PbWO_4$, $PbMoO_4$, and Cs_2HfCl_6, see e.g., [51–53,58,91–104]. Moreover, as other example, rare-earth-doped scintillators (CaF_2(Eu), $LaCl_3$(Ce), etc.) or scintillators, such as $CdWO_4$ and $CaWO_4$, are used to study very specific nuclear rare processes [105–108]. Extensive literature on historical benchmarks and the industrial production of crystals is available, see, e.g., [51,52,58,85–103,105–119].

A case apart concerns the liquid scintillators as liquid noble gases. Liquid noble gas detectors have been proposed and used in different research fields for more than forty years [120–141]. In particular, the application of liquid xenon as a pure scintillator in direct Dark Matter particle investigations dates back to 1990 with the pioneering work conducted by DAMA/LXe [124,127–137] and later one by the UK coll. [142]. The liquid noble gases have also been used to study double beta decay in ^{124}Xe, ^{134}Xe, and ^{136}Xe (see, e.g., [135–137,143–146] and the References therein). Nevertheless, the use of liquid noble gases, especially at low energy, can encounter a number of technical and performance difficulties, in terms of energy resolution, light yield, efficiency, light collection and stability, linearity response, rejection procedure, etc., as reported, for example, in [122,123,138,147–151] and the References therein. The noble gases have also been con-

sidered in either gaseous detectors or two-phase liquid/gaseous detectors, combining the scintillation and ionization responses. These latter experiments are mostly built in the form of time projection chambers (TPC), where the DBD emitter is either the noble gas itself (e.g., ^{136}Xe) or included in liquid scintillators. As already mentioned, the main disadvantages regard the worse energy resolution and stability of the large number of apparatus features (especially in a very large detector).

The cryogenic solid calorimeter is another technique exploited in the DBD, whose detectors are also known as bolometric ones [152]; these detectors work at approximately 10 mK, and the energy resolution is typically very good. Nevertheless, they pay some difficulty in the apparatus stability at that temperature, microphonic problems, etc. [153–156]. Reference [42] reports examples of such detectors in the DBD sector.

In all of the experimental techniques, the natural abundance of the isotope of interest is a common problem. In the Tables of the next Sections, the natural abundance (δ) of all DBD+ emitters is listed. In particular, ^{40}Ca, ^{58}Ni, and ^{64}Zn have a very high natural abundance $\delta > 40\%$; ^{50}Cr, ^{54}Fe, ^{92}Mo, and ^{96}Ru have $5\% < \delta < 15\%$; ^{102}Pd, ^{106}Cd, ^{144}Sm, and ^{164}Er have $1\% < \delta < 4\%$ and all other isotopes have a very low natural abundance, $\delta < 1\%$. Thus, the isotopic enrichment is often a critical experimental requirement.

The modern techniques for isotopic enrichment have their origin in the developments to separate the ^{235}U. In fact, apart from the oldest method known as calutrons (usable for a small sample: a few grams), the gas centrifugation is one of the most adopted techniques, which requires—to be implemented—a stable hexafluoride gaseous compound for the element of interest. An alternative method uses a high-power laser to preferentially ionize the element of interest to remove it using an electric field. The molecular laser isotope separation is a hybrid technique between the two previous ones that operates on a gaseous hexafluoride compound as an alternative to centrifugal gas separation. Finally, the so-called isotopic distillation is another common technique [157,158].

Besides all of these points, the use of simulations and the control of key parameters to extract accurate and reliable measures and uncertainties from the data analysis are crucial aspects to consider [159]. These methods are usually dependent upon experimental techniques, but we can underline some general aspects. The Monte Carlo method is widely used to estimate the presence of some contaminants. It can profit from the preliminary screening of the materials to estimate the abundance of some radio-nuclides, but, in any case, strong assumptions regarding their distribution into the detectors and the housing are required. Thus, it is practically impossible to precisely know the background events distribution. However, while assuming to know the shape of the pulses that are searched for (as in the case of β/γ events with respect to the α ones), procedures adopting the Pulse Shape Discrimination (PSD) method can be helpful in the statistical reduction of the α background, especially at relatively high energy where the PSD is more effective. Another technique for tagging quite fast sequences of correlated events is the so-called Time-Amplitude Analysis (see e.g., Reference [80] and the references therein). Other key aspects are the control of the stability of important parameters that can affect the energy scale and detection efficiency; they are, e.g., the temperature, the light-yield, the self-absorption of the light scintillation, the gain of PMT or sensors in general, the contaminant dispersion in the experimental environmental or in the liquid/gaseous detectors, etc.

2.1. Examples of Energy Distributions in Case of an Experiment of DBD+ with "Source = Detector"

When considering a DBD- in 2ν mode, the energy spectrum of the two electrons' energy sum has a continuum shape with an endpoint at $Q_{\beta\beta}$ due to neutrinos carrying part of the energy away. In the 0ν mode, the spectrum is a delta at $Q_{\beta\beta}$ energy. Typically, a calorimetric experiment for DBD- with an active source has size and density dimensions significant enough to stop the emitted electrons; thus, the energy spectrum is broadened due to the detector's energy response. Instead, in the case of DBD+, the energy spectrum that is convoluted with the detector response is more complicated, due to the gamma quanta that are emitted by the positron(s) annihilation and/or the emission of X-rays

following electron capture. This section briefly describes the energy distributions while considering some DBD+ transitions (adopting the active source approach) to emphasize the differences in the case of a DBD- transition. In particular, we simulate some DBD+ processes in ^{106}Cd that occur in a cadmium tungstate crystal scintillator enriched in ^{106}Cd at 66% ($^{106}CdWO_4$), with a cylindrical shape, size of Ø27 mm × 50 mm, and mass of 215.4 g [160]. The energy resolution—as measured in dedicated calibrations (see Reference [160])—can be written as: $\sigma/E = 0.023 + 0.86/\sqrt{E(\text{keV})}$. The Monte-Carlo simulation uses the GEANT4 toolkit [161,162], with the initial kinematics of the decay products being provided by the DECAY0 event generator [163,164]. Thus, the results of the simulation of the DBD+ transitions to the ground state (g.s.) of ^{106}Pd ($2\beta^+$, $\varepsilon\beta^+$, and 2ε, with and without neutrinos) and of the resonant transitions for the case of $0\nu2\epsilon$ decay to the excited energy levels of ^{106}Pd (2718 keV and 2741 keV, respectively), $0\nu2K$, and $0\nu KL$ electron captures, are reported in Figure 6.

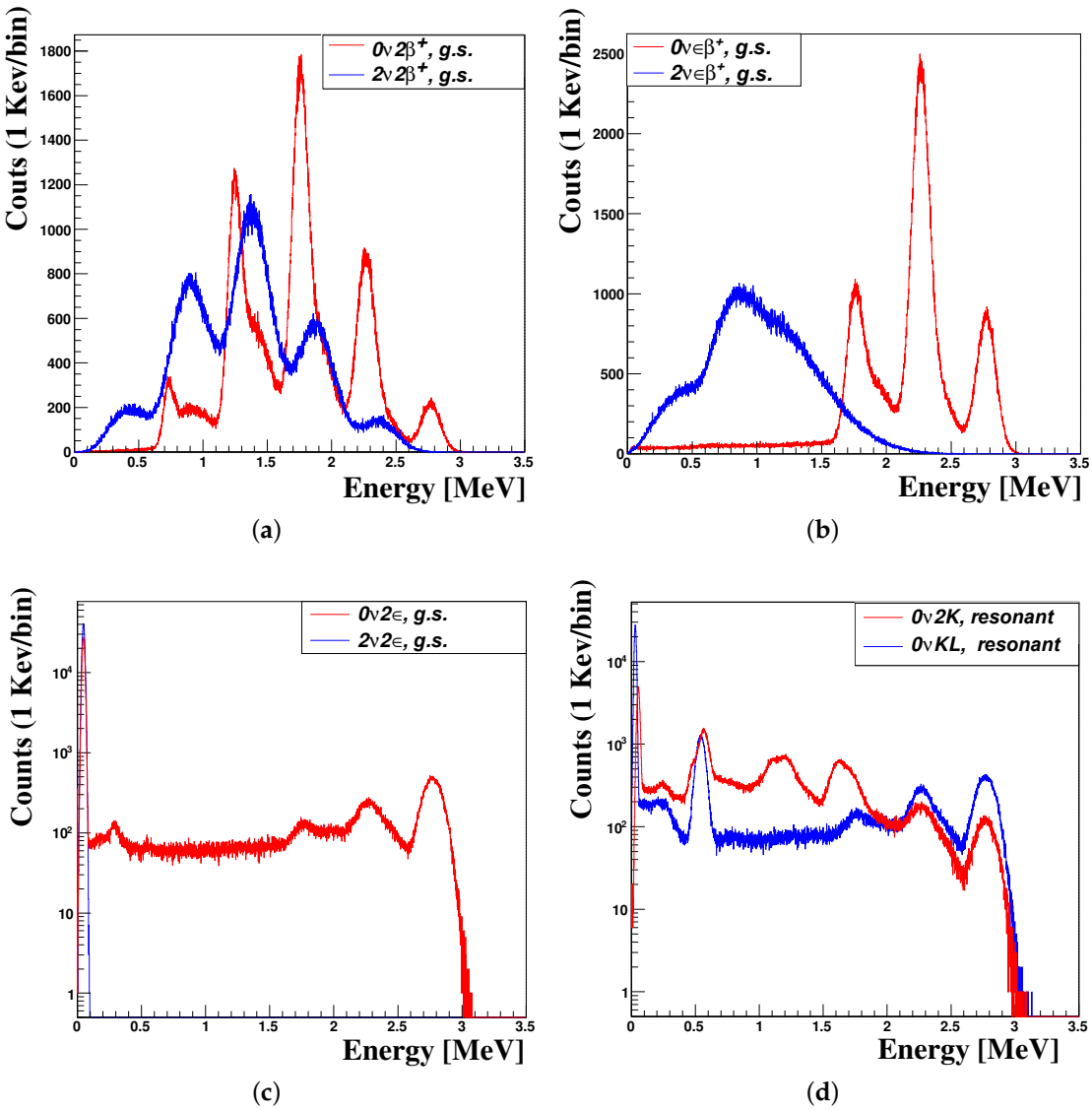

Figure 6. (Color on-line) Some examples of the simulated response functions of the $^{106}CdWO_4$ detector to $2\beta^+$, $\epsilon\beta^+$ and 2ϵ processes in ^{106}Cd ($Q_{\beta\beta} = 2775.39(10)$ [165]) with and without neutrinos. The structures are due to the gamma quanta detection efficiency, the number of escaping annihilation photons, the presence/absence of the neutrinos, and the possible decay in an excited state of daughter ^{106}Pd (see text). In the panels (**a**–**d**) are respectively reported the energy distributions of the following transitions: $0\nu2\beta^+$ and $2\nu2\beta^+ \rightarrow$ g.s.; $0\nu\epsilon\beta^+$ and $2\nu\epsilon\beta^+ \rightarrow$ g.s. ; $0\nu2\epsilon$ and $2\nu2\epsilon \rightarrow$ g.s.; $0\nu2K$ and $2\nu KL$ resonants. Reprinted from Reference [160].

In case of the "source = detector" approach the energy distribution of $0\nu2\beta^+$ is characterized, while taking the gamma-quanta detection efficiency into account, by five peaks (see Figure 6a) at the $Q_{\beta\beta} - km_e$ energy (m_e is the electron's mass) due to the energy deposition of the positrons plus the full deposition of energy of the detected annihilation γ's; and, k is the number of how many annihilation γ's escape the detector. In the $2\nu2\beta^+$ mode, the energy distribution is similar to the previous one, but with the following differences: (i) the peak due to positron detection is broadened due to the energy fraction that is carried out by the neutrinos; (ii) the peaks due to the annihilation photons show the same trend as in the 0ν mode, but shifted by a quantity of $\sim \frac{1}{2}(Q_{\beta\beta} - 4m_e)$ due to the lower mean energy of the positrons.

In the case of $\epsilon\beta^+$ decay, the energy distribution is mainly composed of three main peaks (see Figure 6b). In the 0ν mode, the average position of the peaks is at $Q_{\beta\beta} - 2m_e$, $Q_{\beta\beta} - m_e$, and $Q_{\beta\beta}$. The 2ν mode has a similar energy distribution, but with the following important differences: (i) the peaks are enlarged due to the energy that is carried away by the neutrinos; and, (ii) the peaks are shifted of $\sim \frac{2}{3}(Q_{\beta\beta} - 2m_e - E_b)$ due to the lower energy of the emitted positron; E_b is the bounding atomic energy of the captured electron.

In the $2\nu2\epsilon$ mode, the emitted energy ($Q_{\beta\beta} - 2E_b$) is carried out by the two neutrinos. On the contrary, in the $0\nu2\epsilon$ mode, the full energy is carried out by a single bremsstrahlung gamma quanta. Besides this, the energy distributions show two peaks at E_b and $2E_b$, due to the atomic shell re-organization (see Figure 6c, the binding energies of the electrons on the K and L shell are 24.4 keV and 3.2 keV, respectively).

Finally, the 2ϵ transition from either KK or KL shells in which the released energy is approximatively equal (taking the errors into account) to the two excited energy levels of daughter ^{106}Pd (in the present case, the energy levels are 2718 keV and 2741 keV, respectively) can show the so-called resonant effect. As before, the lowest energy peak is due to the X-rays/Auger electrons cascades. The peak shown at $Q_{\beta\beta}$ is given by the absorption of all the energy of the decay. Instead, the intermediate structures are mainly due to the photons coming out the excited state of ^{106}Pd.

3. Status of Experimental Sensitivities

The most sensitive DBD experiments are $2\beta^-$ decay experiments with the sensitivity at the level of $10^{24} - 10^{26}$ yr and, thus, a sensitivity for the effective Majorana neutrino mass in the range $\langle m_\nu \rangle < (0.1 - 0.7)$ eV is achieved (see, e.g., References [27,28]). The uncertainties are mainly due to the nuclear matrix elements calculations and the assumptions on the nuclear model and the axial-vector coupling constant, as mentioned in Section 1. Instead, the best present sensitivities of experiments for DBD in positive modes are more modest, at the level of $10^{21} - 10^{22}$ yr.

The different experimental sensitivities reached are due, for example, to the progress about the germanium detectors' developments often used in gamma spectroscopy and in the screening of the materials. Historically, progress and efforts in improving the low-level radioactivity measurements technique have favored studies on the double beta decay of the ^{76}Ge isotope. This is the case, e.g., of the half-life limits achieved for the $(2\nu + 0\nu)2\beta^-$ of ^{76}Ge to excited states of ^{76}Se deduced from the background screening of a passive shield using an HP-Ge detector, as shown in Reference [166]. The present results have profited from a long story of experimental technical improvements, new deep underground laboratories, and an increase in researcher expertise in the sector. Most recently, important efforts are in progress to increase the sensitivity on DBD+ to profit from the advantages that are listed in Section 1.

In the following, the experimental limits and positive claims on half-life of some DBD+ modes are given for both 2ν and 0ν modes. All of the measured transitions and the experimental techniques are also reported.

3.1. Positive Claims for Some 2ν DBD+ Modes

In this Section, we briefly address the few positive claims for the detection of $2\nu2\epsilon$ decay in ^{78}Kr, ^{124}Xe, ^{130}Ba, and ^{132}Ba present in literature. These isotopes can decay to the daughters ^{78}Se, ^{124}Te, ^{130}Xe, and ^{132}Xe, respectively, by $2\beta^+$, $\epsilon\beta^+$, 2ϵ, and 2ϵ transitions. In Table 1, we report the results, both positive claims and experimental limits, for those isotopes.

Table 1. The present best half-lives limits or claims on 2ν and 0ν DBD+ in ^{78}Kr, ^{130}Ba, ^{132}Ba, and ^{124}Xe (if not specified, the C.L. of experimental limits is 90%). In the square bracket, the experimental technique is reported: Low background Proportional Counter (LPC), High Pressure Ionization Chamber (HPIC), Geochemical method (GEO), Scintillator detector (S), Liquid Xenon (LXe), and Time Projection Chamber (TPC).

Transition	$Q_{\beta\beta}$ (keV) [165]	Natural Abundance (%) [167]	Process	$T_{1/2}$ (yr)	
				2ν	0ν
^{78}Kr $\rightarrow$ ^{78}Se	2847.67(26)	0.355(3)	KK	$= (9.2^{+5.5}_{-2.6}\text{stat} \pm 1.3\text{sys}) \times 10^{21}$ [LPC] [168] $= (1.9^{+1.3}_{-0.7}\text{stat} + 0.3\text{sys}) \times 10^{22}$ [LPC] [169]	$\geq 5.5 \times 10^{21}$ [LPC] [168]
			KK (0^+_1, 1498.6)	$\geq 5.4 \times 10^{21}$ [LPC] [168]	–
			KK ((2^+), 2838.5) (a)	–	$\geq 5.4 \times 10^{21}$ [LPC] [168]
			$K\beta^+$	$\geq 1.1 \times 10^{20}$ (68%) [LPC] [170]	$\geq 5.1 \times 10^{21}$ (68%) [LPC] [170]
			$2\beta^+$	$\geq 2.0 \times 10^{21}$(b) (68%) [LPC] [170]	
^{124}Xe $\rightarrow$ ^{124}Te	2863.9(22)	0.095(5)	2ϵ	$= (1.8 \pm 0.5_{\text{stat}} \pm 0.1_{\text{sys}}) \times 10^{22}$ [LXe (TPC)] [171]	–
			KK	$\geq 2.1 \times 10^{22}$ [LXe (S)] [172]	–
			$K\beta^+$	$\geq 4.8 \times 10^{16}$ (68%) [Xe (HPIC)] [173]	$\geq 1.2 \times 10^{18}$ (68%) [Xe (HPIC)] [173]
			$K\beta^+$ (2^+ 602.7)	$\geq 4.2 \times 10^{17}$ (68%) [Xe (HPIC)] [173]	–
			$2\beta^+$	$\geq 2.0 \times 10^{14}$ (68%) [Xe (HPIC)] [173]	$\geq 4.2 \times 10^{17}$ (68%) [Xe (HPIC)] [173]
^{130}Ba $\rightarrow$ ^{130}Xe	2618.9(26)	0.11(1)	$2\epsilon + \epsilon\beta^+ + 2\beta^+$	$= (2.16 \pm 0.52) \times 10^{21}$ (b) [GEO] [174] $= (6.0 \pm 1.1) \times 10^{20}$(b) [GEO] [175] $= 2.1^{+3.0}_{-0.8} \times 10^{21}$ (b,c)[GEO] [176] $\geq 4 \times 10^{21}$ (68%) (b,c) [GEO] [176]	
			2ϵ	–	–
			$\epsilon\beta^+$	–	$\geq 1.4 \times 10^{17}$ [BaF_2 (S)] [93]
			$\epsilon\beta^+$ (2^+_1 536.1)	–	$\geq 1.1 \times 10^{17}$ [BaF_2 (S)] [93]
			$\epsilon\beta^+$ (2^+_2 1122.1)	–	$\geq 1.4 \times 10^{17}$ [BaF_2 (S)] [93]
			$\epsilon\beta^+$ (4^+ 1204.6)	–	$\geq 7.6 \times 10^{16}$ [BaF_2 (S)] [93]
			$2\beta^+$	–	$\geq 7.6 \times 10^{16}$ [BaF_2 (S)] [93]
			$2\beta^+$ (2^+_1 536.1)	–	$\geq 1.0 \times 10^{17}$ [BaF_2 (S)] [93]
^{132}Ba $\rightarrow$ ^{132}Xe	843.9(11)	0.10(1)	2ϵ	$= (1.3 \pm 0.9) \times 10^{21}$ (b,d) [GEO] [174] $\geq 2.2 \times 10^{21}$ (68%) (b) [GEO] [174] $\geq 3.0 \times 10^{21}$(68%) (b,c) [GEO] [176]	

(a) Resonant effect. (b) $0\nu + 2\nu$ double beta decay. (c) The result of Reference [176] has been inferred re-analyzing the geochemical measurements of Reference [177]. (d) See the last paragraph of Section 3.1.

The natural abundance of ^{78}Kr is 0.355(3)% [167] and its $Q_{\beta\beta}$ value is 2847.67(26) keV [165] (Figure 7 presents a simplified decay scheme of ^{78}Kr). The theoretical half-life of DBD+ of ^{78}Kr decay to the g.s. of ^{78}Se spreads over a wide range [178–183]: 10^{24}–10^{29} yr for the $2\nu2\beta^+$ case and 10^{21}–10^{25} yr for the $2\nu\epsilon\beta^+$ and $2\nu2\epsilon$ cases. The first positive claim of 2νDBD+ of ^{78}Kr occurred in 2013 [168] using a low background proportional counter (LPC). The adopted LPC was a cylinder with inner and outer diameters of 140 mm and 150 mm, respectively. A gold-plated tungsten wire of 10 µm in diameter was stretched along the LPC axis and it was used as anode. A potential of +2400 V was applied to the wire, and the casing (the cathode) was grounded. The LPC volume was 9.159 L; it was placed inside a shielding of 18 cm of copper, 15 cm of lead, and 8 cm of borated polyethylene layers. The installation was located at the Baksan Neutrino Observatory, INR RAS, (4700 m water equivalent depth), where the cosmic ray flux is lowered by $\sim 10^7$ times as compared to the flux at sea level. The counter was filled with pure krypton gas (enriched in ^{78}Kr to 99.81%) up to 4.42 bar having no quenching or accelerating gaseous additions. After a total exposure of 0.343 kg $\times$ yr, the authors of Reference [168] quotes a possible hint at 2.5 σ of statistical significance with a half-life of ^{78}Kr relative to $2\nu2K$ capture: $T_{1/2} = (9.2^{+5.5}_{-2.6}\text{stat} \pm 1.3\text{sys}) \times 10^{21}$ yr [168]. Later, a comparative study on double electron capture re-estimated the previous value at $T_{1/2} = (1.9^{+1.3}_{-0.7}\text{stat} \pm 0.3\text{sys}) \times 10^{22}$ yr [169] (see Table 1). We also remind the previous limits at the level of 10^{20}–10^{21} yr set since 1994 [170,184,185].

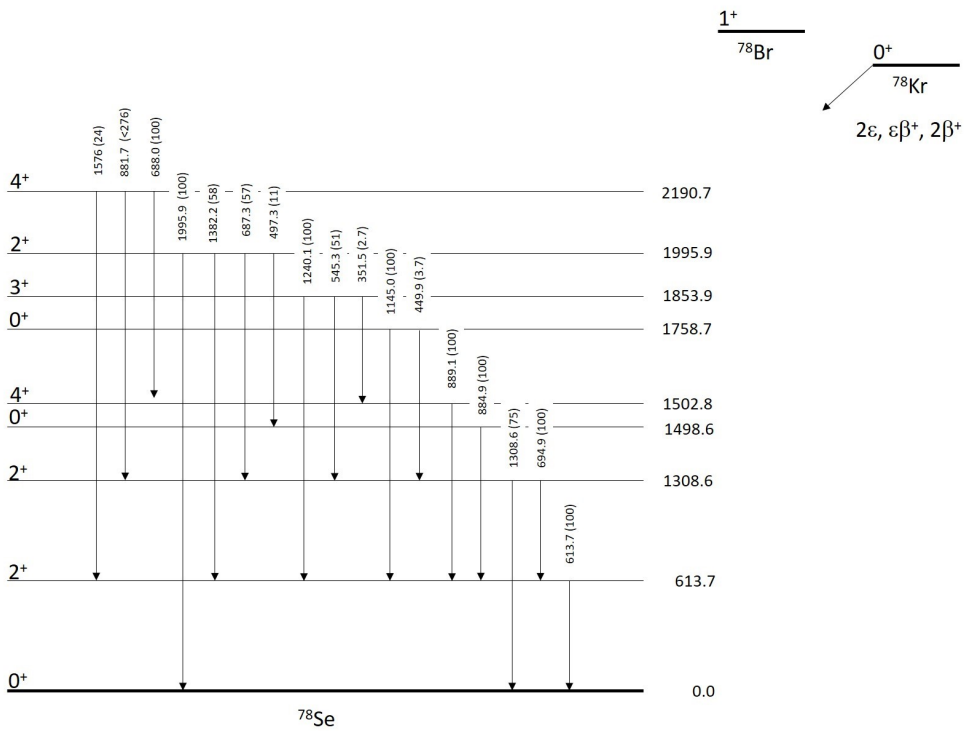

Figure 7. The simplified decay scheme of ^{78}Kr to the ground state and to the first excited levels of ^{78}Se. The energies of the levels (in keV) and relative main branching ratios (in %) are taken from Reference [186].

The natural abundance of ^{124}Xe is 0.095(5)% [167] and its $Q_{\beta\beta}$ value is 2863.9(22) keV [165] enough to account for all of the DBD+ modes (Figure 8 presents a simplified decay scheme of ^{124}Xe). The theoretical half-life of the $2\nu2\epsilon$ transition in ^{124}Xe to the g.s. of ^{124}Te spreads over a wide range between $10^{20} - 10^{24}$ yr [178,179,187–190]. Assuming that the two vacancies of the daughter atom are in the K-shell, the ^{124}Te relaxing emits X-rays and/or Auger electrons with a total energy of $E_{2K} = 64.46$ keV [191]. XENON1T is a detector exploiting the primary scintillation in the liquid phase and the secondary proportional scintillation in the gas phase with the limitations addressed in [147,148] and References therein. It uses 3.2 t of ultra-pure liquid xenon (LXe), and 2 t of them are within the sensitive volume of the time projection chamber (TPC): a cylinder of ∼96 cm diameter and height with walls of highly-reflective PTFE that is instrumented with 248 photomultipliers (Hamamatsu R11410-21, with 76.2 mm diameter) in two arrays (top and bottom). Both of the arrays consist of a massive OFHC copper support plate with circular cut-outs for the PMTs. The TPC is surrounded by 74 field-shaping electrodes with a cross-section of $\sim 10 \times 5$ mm^2; they are made from low-radioactivity oxygen-free high thermal conductivity (OFHC) copper. The LXe-TPC is encapsulated in a stainless-steel cryostat that is installed inside a 740 m^3 water shield equipped with 84 PMTs deployed on the lateral walls. A neutron gun is placed close the side external layer of the stainless-steel cryostat. The neutrons, with energies that are around 2.2 MeV and 2.7 MeV from a neutron generator exploiting the deuterium–deuterium fusion, are used for routine calibrations despite their effects in the activation of all the set-up's materials. The collaboration quoted a signal due to the $2\nu2\epsilon$ decay in ^{124}Xe with the half-life of $(1.8 \pm 0.5_{\text{stat}} \pm 0.1_{\text{sys}}) \times 10^{22}$ yr [171]. However, the significance of the effect is only 4.4 σ, as addressed in the literature (see e.g., Reference [192]). To be thorough, it should also be noted that a limit $T_{1/2} \geq 2.1 \times 10^{22}$ yr was previously obtained in Reference [172] (see Table 1). We are also reminded of the previous limits at the level of $(0.65–4.7) \times 10^{21}$ yr [193–195].

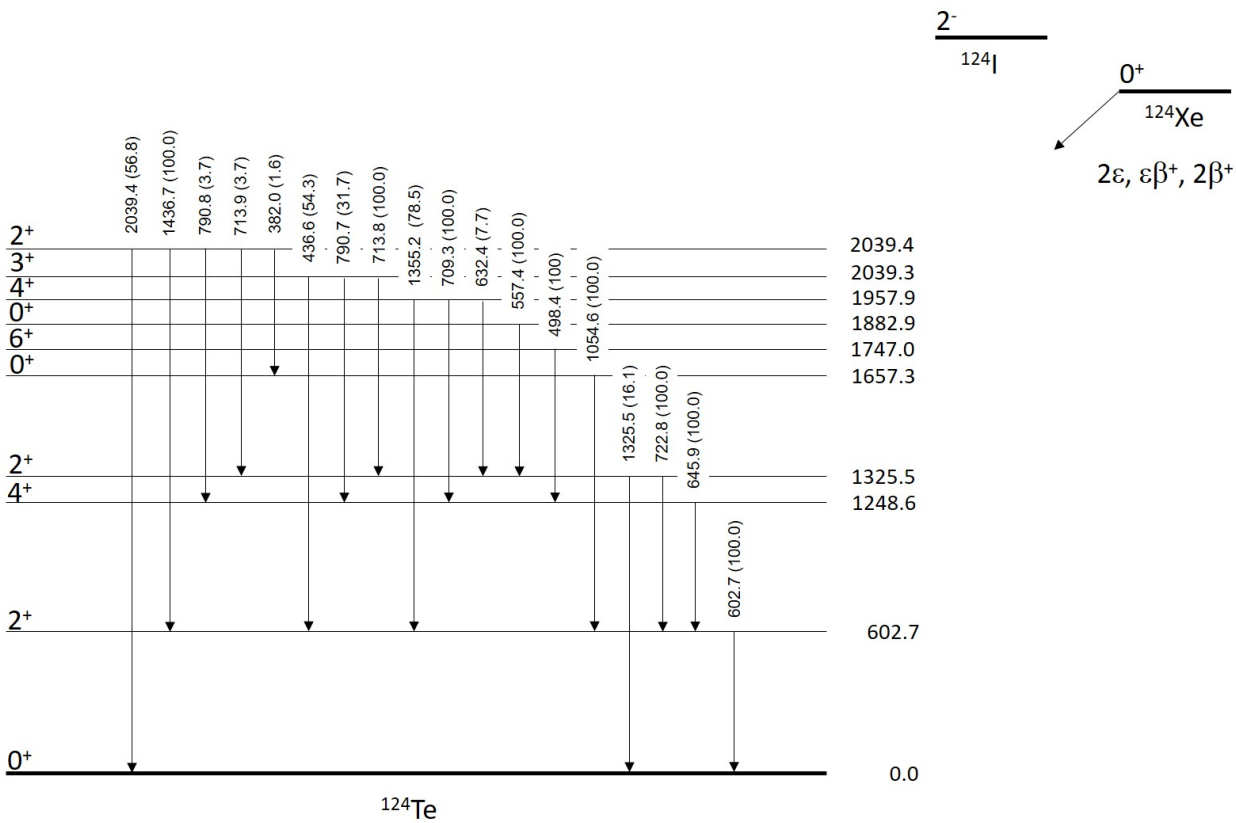

Figure 8. A simplified decay scheme of ^{124}Xe to the ground state and the first excited levels of ^{124}Te. The energies of the levels (in keV) and relative main branching ratios (in %) are taken from Reference [196].

Finally, the natural abundance of ^{130}Ba is 0.11(1)% [167] and its $Q_{\beta\beta}$ value is 2618.9(26) keV [165] (a simplified decay scheme of ^{130}Ba is presented in Figure 9). The theoretical half-life of DBD+ in ^{130}Ba to the g.s. of ^{130}Xe spreads over a wide range [3,178–180,190,197]: 10^{28}–10^{31} yr for the $2\nu2\beta^+$ case, 10^{22}–10^{24} yr for the $2\nu\epsilon\beta^+$ case, and 10^{20}–10^{23} yr for the $2\nu2\epsilon$ case. In 1976, an anomalous amount of ^{130}Xe in a sedimentary barite sample ($BaSO_4$) from South Africa and Western Australia (3×10^9 years old) was found [177]. The adopted experimental technique was the geochemical method that relies on the extraction of decay products (^{130}Xe noble gas) from ancient minerals using mass spectrometer analysis. In Reference [176], reanalyzing the data presented in Reference [177], the limit of $T_{1/2} \geq 4 \times 10^{21}$ yr was set for all of the decay modes of DBD in ^{130}Ba. In the same work of Reference [176], but using a different sample of barite in Reference [177], the authors set a DBD indication with $T_{1/2} = (2.1^{+3.0}_{-0.8}) \times 10^{21}$ yr. Later, in Reference [174], using the geochemical measurement of ^{130}Xe amount in natural barite (from the Belorechenskoe deposit in North Caucasus, Russia), the half-life for ^{130}Ba for all of the DBD decay modes was set to $(2.16 \pm 0.52) \times 10^{21}$ yr. However, in a following geochemical experiment, a $T_{1/2} = (6.0 \pm 1.1) \times 10^{20}$ yr [175] was obtained in disagreement with the previous results. More recently, in Reference [198], a summary of the previous measurements was attempted while considering a more reliable value of $T_{1/2} = (2.2 \pm 0.5) \times 10^{21}$ yr, as recommended in Reference [192] (see Table 1).

To be thorough, a possible claim also exists for the $(2\nu + 0\nu)2\epsilon$ transitions in ^{132}Ba to the g.s. of ^{132}Xe (see Table 1). In fact, in Reference [174], the apparent excess in one barite sample of ^{132}Xe (not evident in the other samples) can be used to estimate the half-life of DBD+ in ^{132}Ba $T_{1/2} = (1.3 \pm 0.9) \times 10^{21}$ yr. However, in the same work, the authors also give a cautious lower limit: $T_{1/2} \geq 2.2 \times 10^{21}$ yr. Moreover, a more stringent half-life limit is also addressed ($T_{1/2} \geq 3.0 \times 10^{21}$ yr) in Reference [176]. The related theoretical half-life prediction spans over a range of 10^{25}–10^{26} yr [190].

Recently, several developments are aimed at increasing the performance of some low radioactive Ba-based scintillation detectors, as in References [93,95], with the goal to improve the experimental sensitivity to DBD+ in ^{130}Ba and ^{132}Ba by direct measurements.

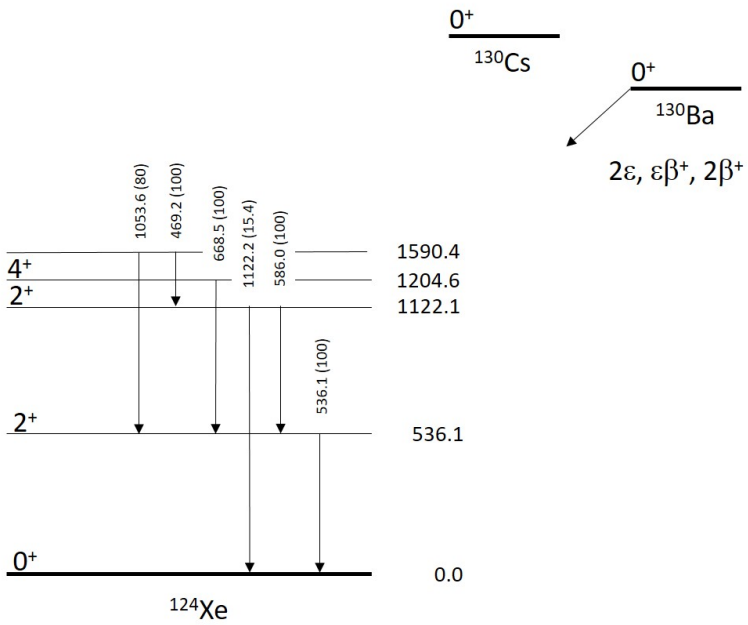

Figure 9. The simplified decay scheme of ^{130}Ba to the ground state and to the first excited levels of ^{130}Xe. The energies of the levels (in keV) and the relative main branching ratios (in %) are taken from Reference [199].

3.2. Experiments Using Solid Detectors as "Source = Detector"

The use of a solid detection medium, thanks, for example, to their high densities and the possibility to implement a modularity approach, is of great advantage. Moreover, when considering the "source = detector" approach, three kinds of solid detectors can be addressed: semiconductor, scintillator, and bolometric detectors. Among them, the most diffused detection method for DBD+ investigations uses the crystal scintillator detectors, since almost all of the best limits of DBD+ transitions are achieved by their use (see the Tables in this Section). In the following, we will first summarize some of the results of bolometers and semiconductors and, later, those of scintillators.

The bolometer/scintillating-bolometers (B/SB) and the semiconductors (SC) ("source = detector") only obtained the best limits for a few DBD+ transitions in ^{48}Ca, ^{64}Zn, ^{120}Te, and ^{180}W achieved by the CRESST (SB), COBRA (SC), CUORE (B), and CUPID (SB) collaborations. CUPID, the upgrade of CUORE, in turn the upgrade of CUORE-0 (B), which was the upgrade of CUORICINO (B) experiment.

CRESST (SB, Cryogenic Rare Event Search with Superconducting Thermometers) consists of scintillating bolometers that are based on $CaWO_4$ crystals. The detector volume (installed deep underground at LNGS in Italy) is surrounded by a passive shield that consists of 14 cm thick low background copper and 20 cm of lead. This inner shield is entirely enclosed within a gas-tight radon box that is continuously flushed with N_2 gas. The data that were collected with the phase-II of the experiment (exposure of 2 kg $\times$ yr) have been used to study some DBD+ transition in ^{40}Ca and ^{180}W [200] (also see Table 2).

COBRA (SC, Cadmium zinc telluride 0-neutrino double-Beta Research Apparatus) collaboration aims at using semiconductor detectors at room temperature, adopting CdTe or CdZnTe crystals (mainly to explore the DBD- in ^{116}Cd and ^{130}Te decays). The experiment, in the upgrading phase at LNGS, is composed by an array of 64 cubic CdZnTe detectors that are arranged in four layers of 16 detectors each one (with 1 cm edge and mass of $\sim$6 g), and, in 2018, nine new crystals (with a size of 1.5 cm $\times$ 2 cm $\times$ 2 cm, mass of $\sim$28 g) have

been added [201]. The technology is not yet mature and, thus, the sensitivity for the DBD+ in ^{120}Te is at the level of 10^{15}–10^{16} yr. However, CdZnTe crystals have nine double-beta emitters: ^{64}Zn, ^{70}Zn, ^{106}Cd, ^{108}Cd, ^{114}Cd, ^{116}Cd, ^{120}Te, ^{128}Te, and ^{130}Te, but, as before, the sensitivity that is reached for their DBD+ is often not competitive [202].

CUORE-0 (B, Cryogenic Underground Observatory for Rare Events, step 0) consisted of 52 TeO_2 crystals with natural Te composition. The crystals were 5 cm cubes mounted in a tower of 13 floors, with four crystals per floor (the total crystals array is named tower). They were operated at a temperature of ∼10 mK and read-out with neutron transmutation-doped germanium thermistors. The total TeO_2 mass is 39 kg and the ^{120}Te mass was 28 g, which correponded to 1.3×10^{23} atoms of ^{120}Te. At present, its upgrade, the CUORE experiment, is running using 19 towers of CUORE-0 with an isotopic mass of ^{120}Te of 532 g. Different layers of shielding, such as, e.g., an internal low-background Roman lead layer and an external anti-radon box, surround the cryostat and the crystals [203–205].

CUPID (SB, CUORE Upgrade with Particle Identification [206]) aims at upgrading the CUORE experiment, but using its infrastructure. The idea is to exploit the scintillator-bolometers technique. For this purpose, the project has been testing a few crystal bolometers. The first phase adopting ZnSe crystals was named CUPID-0 (B), and it uses the CUORICINO cryostat.

The bolometric experiments have only achieved the best limits for only a few DBD+ transitions in ^{48}Ca, ^{64}Zn, and ^{120}Te, as previously mentioned. In particular, ^{40}Ca has a natural abundance of 96.941(156)% [167], and its $Q_{\beta\beta}$ value is 193.51(2) keV [165]; it can decay via the 2ϵ mode. The theoretical half-life for the DBD+ of ^{40}Ca to the g.s. of ^{40}Ar is $T_{1/2} \geq 1.2 \times 10^{33}$ yr [207]. The best limits currently established are at the level of $10^{21} - 10^{22}$ yr by the CRESST experiment (or by a based scintillator experiment using a CaF_2(Eu) crystal [208]), as reported in Table 2.

Table 2. The present best half-life limits on 2ν and 0ν DBD+ in ^{40}Ca, ^{64}Zn, ^{120}Te, and ^{180}W (if not specified, the C.L. is at 90%). Only for such isotopes the bolometers (B) or scintillating-bolometers (SB) have achieved the best limits. In the square bracket, the experimental technique and adopted crystal detector are reported: crystal Scintillator detector (S), High Pure Germanium detector (HPGe), B, SB, and crystal semiconductors in CdTe and CdZnTe working at room temperature (SC).

Transition	$Q_{\beta\beta}$ (keV) [165]	Natural Abundance (%) [167]	Process	$T_{1/2}$ (yr)	
				2ν	0ν
^{40}Ca → ^{40}Ar	193.51(2)	96.941(156)	$2K$	$\geq 9.92 \times 10^{21}$ [$CaWO_4$ (SB)] [200]	–
			2ϵ	$\geq 5.9 \times 10^{21}$ [CaF_2(Eu) (S)] [208]	$\geq 1.40 \times 10^{22}$ [$CaWO_4$ (SB)] [200]
^{64}Zn → ^{64}Ni	1094.9(7)	49.17(75)	2K	$\geq 1.1 \times 10^{19}$ [$ZnWO_4$ (S)] [100]	–
			2ϵ	–	$\geq 2.5 \times 10^{21}$ [HPGe] [209]
			$\epsilon\beta^+$	$\geq 9.4 \times 10^{20}$ (a) [$ZnWO_4$ (S)] [100]	$\geq 1.2 \times 10^{22}$ [ZnSe (SB)] [210]
				$\geq 2.7 \times 10^{21}$ (b) [HPGe] [209]	
^{120}Te → ^{120}Sn	1730(3)	0.09(1)	2ϵ	$\geq 9.4 \times 10^{15}$ [CdTe, CdZnTe (SC)] [211]	–
			KK/KL/LL	–	$\geq (6.0/3.9/2.9) \times 10^{17}$ [HPGe] [212]
			2ϵ (2^+ 1171.3)	$\geq 7.5 \times 10^{17}$ (b) [HPGe] [212]	$\geq 1.8 \times 10^{16}$ [CdZnTe (SC)] [213]
			$\epsilon\beta^+$	$\geq 7.6 \times 10^{19}$ [TeO_2 (B)] [214]	$\geq 2.7 \times 10^{21}$ [TeO_2 (B)] [203]
^{180}W † → ^{180}Hf †	143.23(28)	0.12(1)	KK	$\geq 3.1 \times 10^{19}$ [$CaWO_4$ (SB)] [200]	–
			2ϵ	–	$\geq 9.4 \times 10^{18}$ [$CaWO_4$ (SB)] [200]

(†) The nucleus is unstable with respect to the α decay [51,78]. (a) We also remind a quoted claim with $T_{1/2} = 1.1(9) \times 10^{19}$ yr in Reference [215]. (b) $0\nu + 2\nu$ double beta decay.

The ^{64}Zn nuclide has a natural abundance of 49.17(75)% [167], and its $Q_{\beta\beta}$ value is 1094.9(7) keV [165], and it can decay via $\epsilon\beta^+$ and 2ϵ modes. The half-life that is predicted in the literature for the DBD+ in ^{64}Zn to the g.s. of ^{64}Ni spreads over a range of [182,183]: 10^{34}–10^{36} yr for the $2\nu\epsilon\beta^+$ case and 10^{26}–10^{27} yr for the $2\nu 2\epsilon$ case. The best limit for the transition $0\nu\epsilon\beta^+$ (g.s.) is achieved by the CUPID-0 with $T_{1/2} \geq 1.2 \times 10^{22}$ yr, while all of the other transitions are measured by the DAMA-INR Kyiv collaboration with the help of $ZnWO_4$ crystal scintillators [100]; the sensitivity reached is at the level of 10^{19}–10^{21} yr. To be thorough, a quoted claim with $T_{1/2} = 1.1(9) \times 10^{19}$ yr [215] is present in the literature while using a passive source approach.

The ^{120}Te nuclide has a natural abundance of 0.09(1)% [167], and its $Q_{\beta\beta}$ value is 1730(3) keV [165] and it can decay via $\epsilon\beta^+$ and 2ϵ modes. The half-life that is predicted in the literature for the DBD+ in ^{120}Te to the g.s. of ^{120}Sn spreads over a wide range [216]: 10^{26}–10^{27} yr for the $2\nu\epsilon\beta^+$ case and 10^{23}–10^{24} yr for the $2\nu2\epsilon$ case. Instead, the theoretical prediction for $2\nu2\epsilon$ decay of ^{120}Te to the first exited level of ^{120}Sn spans [216] in 10^{33}–10^{34} yr. The COBRA experiment [211] and a passive source approach, using an HP-Ge detector [212], determined the best limits for the 2ϵ transition to g.s. of daughter nucleus and 2ϵ to the 2^+ exited level of the daughter nucleus (see Table 2). Instead, the best limits of $\epsilon\beta^+$ were achieved by the CUORICINO and CUORE-0 collaborations [203,214] (see Table 2).

Finally, ^{180}W has a natural abundance of 0.12(1)% [167] and its $Q_{\beta\beta}$ value is 143.23(28) keV [165], and it can decay via he 2ϵ modes. The best limits currently established are at the level of 10^{18}–10^{19} yr by the CRESST experiment, as reported in Table 2 (or by a based scintillator experiment using a $^{116}CdWO_4$ crystal scintillator, as in Reference [217]).

The most competitive crystal scintillators used to study the DBD+ are: $CaMoO_4$, $ZnWO_4$, CaF_2, SrI_2, Cs_2HfCl_6, $CdWO_4$, BaF_2, and $CeCl_3$. Most of the listed crystal scintillators have been developed in the framework of DAMA and DAMA-INR Kyiv collaborations. These scintillators contain DBD+ emitters that are of great interest in the sector: ^{40}Ca, ^{64}Zn, ^{84}Sr, ^{106}Cd, ^{108}Cd, ^{130}Ba, ^{132}Ba, ^{136}Ce, ^{138}Ce, and ^{174}Hf. This motivated the DAMA and DAMA-INR Kyiv efforts. Besides this, the intriguing possibility to either develop or improve new low background crystal scintillators for both rare event investigations and industrial/medical applications has further motivated different DAMA and DAMA-INR Kyiv R&Ds [30,42,50,55,59]. Table 3 shows the best limits that are mainly achieved using crystal scintillator detectors, besides those already listed in Tables 1, 2 and 4. In the following, as an interesting example, the experimental results on DBD+ in ^{106}Cd will be summarized.

Table 3. The present best half-lives limits on 2ν and 0ν DBD+ of ^{84}Sr, ^{92}Mo, ^{106}Cd, ^{108}Cd, ^{126}Xe, and ^{138}Ce mainly obtained by crystal scintillator detectors (if not specified, the C.L. is at 90%). In the square bracket, the experimental technique and adopted crystal detector is reported: crystal Scintillator detector (S) and High Pure Germanium detector (HPGe). To be thorough, some other best limits for transitions using S are also shown in Tables 1, 2 and 4.

Transition	$Q_{\beta\beta}$ (keV) [165]	Natural Abundance (%) [167]	Process	$T_{1/2}$ (yr)	
				2ν	0ν
^{84}Sr → ^{84}Kr	1789.8(12)	0.355(3)	KK/KL/LL	–	≥(6.0/1.9/5.9) × 10^{16} [SrI_2 (S)] [89]
			2ϵ (2^+ 881.6)	≥2.6 × 10^{16} [SrI_2 (S)] [89]	≥3.1 × 10^{16} [SrI_2 (S)] [89]
			$\epsilon\beta^+$	≥6.9 × 10^{15} [SrI_2 (S)] [89]	≥6.9 × 10^{15} [SrI_2 (S)] [89]
^{92}Mo → ^{92}Zr	1650.45(19)	14.649(2)	2ϵ	–	≥6.8 × 10^{19} [HPGe + $CaMoO_4$ (S)] [218]
			2ϵ (2_1^+, 934.5)	≥8.9 × 10^{20} (a)[HPGe] [219]	≥3.7 × 10^{19} [HPGe + $CaMoO_4$ (S)] [218]
			2ϵ (0_1^+, 1382.7)	≥8.1 × 10^{20} (a)[HPGe] [219]	≥1.9 × 10^{19} [HPGe + $CaMoO_4$ (S)] [218]
			2ϵ (4_1^+, 1495.5)	≥6 × 10^{18} (a) [Ge(Li)] [220]	
			$\epsilon\beta^+$	≥1.9 × 10^{20} (a)[HPGe] [219]	≥2.3 × 10^{20} [CsI(Tl) (S) + $CaMoO_4$ (S)] [221]
^{106}Cd → ^{106}Pd	2775.39(10)	1.245(22)	2ϵ	≥4.2 × 10^{20} [HPGe] [222]	≥1.0 × 10^{21} [$CdwO_4$ (S)] [80]
			2ϵ (2^+ 511.9)	≥9.9 × 10^{20} [$CdwO_4$ (S) + HPGe] [82]	≥5.1 × 10^{20} [$CdWO_4$ (S)] [80]
			2ϵ (2^+ 1128.0)	≥6.6 × 10^{20} [$CdWO_4$ (S)] [48]	≥5.1 × 10^{20} [$CdWO_4$ (S) + HPGe] [82]
			2ϵ (0^+ 1133.8)	≥1.0 × 10^{21} [$CdWO_4$ (S) + HPGe] [82]	≥1.1 × 10^{21} [$CdWO_4$ (S) + HPGe] [82]
			2ϵ (2^+ 1562.3)	≥7.8 × 10^{20} [$CdWO_4$ (S)] [48]	≥1.4 × 10^{21} [$CdWO_4$ (S)] [48]
			2ϵ (0^+ 1706.4)	≥7.1 × 10^{20} [$CdWO_4$ (S) + HPGe] [82]	≥2.0 × 10^{21} [$CdWO_4$ (S)] [48]
			2ϵ (0^+ 2001.5)	≥1.5 × 10^{21} [$CdWO_4$ (S)] [48]	≥1.2 × 10^{21} [$CdWO_4$ (S) + HPGe] [82]
			2ϵ (0^+ 2278.1)	≥3.1 × 10^{20} [$CdWO_4$ (S)] [48]	≥1.2 × 10^{21} [$CdWO_4$ (S)] [48]
			KK (2718) (b)	–	≥29 × 10^{20} [$CdWO_4$ (S)] [48,80]
			KL_1 (4^+ 2741) (b)	–	≥9.5 × 10^{20} [$CdWO_4$ (S)] [48,80]
			KL_3 ($2,3^-$ 2748) (b)	–	≥14 × 10^{20} [$CdWO_4$ (S)] [48,80]
			$\epsilon\beta^+$	≥2.1 × 10^{21} [$CdWO_4$ (S)] [48]	≥1.4 × 10^{22} [$CdWO_4$ (S)] [80]
			$\epsilon\beta^+$ (2^+ 511.9)	≥2.7 × 10^{21} [$CdWO_4$ (S)] [48]	≥9.7 × 10^{21} [$CdWO_4$ (S)] [48]
			$\epsilon\beta^+$ (2^+ 1128.0)	≥1.3 × 10^{21} [$CdWO_4$ (S)] [48]	≥1.0 × 10^{22} [$CdWO_4$ (S)] [48]
			$\epsilon\beta^+$ (0^+ 1133.8)	≥8.5 × 10^{20} [$CdWO_4$ (S)] [48]	≥1.9 × 10^{21} [$CdWO_4$ (S) + HPGe] [82]
			$2\beta^+$	≥2.3 × 10^{21} [$CdWO_4$ (S) + HPGe] [82]	≥5.9 × 10^{21} [$CdWO_4$ (S)] [48]
			$2\beta^+$ (2^+ 511.9)	≥2.5 × 10^{21} [$CdWO_4$ (S) + HPGe] [82]	≥4.3 × 10^{21} [$CdWO_4$ (S)] [48]
^{108}Cd → ^{108}Pd	271.8(8)	0.888(11)	2K	≥1.1 × 10^{18} [$CdWO_4$ (S)] [92]	–
			2ϵ	–	≥1.0 × 10^{18} [$CdWO_4$ (S)] [92]
^{126}Xe → ^{126}Te	918(4)	0.089(3)	KK	≥1.9 × 10^{22} [LXe] [172]	–
^{138}Ce → ^{138}Ba	691(5)	0.251(2)	KK/KL/LL	≥(4.4/ − /−) × 10^{16} [$CeCl_3$ (S)] [86]	≥(5.5/8.3/42) × 10^{17} [HPGe] [223,224]

(a) $0\nu + 2\nu$ double beta decay. (b) Resonant effect.

In 2012, the result of a search for the double β processes in ^{106}Cd was carried out at the LNGS (Italy) with the help of a $^{106}CdWO_4$ crystal scintillator (215 g) enriched in ^{106}Cd up to 66% [80]. After 6590 h of data taking, several half-life limits on the double beta processes, including the possible resonant $0\nu2\epsilon$ transitions (see Section 2.1), in ^{106}Cd were established at the level of 10^{19}–10^{21} yr (Figure 10 presents a simplified decay scheme of ^{106}Cd).

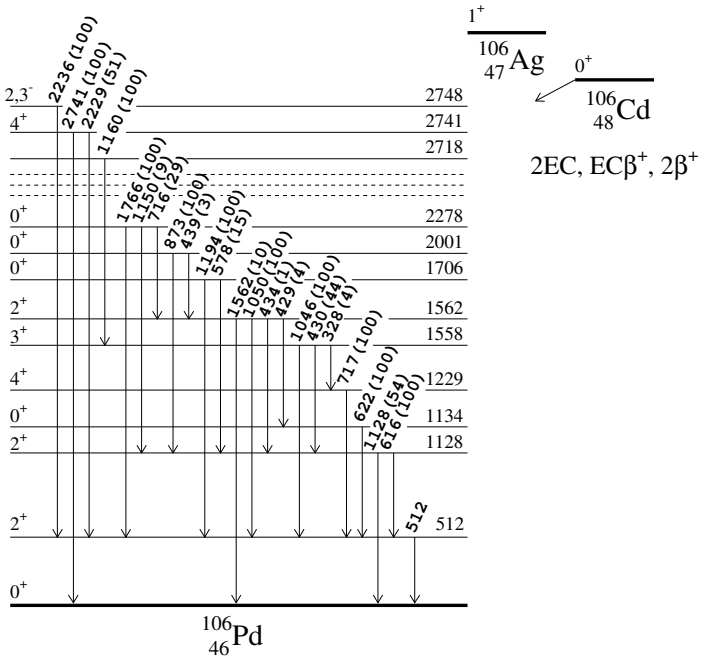

Figure 10. The simplified decay scheme of ^{106}Cd to the ground state and to the first excited levels of ^{106}Pd. The energies of the levels (in keV) and the relative main branching ratios (in %) are taken from Reference [225]. Reprinted from Reference [48].

The $^{106}CdWO_4$ scintillator was placed inside a low background HPGe detector with four Ge crystals to increase the experimental sensitivity to the 2β processes with emission of γ quanta. The final result of this stage, after 13085 h of data taking, with the $^{106}CdWO_4$ scintillation detector operated in coincidence (anticoincidence) with the four crystals HPGe γ detector, further improved the lower limits of several DBD+ [82]. The preliminary results of the experiment have been presented in conference proceedings [81,226–228].

The third stage of the experiment, which was hosted in the DAMA/CRYS set-up at LNGS, added two other low background $CdWO_4$ detectors to profit from the coincidences with gammas emitted in the DBD+. After 26033 h of data taking, new improved half-life limits were set on the different channels and modes of the ^{106}Cd double beta decay at a level of lim $T_{1/2} \sim 10^{20}$–10^{22} yr. The limit for the two neutrino electron capture with positron emission in ^{106}Cd to the ground state of ^{106}Pd, $T_{1/2}^{2\nu\epsilon\beta^+} \geq 2.1 \times 10^{21}$ yr, was set by the analysis of the $^{106}CdWO_4$ data in coincidence with the energy release 511 keV in both of the $CdWO_4$ counters [48]. The sensitivity approaches the theoretical predictions for the half-life that is in the range of $T_{1/2} \sim 10^{21}$–10^{22} yr [48]. The resonant neutrinoless double-electron capture to the 2718 keV excited state of ^{106}Pd is restricted at the level of $T_{1/2}^{0\nu2K} \geq 2.9 \times 10^{21}$ yr (see Table 3). In particular, Figure 11 shows the energy spectrum of the γ and β events that were measured for 26033 h by the $^{106}CdWO_4$ detector in coincidence with 511 keV events in at least one of the $CdWO_4$ counters [48]. The fit of the data by the background model and the excluded distributions for $0\nu\epsilon\beta^+$ and $0\nu2\beta^+$ decays of ^{106}Cd to the ground state of ^{106}Pd with the half-lives $T_{1/2} = 1.4 \times 10^{22}$ yr and $T_{1/2} = 5.9 \times 10^{21}$ yr, respectively, are also shown [48].

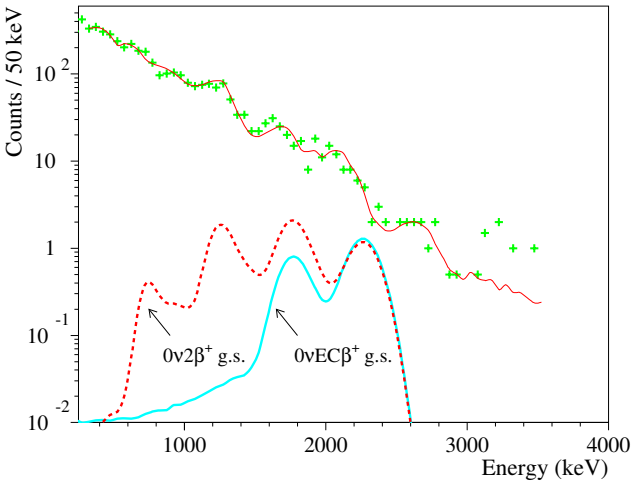

Figure 11. The energy spectrum of the γ and β events measured for 26,033 h by the $^{106}CdWO_4$ detector in coincidence with events in at least one of the $CdWO_4$ counters with energy $E = (511 \pm 2\sigma)$ keV (crosses). The solid red line shows the fit of the data by the background model (see Reference [48]). The excluded distributions of $0\nu\epsilon\beta^+$ and $0\nu2\beta^+$ decays of ^{106}Cd to the ground state of ^{106}Pd with the half-lives $T_{1/2} = 1.4 \times 10^{22}$ yr and $T_{1/2} = 5.9 \times 10^{21}$ yr, respectively, are shown. Reprinted from Reference [48].

Being aimed at the possibility to cover the theoretical predictions for the decay half-life of $2\nu\epsilon\beta^+$ in ^{106}Cd, a new stage with an improved apparatus is in data taking in the DAMA/R&D set-up. Figure 12 shows the scheme of the improved experimental set-up. The two $CdWO_4$ crystal scintillators include a cylindrical cut-out to house the $^{106}CdWO_4$ crystal. The detector system is surrounded by four high purity copper bricks, low radioactive copper and lead, cadmium, and polyethylene in order to reduce the external background.

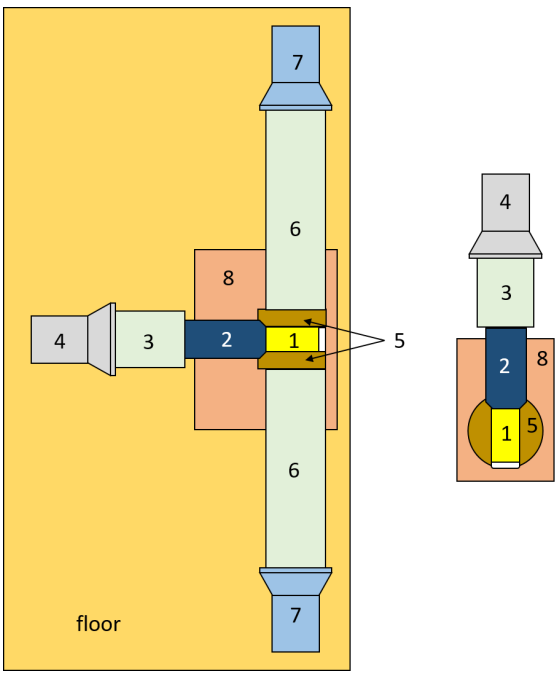

Figure 12. The scheme of the experimental set-up with the $^{106}CdWO_4$ crystal scintillation detector (1), viewed through plastic scintillator (2) and a quartz light-guide (3) by a metallic PMT (4). The two $CdWO_4$ crystal scintillators (5) are viewed through two quartz light-guides (6) by PMTs (7). The detector system was shielded by copper, lead, cadmium, and polyethylene (not shown). Only part of the copper details (8) is shown.

Table 4. The present best half-lives limits on 2ν and 0ν DBD+ in ^{136}Ce, ^{144}Sm, ^{152}Gd, and ^{156}Dy being mainly achieved using the passive source approach (if not specified, the C.L. is at 90%). In the square brackets, the adopted detector is reported: High Pure Germanium detector (HPGe) and Geochemical method (GEO). A few other best limits for transitions using such approach are also listed in Tables 1–6.

Transition	$Q_{\beta\beta}$ (keV) [165]	Natural Abundance (%) [167]	Process	$T_{1/2}$ (yr)	
				2ν	0ν
^{136}Ce → ^{136}Ba	2378.55(27)	0.186(2)	KK/KL/LL	$\geq(3.2/-/-)\times10^{16}$ [$CeCl_3$ (S)] [86]	$\geq(2.1/3.4/8.4)\times10^{18}$ [HPGe] [224]
			2ϵ (2^+ 818.5)	$\geq2.9\times10^{18}$ [HPGe] [224]	$\geq3.0\times10^{18}$ [HPGe] [224]
			2ϵ (2^+ 1551.0)	$\geq3.4\times10^{18}$ [HPGe] [224]	$\geq2.9\times10^{18}$ [HPGe] [224]
			2ϵ (0^+ 1579.0)	$\geq2.5\times10^{18}$ [HPGe] [224]	$\geq2.2\times10^{18}$ [HPGe] [224]
			2ϵ (2^+ 2080.1)	$\geq2.8\times10^{18}$ [HPGe] [224]	$\geq2.6\times10^{18}$ [HPGe] [224]
			2ϵ (2^+ 2128.9)	$\geq1.4\times10^{18}$ [HPGe] [224]	$\geq1.6\times10^{18}$ [HPGe] [224]
			2ϵ (0^+ 2141.4)	$\geq4.4\times10^{18}$ [HPGe] [224]	$\geq4.2\times10^{18}$ [HPGe] [224]
			2ϵ ($(2)^+$ 2222.7)	$\geq2.0\times10^{18}$ [HPGe] [224]	$\geq2.0\times10^{18}$ [HPGe] [224]
			2ϵ (0^+ 2315.3)	$\geq2.5\times10^{18}$ [HPGe] [224]	$\geq2.5\times10^{18}$ [HPGe] [224]
			$\epsilon\beta^+$	$\geq2.7\times10^{18}$ (a) [HPGe] [224]	$\geq2.6\times10^{18}$ [HPGe] [224]
			$\epsilon\beta^+$ (2^+ 818.5)	$\geq2.4\times10^{18}$ [HPGe] [224]	$\geq2.3\times10^{18}$ [HPGe] [224]
			$2\beta^+$	$\geq4.1\times10^{18}$ [HPGe] [224]	$\geq4.1\times10^{18}$ [HPGe] [224]
^{144}Sm → ^{144}Nd †	1782.4(8)	3.08(4)	KK/KL/LL	–	$\geq(4.4/1.7/1.4)\times10^{19}$ [HPGe] [56]
			KK (2^+ 696.6)	$\geq1.6\times10^{19}$ [HPGe] [56]	$\geq1.4\times10^{19}$ [HPGe] [56]
			KK (2^+ 1560.9)	$\geq1.3\times10^{19}$ [HPGe] [56]	$\geq1.3\times10^{20}$ [HPGe] [56]
			$\epsilon\beta^+$	$\geq3.6\times10^{19}$ [HPGe] [56]	$\geq3.5\times10^{20}$ [HPGe] [56]
			$\epsilon\beta^+$ (2^+ 696.6)	$\geq3.2\times10^{19}$ [HPGe] [56]	$\geq3.2\times10^{20}$ [HPGe] [56]
^{152}Gd † → ^{152}Sm †	55.69(18)	0.20(3)	2ϵ	$\geq6.0\times10^{8}$ (b,c) [GEO] [229]	
^{156}Dy † → ^{156}Gd †	2005.95(10)	0.056(3)	KK/KL/LL	$\geq6.1\times10^{14}$ [HPGe] [230]	$\geq(1.7/1.7/2.2)\times10^{16}$ [HPGe] [230]
			2ϵ (2^+ 89.0)	$\geq1.8\times10^{14}$ [HPGe] [230]	$\geq1.5\times10^{14}$ [HPGe] [230]
			2ϵ (0^+ 1049.5)	$\geq7.1\times10^{16}$ [HPGe] [230]	$\geq6.4\times10^{16}$ [HPGe] [230]
			2ϵ (2^+ 1129.4)	$\geq1.4\times10^{16}$ [HPGe] [230]	$\geq1.4\times10^{16}$ [HPGe] [230]
			2ϵ (2^+ 1154.2)	$\geq4.7\times10^{15}$ [HPGe] [230]	$\geq4.1\times10^{15}$ [HPGe] [230]
			2ϵ (0^+ 1168.2)	$\geq8.9\times10^{15}$ [HPGe] [230]	$\geq8.0\times10^{15}$ [HPGe] [230]
			2ϵ (0^+ 1715.2)	$\geq3.0\times10^{16}$ [HPGe] [230]	$\geq2.8\times10^{16}$ [HPGe] [230]
			2ϵ (2^+ 1771.1)	$\geq1.0\times10^{16}$ [HPGe] [230]	$\geq8.9\times10^{15}$ [HPGe] [230]
			2ϵ (2^+ 1827.8)	$\geq1.9\times10^{16}$ [HPGe] [230]	$\geq1.9\times10^{16}$ [HPGe] [230]
			2ϵ (0^+ 1851.3)	$\geq1.5\times10^{15}$ [HPGe] [230]	$\geq1.5\times10^{16}$ [HPGe] [230]
			KK (2^+ 1914.8) (d)	$\geq1.1\times10^{16}$ (c) [HPGe] [230]	
			KL_1 (1^- 1946.4) (d)	$\geq0.96\times10^{16}$ (c) [HPGe] [230]	$\geq1.8\times10^{18}$ [HPGe] [231]
			KL_1 (0^+ 1952.4) (d)	$\geq2.6\times10^{16}$ (c) [HPGe] [230]	$\geq2.2\times10^{17}$ [HPGe] [231]
			$2L_1$ (2^+ 1988.5) (d)	$\geq1.9\times10^{16}$ (c) [HPGe] [230]	$\geq9.5\times10^{17}$ [HPGe] [231]
			$2L_3$ (2^+ 2003.7) (d)	$\geq2.8\times10^{14}$ [HPGe] [230]	$\geq6.7\times10^{16}$ [HPGe] [231]
			$\epsilon\beta^+$	$\geq1.9\times10^{16}$ (c) [HPGe] [230]	
			$\epsilon\beta^+$ (2^+ 89.0)	$\geq1.9\times10^{16}$ (c) [HPGe] [230]	

(†) The nucleus is unstable with respect to the α decay [78]. (a) The limit obtained in Reference [224] is erroneously swapped with the limit of Reference [223]. (b) The limit takes all possible processes into account. (c) $0\nu+2\nu$ double beta decay. (d) Resonant effect.

3.3. Experiments Based on the "Source ≠ Detector" Approach

Despite the numerous efforts to implement the "source=detector" approach, since it also offers a good detection efficiency, several DBD+ emitters can be investigated by the passive source method. The isotopes that were studied by this technique, with the best performance in terms of half-life for different DBD+ transitions, are: ^{50}Cr, ^{54}Fe, ^{58}Ni, ^{74}Se, ^{92}Mo, ^{96}Ru, ^{102}Pd, ^{112}Sn, ^{120}Te, ^{136}Ce, ^{138}Ce, ^{144}Sm, ^{156}Dy, ^{158}Dy, ^{162}Er, ^{168}Yb, ^{174}Hf, ^{184}Os, ^{190}Pt, and ^{196}Hg.

The most adopted passive-source experiments use the HPGe γ spectrometers, as shown in Tables 4–6. The DAMA-INR Kyiv collaboration holds the most stringent limits for mostly all of the isotopes investigated by this technique. Thus, in this Section, we briefly summarize the measurements that were carried out by the HPGe γ spectrometers at the STELLA facility of LNGS [232] by the DAMA-INR Kyiv collaboration (also see [42,59] and the References therein).

Table 5. The present best half-lives limits on 2ν and 0ν DBD+ in ^{36}Ar, ^{50}Cr, ^{54}Fe, ^{58}Ni, ^{74}Se, ^{96}Ru, ^{102}Pd, and ^{112}Sn mainly achieved using the passive source approach (if not specified, the C.L. is at 90%). In the square brackets, the detector adopted is reported: High Pure Germanium detector (HPGe). A few other best limits for transitions using such approach are also listed in Tables 1–4 and 6.

Transition	$Q_{\beta\beta}$ (keV) [165]	Natural Abundance (%) [167]	Process	$T_{1/2}$ (yr)	
				2ν	0ν
^{36}Ar $\rightarrow$ ^{36}Se	432.58(19)	0.3336(210)	2ϵ	–	$\geq 3.6 \times 10^{21}$ [HPGe] [233]
^{50}Cr $\rightarrow$ ^{50}Ti	1169.6(5)	4.345(13)	2ϵ	$\geq 1.8 \times 10^{17}$ (68%)(a) [HPGe] [234]	
			$\epsilon\beta^+$	$\geq 1.3 \times 10^{18}$ (95%)(a) [HPGe] [235]	
^{54}Fe $\rightarrow$ ^{54}Cr	680.3(4)	5.845(105)	KK/KL/LL	–	$\geq (4.4/4.1/5.0) \times 10^{20}$ (68%) [HPGe] [236]
^{58}Ni $\rightarrow$ ^{58}Fe	1926.4(3)	68.0769(100)	2ϵ	–	$\geq 4.1 \times 10^{22}$(b) [HPGe] [237]
			2ϵ (2^+_1, 810.8)	$\geq 3.3 \times 10^{22}$ [HPGe] [237]	–
			2ϵ (2^+_2, 1674.7)	$\geq 3.4 \times 10^{22}$ [HPGe] [237]	–
			$\epsilon\beta^+$	$\geq 1.7 \times 10^{22}$ [HPGe] [237]	–
			$\epsilon\beta^+$ (2^+_1, 810.8)	$\geq 2.3 \times 10^{22}$ [HPGe] [237]	–
^{74}Se $\rightarrow$ ^{74}Ge	1209.24(1)	0.86(3)	2ϵ	$\geq 1.5 \times 10^{19}$ (a) [HPGe] [238]	
			KK/KL/LL	–	$\geq (4.83/3.48/6.47) \times 10^{19}$ [HPGe] [239]
			KK/KL/LL (2^+_1, 595.9)	$\geq 1.83 \times 10^{19}$ [HPGe] [239]	$\geq (1.57/4.37/4.58) \times 10^{19}$ [HPGe] [239]
			2ϵ (2^+_2, 1204.2)	$\geq 4.3 \times 10^{19}$ (a,c) [HPGe] [240]	$\geq 1.10 \times 10^{19}$ [HPGe] [239]
			$\epsilon\beta^+$	$\geq 2.3 \times 10^{19}$ (a) [HPGe] [239]	
^{96}Ru $\rightarrow$ ^{96}Mo	2714.50(12)	5.54(14)	KK/KL/LL	–	$\geq (10/2.3/2.3) \times 10^{20}$ [HPGe] [241]
			KL (b)/LL (b)	–	$\geq (2.0/3.6) \times 10^{20}$ [HPGe] [241]
			2ϵ (2^+ 778.2)	$\geq 2.6 \times 10^{20}$ [HPGe] [241]	$\geq 2.4 \times 10^{20}$ [HPGe] [241]
			2ϵ (0^+ 1148.1)	$\geq 2.5 \times 10^{20}$ [HPGe] [241]	$\geq 2.3 \times 10^{20}$ [HPGe] [241]
			2ϵ (2^+ 1497.8)	$\geq 1.7 \times 10^{20}$ [HPGe] [241]	$\geq 1.6 \times 10^{20}$ [HPGe] [241]
			2ϵ (2^+ 1625.9)	$\geq 3.6 \times 10^{20}$ [HPGe] [241]	$\geq 3.3 \times 10^{20}$ [HPGe] [241]
			2ϵ (2^+ 2095.7)	$\geq 2.4 \times 10^{20}$ [HPGe] [241]	$\geq 2.2 \times 10^{20}$ [HPGe] [241]
			2ϵ (2^+ 2426.1)	$\geq 2.1 \times 10^{20}$ [HPGe] [241]	$\geq 2.1 \times 10^{20}$ [HPGe] [241]
			2ϵ ($(0)^+$ 2622.5)	$\geq 2.4 \times 10^{20}$ [HPGe] [241]	$\geq 2.4 \times 10^{20}$ [HPGe] [241]
			$\epsilon\beta^+$	$\geq 8.0 \times 10^{19}$ [HPGe] [241]	$\geq 7.7 \times 10^{19}$ [HPGe] [241]
			2ϵ (2^+ 778.2)	$\geq 2.3 \times 10^{19}$ [HPGe] [241]	$\geq 2.3 \times 10^{19}$ [HPGe] [241]
			2ϵ (0^+ 1148.1)	$\geq 2.1 \times 10^{19}$ [HPGe] [241]	$\geq 2.1 \times 10^{19}$ [HPGe] [241]
			2ϵ (2^+ 1497.8)	$\geq 1.5 \times 10^{19}$ [HPGe] [241]	$\geq 1.5 \times 10^{19}$ [HPGe] [241]
			2ϵ (2^+ 1625.9)	$\geq 3.1 \times 10^{19}$ [HPGe] [241]	$\geq 3.1 \times 10^{19}$ [HPGe] [241]
			$2\beta^+$	$\geq 1.4 \times 10^{20}$ [HPGe] [241]	$\geq 1.3 \times 10^{20}$ [HPGe] [241]
^{102}Pd $\rightarrow$ ^{102}Ru	1203.3(4)	1.02(1)	2ϵ	–	–
			2ϵ (2^+_1, 475.1)	$\geq 7.6 \times 10^{18}$(a) [HPGe] [242]	
			2ϵ (0^+_1, 943.7)	$\geq 8.8 \times 10^{18}$(a) [HPGe] [242]	
			2ϵ (2^+_2, 1103.0)	$\geq 1.4 \times 10^{19}$(a) [HPGe] [242]	
			$\epsilon\beta^+$	–	–
			$\epsilon\beta^+$ (2^+_1, 475.1)	$\geq 7.6 \times 10^{18}$(a) [HPGe] [242]	
^{112}Sn $\rightarrow$ ^{112}Cd	1919.80(16)	0.97(1)	KK/KL/LL	–	$\geq (10.63/8.15/6.43) \times 10^{20}$ [HPGe] [243]
			2ϵ (2^+_1 617.5)	$\geq 11.94 \times 10^{20}$ [HPGe] [243]	$\geq 9.72 \times 10^{20}$ [HPGe] [243]
			2ϵ (0^+_1 1224.3)	$\geq 16.25 \times 10^{20}$ [HPGe] [243]	$\geq 12.86 \times 10^{20}$ [HPGe] [243]
			2ϵ (2^+_2 1312.4)	$\geq 11.24 \times 10^{20}$ [HPGe] [243]	$\geq 8.89 \times 10^{20}$ [HPGe] [243]
			2ϵ (4^+_1 1415.5)	$\geq 9.57 \times 10^{20}$ [HPGe] [243]	$\geq 7.46 \times 10^{20}$ [HPGe] [243]
			2ϵ (0^+_2 1433.3)	$\geq 8.64 \times 10^{20}$ [HPGe] [243]	$\geq 6.86 \times 10^{20}$ [HPGe] [243]
			2ϵ (2^+_3 1468.8)	$\geq 8.19 \times 10^{20}$ [HPGe] [243]	$\geq 6.46 \times 10^{20}$ [HPGe] [243]
			2ϵ (4^+_2 1870.7)	$\geq 11.03 \times 10^{20}$ [HPGe] [243]	$\geq 11.03 \times 10^{20}$ [HPGe] [243]
			2ϵ (0^+_3 1871.0)	$\geq 13.43 \times 10^{20}$ [HPGe] [243]	$\geq 13.43 \times 10^{20}$ [HPGe] [243]
			$\epsilon\beta^+$	$\geq 9.7 \times 10^{19}$ (a) [HPGe] [243]	
			$\epsilon\beta^+$ (2^+_1 617.5)	$\geq 7.02 \times 10^{20}$ (a) [HPGe] [243]	

(a) $0\nu + 2\nu$ double beta decay. (b) Resonant effect. (c) The value quoted in Reference [240] for the 2ϵ (2^+_2, 1204.2) transition was re-evaluated in Reference [244] with $T_{1/2} \geq 1.4 \times 10^{18}$ yr, and it further decreased to $T_{1/2} \geq 3.9 \times 10^{16}$ yr in Reference [245], as reported in [19]. Recently, a new upper limit at $T_{1/2} \geq 1.10 \times 10^{19}$ was reported in [239].

HPGe detectors can offer high performances in the measurements on samples at very low radioactivity levels, being typically down to the μBq kg^{-1}. The usual experimental approach consists of two phases: in the first one, the sample (source) can be purified at different stages to decease the background for the effect searched for; then, the DBD+ measurements can be done. Examples of purification technique include the evaporation of the impurities from the melted sample, the sedimentation, the liquid-liquid extraction, or, if possible, their combination. However, the protocol is strictly isotope/sample dependent. Some details regarding the different adopted/developed purifications and protocols can be found in [62,224,241,246] and the references therein. Besides this, the material contamination can also be investigated by Inductively Coupled Plasma-Mass Spectrometry [247], especially to evaluate the radio-isotopes concentration in the case their decay is not accom-

panied with a γ emission. For example, present studies on the purification protocol for Gd_2O_3 are in progress at the STELLA facility of LNGS [232], due to the great interest in the DBD+ of ^{152}Gd (and DBD- of ^{160}Gd). There is also great interest in the development of purification techniques for lanthanide's and rare-earth nuclides [57,62,230,247–249].

Table 6. The best half-lives limits on 2ν and 0ν DBD+ in ^{158}Dy, ^{162}Er, ^{164}Er, ^{168}Yb, ^{174}Hf, ^{184}Os, ^{190}Pt, and ^{196}Hg mainly achieved using the passive source approach (if not specified, the C.L. is at 90%). In the square brackets, the adopted detector is reported, where HPGe means High Pure Germanium detector and GEO means the Geochemical method. A few other best limits for transitions using such approach are also listed in Tables 1–4.

Transition	$Q_{\beta\beta}$ (keV) [165]	Natural Abundance (%) [167]	Process	$T_{1/2}$ (yr)	
				2ν	0ν
^{158}Dy † → ^{158}Gd	282.2(24)	0.095(3)	KK	$\geq 1.0 \times 10^{15}$ [HPGe] [230]	$\geq 4.2 \times 10^{16}$ [HPGe] [230]
			2ϵ (2^+ 79.5)	$\geq 3.5 \times 10^{14}$ [HPGe] [230]	$\geq 2.6 \times 10^{14}$ [HPGe] [230]
			$2L_1$ (4^+ 261.5) (a)	$\geq 3.2 \times 10^{16}$ (b) [HPGe] [230]	
^{162}Er † → ^{162}Dy †	1846.96(30)	0.139(5)	KK/KL/LL	$\geq (3.2/-/-) \times 10^{15}$ [HPGe] [62]	$\geq (10/9.6/13) \times 10^{17}$ [HPGe] [62]
			2ϵ (2^+ 80.7)	$\geq 1.2 \times 10^{16}$ [HPGe] [62]	–
			2ϵ (2^+ 888.2)	$\geq 4.2 \times 10^{17}$ [HPGe] [62]	–
			2ϵ (0^+ 1400.3)	$\geq 1.3 \times 10^{18}$ [HPGe] [62]	–
			2ϵ (2^+ 1453.5)	$\geq 3.1 \times 10^{17}$ [HPGe] [62]	–
			2ϵ (0^+ 1666.3)	$\geq 7.7 \times 10^{17}$ [HPGe] [62]	–
			2ϵ (2^+ 1728.3)	$\geq 9.4 \times 10^{17}$ [HPGe] [62]	–
			KL (2^+ 1782.7)	$\geq 5.0 \times 10^{17}$ [HPGe] [62]	–
			KK (2^+ 80.7)	–	$\geq 6.2 \times 10^{17}$ [HPGe] [62]
			KK (2^+ 888.2)	–	$\geq 5.9 \times 10^{17}$ [HPGe] [62]
			KK (0^+ 1400.3)	–	$\geq 1.3 \times 10^{18}$ [HPGe] [62]
			KK (2^+ 1453.5)	–	$\geq 9.1 \times 10^{17}$ [HPGe] [62]
			KK (0^+ 1666.3)	–	$\geq 7.7 \times 10^{17}$ [HPGe] [62]
			KK (2^+ 1728.3)	–	$\geq 9.3 \times 10^{17}$ [HPGe] [62]
			KL_1 (a) (2^+ 1782.7)	–	$\geq 5.0 \times 10^{17}$ [HPGe] [62]
			$\epsilon\beta^+$	$\geq 3.8 \times 10^{17}$ [HPGe] [62]	$\geq 3.7 \times 10^{17}$ [HPGe] [62]
			$\epsilon\beta^+$ (2^+ 80.7)	$\geq 3.8 \times 10^{17}$ [HPGe] [62]	$\geq 3.7 \times 10^{17}$ [HPGe] [62]
^{164}Er † → ^{164}Dy	25.08(11)	1.601(3)	2ϵ	$\geq 1.0 \times 10^{9}$(b,c) [GEO] [229]	
^{168}Yb † → ^{168}Er †	1409.27(25)	0.123(3)	KK/KL/LL	$\geq (8.7, -, -) \times 10^{13}$ [HPGe] [57]	$\geq (7.3/6.9/12) \times 10^{17}$ [HPGe] [57]
			2ϵ (2^+ 78.8)	$\geq 2.3 \times 10^{15}$ [HPGe] [57]	$\geq 4.4 \times 10^{14}$ [HPGe] [57]
			2ϵ (2^+ 821.2)	$\geq 4.4 \times 10^{17}$ [HPGe] [57]	$\geq 3.9 \times 10^{17}$ [HPGe] [57]
			2ϵ (0^+ 1217.2)	$\geq 1.5 \times 10^{18}$ [HPGe] [57]	$\geq 1.5 \times 10^{18}$ [HPGe] [57]
			2ϵ (2^+ 1276.3)	$\geq 8.6 \times 10^{17}$ [HPGe] [57]	$\geq 8.6 \times 10^{17}$ [HPGe] [57]
			M_1M_1 ($(2)^-$ 1403.7) (a)	–	$\geq 1.9 \times 10^{18}$ [HPGe] [57]
			$\epsilon\beta^+$	$\geq 2.8 \times 10^{17}$ [HPGe] [57]	$\geq 2.8 \times 10^{17}$ [HPGe] [57]
			$\epsilon\beta^+$ (2^+ 78.8)	$\geq 2.8 \times 10^{17}$ [HPGe] [57]	$\geq 2.8 \times 10^{17}$ [HPGe] [57]
^{174}Hf † → ^{174}Yb †	1100.0(23)	0.16(12)	KK/KL/LL	$\geq (7.1/4.2/-) \times 10^{16}$ [HPGe] [250]	$\geq (5.8/19/7.8) \times 10^{17}$ [HPGe] [250]
			KK/KL/LL (2^+ 76.5)	$\geq (5.9/3.5/3.9) \times 10^{16}$ [HPGe] [250]	$\geq (7.1/6.2/7.2) \times 10^{17}$ [HPGe] [250]
			$K\beta^+$	$\geq 1.4 \times 10^{16}$(b) [HPGe] [250]	
			$L\beta^+$	$\geq 1.4 \times 10^{16}$(b) [HPGe] [250]	
^{184}Os † → ^{184}W †	1452.8(7)	0.02(2)	KK/KL/LL	$\geq (3.0/2.0/-) \times 10^{16}$ [HPGe] [251]	$\geq (2.0/1.3/1.4) \times 10^{17}$ [HPGe] [252]
			KK/KL/2ϵ (2^+ 112.2)	$\geq (3.6/2.4/0.73) \times 10^{16}$ [HPGe] [251]	$\geq (3.3/0.19/-) \times 10^{17}$ [HPGe] [251,252]
			2ϵ (2^+ 903.3)	$\geq 2.0 \times 10^{17}$ [HPGe] [251]	$\geq 1.7 \times 10^{17}$ [HPGe] [251]
			2ϵ (0^+ 1002.5)	$\geq 3.8 \times 10^{17}$ [HPGe] [252]	$\geq 3.5 \times 10^{17}$ [HPGe] [252]
			2ϵ (2^+ 1121.5)	$\geq 1.0 \times 10^{17}$ [HPGe] [251]	$\geq 9.4 \times 10^{16}$ [HPGe] [251]
			KK ($(0)^+$ 1322.2)	$\geq 1.7 \times 10^{17}$ [HPGe] [251]	$\geq 1.7 \times 10^{17}$ (a) [HPGe] [251]
			KL (2^+ 1386.3)	$\geq 3.0 \times 10^{16}$ [HPGe] [251]	$\geq 6.7 \times 10^{16}$ (a) [HPGe] [252]
			LL ($(3)^+$ 1425.0)	$\geq 8.4 \times 10^{16}$ [HPGe] [251]	$\geq 8.4 \times 10^{16}$ [HPGe] [251]
			LL (2^+ 1431.0)	$\geq 4.4 \times 10^{16}$ [HPGe] [251]	$\geq 8.2 \times 10^{16}$ (a) [HPGe] [252]
			$\epsilon\beta^+$ (2^+ 112.2)	$\geq 1.0 \times 10^{17}$ [HPGe] [251]	$\geq 1.0 \times 10^{17}$ [HPGe] [251]
			$\epsilon\beta^+$ (2^+ 112.2)	$\geq 1.0 \times 10^{17}$ [HPGe] [251]	$\geq 9.9 \times 10^{16}$ [HPGe] [251]
^{190}Pt † → ^{190}Os †	1401.3(4)	0.012(2)	KK/KL/LL	$\geq (8.4, -, -) \times 10^{14}$ [HPGe] [253]	$\geq (5.7/17/31) \times 10^{15}$ [HPGe] [253]
			KK (2^+ 186.7)	$\geq 8.8 \times 10^{14}$ [HPGe] [253]	–
			KK (2^+ 558.0)	$\geq 5.6 \times 10^{15}$ [HPGe] [253]	–
			KK (0^+ 911.8)	$\geq 4.5 \times 10^{15}$ [HPGe] [253]	–
			KK (2^+ 1114.7)	$\geq 1.0 \times 10^{16}$ [HPGe] [253]	–
			2ϵ (2^+ 186.7)	–	$\geq 6.9 \times 10^{14}$ [HPGe] [253]
			2ϵ (2^+ 558.0)	–	$\geq 4.5 \times 10^{15}$ [HPGe] [253]
			2ϵ (0^+ 911.8)	–	$\geq 3.6 \times 10^{15}$ [HPGe] [253]
			2ϵ (2^+ 1114.7)	–	$\geq 9.8 \times 10^{15}$ [HPGe] [253]
			MM/MN/NN (0, 1, 2^+ 1382.4) (a)	$\geq 2.9 \times 10^{16}$(b) [HPGe] [253]	
			$\epsilon\beta^+$	$\geq 9.2 \times 10^{15}$ [HPGe] [253]	$\geq 9.0 \times 10^{15}$ [HPGe] [253]
			$\epsilon\beta^+$ (2^+ 186.7)	$\geq 8.4 \times 10^{15}$(b) [HPGe] [253]	
^{196}Hg † → ^{196}Pt †	818.6(30)	0.15(1)	KK	–	$\geq 9.6 \times 10^{17}$ [HPGe] [254]
			KK (2^+ 355.7)	$\geq 2.5 \times 10^{18}$(b) [HPGe)] [254]	

(†) The nucleus is unstable with respect to the α decay [49,51,78]. (a) Resonant effect. (b) $0\nu + 2\nu$ double beta decay. (c) The limit takes in account all the possible processes.

The experimental set-ups, in the STELLA facility of LNGS [232], are placed in an air-tight poly-methyl-methacrylate box and then flushed with high purity nitrogen gas to remove the environmental radon (some set-ups are also covered by borated polyethylene

of ≈10 cm). Inside this box, the detectors are surrounded by a passive shield made of low radioactivity copper (5–10 cm) and low radioactivity lead (20–25 cm). The samples are typically enclosed in a polystyrene box on the HPGe detector end-cap. The most commonly used HPGe detectors are: (i) GeCris, it is a 465 cm^3 with 120 % relative efficiency with respect to a 3″ × 3″ sodium iodine detector [232]. (ii) GeMulti, it is made of four HPGe detectors inside the same cryostat with ∼225 cm^3 volume each one. (iii) GeBer with a 244 cm^3 volume. The typical energy resolution of the detectors is 2.0 keV at the 1332.5 keV γ peak of ^{60}Co. Other HPGe detectors are also used for radio-purity measurements [232]. The detection efficiencies of the DBD+ that are searched for are estimated while using dedicated Monte-Carlo simulations: EGSnrc [255] and GEANT4 toolkits [161,162], with initial kinematics being provided by the DECAY0 event generator [163,164].

Thanks to these efforts, the DAMA and DAMA-INR Kyiv collaborations have obtained samples with very high-purity levels and high sensitivities to many DBD+ transitions with levels up to 10^{21} yr (see Tables 4–6), even with small-scale experiments. In particular, as an example, Figure 13 shows the results of the first direct search for 2ϵ and $\epsilon\beta^+$ of ^{144}Sm to the ground state and the excited levels of ^{144}Nd [56]. The experiment was realized by measuring—over 1899 h—a 342 g sample of highly purified samarium oxide (Sm_2O_3) with the ultra-low background HPGe γ spectrometer GeCris. No effect was observed, and the half-life limits were estimated at the level of $T_{1/2} \sim (0.1–3.6) \times 10^{20}$ yr (90% C.L.) (see Table 4).

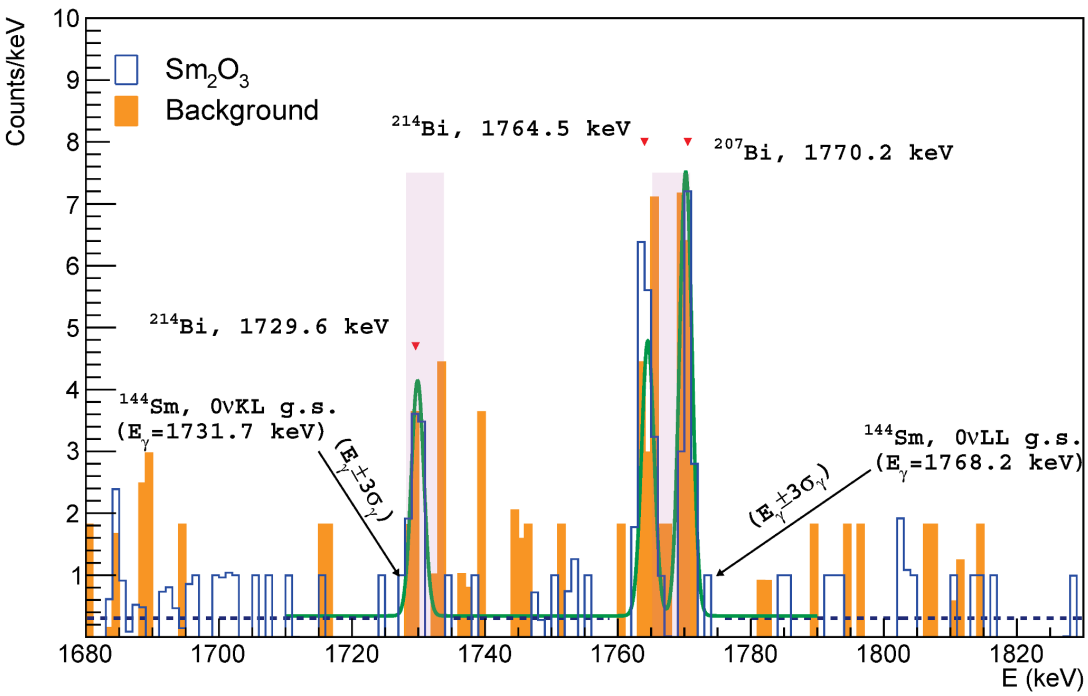

Figure 13. An example: part of the energy spectrum accumulated with a Sm_2O_3 sample of 342 g over 1899 h [56], where the γ peaks from the $0\nu KL$ and $0\nu LL$ processes in ^{144}Sm to the ^{144}Nd g.s. are expected. The fit (green on-line line) of the background data (a straight line plus the 1729.6 keV and 1764.5 keV Gaussian γ peaks from ^{214}Bi and 1770.2 keV peak from ^{207}Bi) is shown [56]. The constant fit (dashed blue on-line) of the data with the Sm_2O_3 6σ far from the mentioned γ lines of ^{214}Bi and ^{207}Bi is also reported. The boxes (transparent pink on-line) indicate the energy range ($E_\gamma \pm 3\sigma_\gamma$) expected for the $0\nu KL$ and $0\nu 2L$ decay processes to the g.s. of ^{144}Nd in the energy spectra that were measured with Sm_2O_3 sample [56]. Reprinted from Reference [56].

4. Perspectives and Conclusions

The current interest and status of the experimental searches for DBD+ to the ground state and excited states of daughter nuclei have been outlined. An introduction regarding the theoretical aspect and interests to the DBD+ studies has been addressed. The great

interest in the field is clearly evident: it is aimed at studying the important nuclear processes predicted from the SM or its extensions; crucial theoretical tests can be inferred. Moreover, very important complementary information in nuclear and interaction theoretical models can be achieved with respect to the DBD- modes (as widely discussed in Section 1). The case of 0ν mode involves the neutrino mass and new specific theoretical scenarios; but, in some models, one can consider the 2ν nuclear matrix element as a test case for the 0ν modes, which is crucial in studying, as much as possible, all of the DBD+ emitters. Another relevant aspect, concerning the 0ν modes, is that the mutual information from the contemporary study of positive and negative DBD can strongly constrain the theoretical parameters with very high confidence (as discussed in Section 1). In addition, a remarkable new effect is the possible so-called "resonant effect" on the $0\nu 2\epsilon$ decay, if the initial and final states are energetically degenerate. Besides this, continuous efforts in this field push an evident progression in new or more performing detectors, which can also be profitable in many other fields. Thus, the experimental methods that are used in the field and the status of art have been summarized. Some claims, which are present in literature, have been reviewed. Many other experimental results using different detector types, sizes, and materials have been discussed.

In the future, improvements in the purification protocol, growing materials, and new detector concept can strongly increase the experimental sensitivity on DBD+ transitions. In particular, dedicated efforts are enlarging the number of DBD+ emitters that can be studied using the "source=detector" approach. In fact, among the other existing efforts (such as, e.g., attempts to use crystal bolometers), the DAMA-INR Kyiv collaboration works to purify several compounds aiming at improving the sensitivity in the passive source approach and enhancing the growing procedure of crystal scintillators with the DBD+ emitters.

Moreover, some positive claims on 2ν DBD+ need further experimental investigation. Some other DBD+ emitters are poorly investigated, such as ^{152}Gd and ^{164}Er. Thus, these latter deficits push the experimentalists to improve new related detectors and methods. In addition, the sensitivity that is reached for a few 2νDBD+ emitters is in the range of theoretical expectations (as some DBD+ transition in ^{106}Cd), which could allow their observations.

Author Contributions: All the authors of this paper have been significantly contributing to the presented review of experimental results. All authors have read and agreed to the published version of the manuscript.

Funding: This research received no external funding.

Acknowledgments: It is a pleasure to thank all our collaborators in the searches on related fields.

Conflicts of Interest: The authors declare no conflict of interest.

References

1. Weizsäcker, C.F. Zur Theorie der Kernmassen. *Z. Phys.* **1935**, *96*, 431. [CrossRef]
2. Goeppert-Mayer, M. Double Beta-Disintegration. *Phys. Rev.* **1935**, *48*, 512. [CrossRef]
3. Suhonen, J.; Civitarese, O. Weak-interaction and nuclear-structure aspects of nuclear double beta decay. *Phys. Rep.* **1998**, *300*, 123–214. [CrossRef]
4. Mohapatra, R.N. New contributions to neutrinoless double-beta decay in supersymmetric theories. *Phys. Rev. D* **1986**, *34*, 3457–3461. [CrossRef]
5. Babu, K.S.; Mohapatra, R.N. New Vector-Scalar contributions to neutrinoless double beta decay and constraints on R-parity violation. *Phys. Rev. Lett.* **1995**, *75*, 2276–2279. [CrossRef] [PubMed]
6. Faessler, A.; Gutsche, T.; Kovalenko, S.; Šimkovic, F. Pion dominance in R-parity violating supersymmetry induced neutrinoless double beta decay. *Phys. Rev. D* **2008**, *77*, 113012. [CrossRef]
7. Vergados, J.D. Pion-double-charge-exchange contribution to neutrinoless double-decay. *Phys. Rev. D* **1982**, *25*, 914–917. [CrossRef]
8. Hirsch, M.; Klapdor-Kleingrothaus, H.V.; Kovalenko, S.G. New contributions to supersymmetric mechanism of neutrinoless double beta decay. *Phys. Lett. B* **1995**, *352*, 1–7. [CrossRef]
9. Frank, M.; Majumdar, C.; Poulose, P.; Senapati, S.; Yajnik, U.A. Exploring $0\nu\beta\beta$ and leptogenesis in the alternative left-right model. *Phys. Rev. D* **2020**, *102*, 075020. [CrossRef]

10. Mitra, M.; Senjanović, G.; Vissani, F. Neutrinoless double beta decay and heavy sterile neutrinos. *Nucl. Phys. B* **2012**, *856*, 26–73. [CrossRef]
11. Masaru Doi, M.; Kotani, T.; Takasugi, E. Double beta decay and Majorana neutrino. *Prog. Theo. Phys. Supp.* **1985**, *83*, 1–175.
12. Zyla, P.A.; Barnett, R.M.; Beringer, J.; Dahl, O.; Dwyer, D.A.; Groom, D.E.; Lin, C.J.; Lugovsky, K.S.; Pianori, E.; Robinson, D.J.; et al. Review of Particle Physics. *Prog. Theor. Exp. Phys.* **2020**, *8*, 083C01. [CrossRef]
13. Hirsch, H. Calculation of double beta plus decay matrix elements. *Nulc. Phys. A* **1994**, *557*, 411c–414c. [CrossRef]
14. Tretyak, V.I.; Zdesenko, Y.G. Tables of double beta decay data: An update. *Atom. Data Nucl. Data Tabl.* **2020**, *80*, 83–116. [CrossRef]
15. Maalampi, J.; Suhonen, J. Neutrinoless Double β^+/EC Decays. *Adv. High Energy Phys.* **2013**, *2013*, 505874. [CrossRef]
16. Winter, R.G. Double K capture and single K capture with positron emission. *Phys. Rev.* **1955**, *100*, 142–144. [CrossRef]
17. Voloshin, M.B.; Mitselmakher, G.V.; Eramzhyan, R.A. Conversion of an atomic electron into a positron and double β^+ decay. *JETP Lett.* **1982**, *35*, 656–659.
18. Bernabeu, J.; De Rujula, A.; Jarlskog, C. Neutrinoless double electron capture as a tool to measure the electron neutrino mass. *Nucl. Phys. B* **1983**, *223*, 15–28. [CrossRef]
19. Blaum, K.; Eliseev, S.; Danevich, F.A.; Tretyak, V.I.; Kovalenko, S.; Krivoruchenko, M.I.; Novikov, Y.N.; Suhonen, J. Neutrinoless double-electron capture. *Rev. Mod. Phys.* **2020**, *92*, 045007. [CrossRef]
20. Krivoruchenko, M.I.; Šimkovic, F.; Frekers, D.; Faessler, D. Resonance enhancement of neutrinoless double electron capture. *Nucl. Phys. A* **2011**, *859*, 140. [CrossRef]
21. Georgi, H.M.; Glashow, S.L.; Nussinov, S. Unconventional model of neutrino masses. *Nucl. Phys. B* **1981**, *193*, 297–316. [CrossRef]
22. Eliseev, S.A.; Novikov, Y.N.; Blaum, K. Search for resonant enhancement of neutrinoless double-electron capture by high-precision Penning-trap mass spectrometry. *J. Phys. G* **2012**, *39*, 124003. [CrossRef]
23. Klapdor-Kleingrothaus, H.V.; Krivosheina, I.V. Nuclear Double Beta Decay, Fundamental Particle Physics, Hot Dark Matter, And Dark Energy. In Proceedings of the 7th International Heidelberg Conference: Dark Matter in Astrophysics and Particle Physics, Christchurch, New Zealand, 18–24 January 2009; pp. 137–169.
24. Kuzmin, V.A.; Rubakov, V.A.; Shaposhnikov, M.E. On anomalous electroweak baryon-number non-conservation in the early universe. *Phys. Lett. B* **1985**, *155*, 36–42. [CrossRef]
25. Barabash, A.S. Possibilities of future double beta decay experiments to investigate inverted and normal ordering region of neutrino mass. *Front. Phys.* **2019**, *6*, 160. [CrossRef]
26. Gando, A.; Gando, Y.; Hachiya, T.; Hayashi, A.; Hayashida, S.; Ikeda, H.; Inoue, K.; Ishidoshiro, K.; Karino, Y.; Koga, M.; et al. Search for Majorana Neutrinos Near the Inverted Mass Hierarchy Region with KamLAND-Zen. *Phys. Rev. Lett.* **2016**, *117*, 082503 [CrossRef]
27. Adams, D.Q.; Alduino, C.; Alfonso, K.; Avignone, F.T.; Azzolini, O.; Bari, G.; Bellini, F.; Benato, G.; Biassoni, M.; Branca, A.; et al. Improved Limit on Neutrinoless Double-Beta Decay in ^{130}Te with CUORE. *Phys. Rev. Lett.* **2020**, *124*, 122501. [CrossRef] [PubMed]
28. Agostini, M.; Araujo, G.R.; Bakalyarov, A.M.; Balata, M.; Barabanov, I.; Baudis, L.; Bauer, C.; Bellotti, E.; Belogurov, S.; Bettini, A.; et al. Final Results of GERDA on the Search for Neutrinoless Double–β Decay. *Phys. Rev. Lett.* **2020**, *125*, 252502. [CrossRef] [PubMed]
29. Arnold, R.; Augier, C.; Baker, J.D.; Barabash, A.S.; Basharina-Freshville, A.; Blondel, S.; Blot, S.; Bongrand, M.; Brudanin, V.; Busto, J.; et al. Results of the search for neutrinoless double-β decay in ^{100}Mo with the NEMO-3 experiment. *Phys. Rev. D* **2015**, *92*, 072011. [CrossRef]
30. Tretyak, V.I.; Barabash, A.S.; Belli, P.; Bernabei, R.; Cappella, F.; Caracciolo, V.; Cerulli, R.; Chernyak, D.M.; Danevich, F.A.; d'Angelo, S.; et al. Aurora experiment: Final results of studies of ^{116}Cd 2β decay with enriched $^{116}CdWO_4$ crystal scintillators. *AIP Conf. Proc.* **2019**, *2165*, 020029.
31. Barabash, A.S.; Belli, P.; Bernabei, R.; Cappella, F.; Caracciolo, V.; Cerulli, R.; Chernyak, D.M.; Danevich, F.A.; d'Angelo, S.; Incicchitti, A.; et al. Final results of the Aurora experiment to study 2β decay of ^{116}Cd with enriched $^{116}CdWO_4$ crystal scintillators. *Phys. Rev. D* **2018**, *98*, 092007. [CrossRef]
32. Abada, A.; Bhattacharyya, G. Impact of CP phases on neutrinoless double beta decay. *Phys. Rev. D* **2003**, *68*, 033004. [CrossRef]
33. Cremonesi, O.; Pavan, M. Challenges in Double Beta Decay. *Adv. High Energy Phys.* **2014**, *2014*, 951432. [CrossRef]
34. Bilenky, S.M.; Giunti, C. Neutrinoless double-beta decay: A probe of physics beyond the Standard Model. *Int. J. Mod. Phys. A* **2015**, *30*, 1530001. [CrossRef]
35. Suhonen, J.T. Value of the axial-vector coupling strength in β and $\beta\beta$ decays: A review. *Front. Phys.* **2017**, *5*, 55. [CrossRef]
36. Beringer, J.; Arguin, J.F.; Barnett, R.M.; Copic, K.; Dahl, O.; Groom, D.E.; Lin, C.J.; Lys, J.; Murayama, H.; Wohl, C.G.; et al. Review of particle physics. *Phys. Rev. D* **2012**, *86*, 010001. [CrossRef]
37. Engel, J.; Menendez, J. Status and future of nuclear matrix elements for neutrinoless double-beta decay: A review. *Rep. Prog. Phys.* **2017**, *80*, 046301. [CrossRef]
38. Suhonen, J. Impact of the quenching of g_A on the sensitivity of $0\nu\beta\beta$ experiments. *Phys. Rev. C* **2017**, *96*, 055501. [CrossRef]
39. Suhonen, J.; Kostensalo J. Double β decay and the axial strength. *Front. Phys.* **2019**, *7*, 00029. [CrossRef]
40. Ejiri, H. Axial-vector weak coupling at medium momentum for astro neutrinos and double beta decays. *J. Phys. G Nucl. Part. Phys.* **2019**, *46*, 125202. [CrossRef]
41. Ejiri, H.; Suhonen, J.; Zuber, K. Neutrino–nuclear responses for astro-neutrinos, single beta decays and double beta decays. *Phys. Rep.* **2019**, *797*, 1–102. [CrossRef]

42. Belli, P.; Bernabei, R.; Cappella, F.; Caracciolo, V.; Cerulli, R.; Incicchitti, A.; Merlo, V. Double beta decay to excited states of daughter nuclei. *Universe* **2020**, *6*, 239. [CrossRef]
43. Ejiri, H.; Elliott, S.R. Charged current neutrino cross section for solar neutrinos, and background to $\beta\beta(0\nu)$ experiments. *Phys. Rev. C* **2014**, *89*, 055501. [CrossRef]
44. Ianni, A. Considerations on Underground Laboratories. *J. Phys. Conf. Ser.* **2020**, *1342*, 012003. [CrossRef]
45. Bernabei, R.; Belli, P.; Montecchia, F.; Di Nicolantonio, W.; Ignesti, G.; Incicchitti, A.; Prosperi, D.; Dai, C.J.; Ding, L.K.; Kuang, H.H.; et al. Performances of the $\simeq$ 100 kg NaI(Tl) set-up of the DAMA experiment at Gran Sasso. *Nuovo Cimento A* **1999**, *112*, 6. [CrossRef]
46. Belli, P.; Bernabei, R.; d'Angelo, S.; De Pascale, M.P.; Paoluzi, L.; Santonico, R.; Taborgna, R.; Iucci, N.; Villoresi, G. Deep Underground Neutron Flux Measurement With Large BF_3 Counters. *Nuovo Cimento A* **1998**, *101*, *959–966*. [CrossRef]
47. Barabash, A.S.; Belli, P.; Bernabei, R.; Borovlev, Y.A.; Cappella, F.; Caracciolo, V.; Cerulli, R.; Danevich, F.A.; Incicchitti, A.; Kobychev, V.V.; et al. Improvement of radiopurity level of enriched $^{116}CdWO_4$ and $ZnWO_4$ crystal scintillators by recrystallization. *Nucl. Instrum. Methods* **2016**, *883*, 77–81. [CrossRef]
48. Belli, P.; Bernabei, R.; Brudanin, V.B.; Cappella, F.; Caracciolo, V.; Cerulli, R.; Danevich, F.A.; Incicchitti, A.; Kasperovych, D.V.; Klavdiinienko, V.R.; et al. Search for Double Beta Decay of ^{106}Cd with an Enriched $^{106}CdWO_4$ Crystal Scintillator in Coincidence with $CdWO_4$ Scintillation Counters. *Universe* **2020**, *6*, 182. [CrossRef]
49. Belli, P.; Bernabei, R.; Cappella, F.; Caracciolo, V.; Cerulli, R.; Danevich, F.A.; Incicchitti, A.; Kasperovych, D.V.; Kobychev, V.V.; Kovtun, G.P.; et al. Search for α decay of naturally occurring osmium nuclides accompanied by γ quanta. *Phys. Rev. C* **2020**, *102*, 024605. [CrossRef]
50. Barabash, A.S.; Belli, P.; Bernabei, R.; Cappella, F.; Caracciolo, V.; Cerulli, R.; Danevich, F.A.; Di Marco, A.; Incicchitti, A.; Kasperovych, D.V.; et al. Low background scintillators to investigate rare processes. *JINST* **2020**, *15*, C07037. [CrossRef]
51. Caracciolo, V.; Nagorny, S.S.; Belli, P.; Bernabei, R.; Cappella, F.; Cerulli, R.; Incicchitti, A.; Laubenstein, M.; Merlo, V.; Nisi, S.; et al. Search for α decay of naturally occurring Hf-nuclides using a Cs_2HfCl_6 scintillator. *Nucl. Phys. A* **2002**, *1002*, 121941. [CrossRef]
52. Belli, P.; Bernabei, R.; Cappella, F.; Caracciolo, V.; Cerulli, R.; Cherubini, N.; Danevich, F.A.; Incicchitti, A.; Kasperovych, D.V.; Merlo, V.; et al. Developments and improvements of radiopure $ZnWO_4$ anisotropic scintillators. *JINST* **2020**, *15*, C05055. [CrossRef]
53. Belli, P.; Bernabei, R.; Cappella, F.; Caracciolo, V.; Cerulli, R.; Danevich, F.; Incicchitti, A.; Kasperovych, D.; Merlo, V.; Polischuk, O.; et al. The Future Role of Inorganic Crystal Scintillators in Dark Matter Investigations. *Instruments* **2021**, *5*, 16. [CrossRef]
54. Polischuk, O.G.; Belli, P.; Bernabei, R.; Brudanin, V.B.; Cappella, F.; Caracciolo, V.; Cerulli, R.; Danevich, F.A.; Incicchitti, A.; Kasperovych, D.V.; et al. New limit on two neutrino electron capture with positron emission in ^{106}Cd. *AIP Conf. Proc.* **2019**, *2165*, 020020.
55. Kasperovych, D.V.; Barabash, A.S.; Belli, P.; Bernabei, R.; Boiko, R.S.; Cappella, F.; Caracciolo, V.; Cerulli, R.; Danevich, F.A.; Di Marco, A.; et al. Study of double-β decay of ^{150}Nd to the first 0^+ excited level of ^{150}Sm. *AIP Conf. Proc.* **2019**, *2165*, 020014.
56. Belli, P.; Bernabei, R.; Boiko, R.S.; Cappella, F.; Caracciolo, V.; Cerulli, R.; Danevich, F.A.; Di Marco, A.; Incicchitti, A.; Kropivyansky, B.N.; et al. First direct search for 2ϵ and $\epsilon\beta^+$ decay of ^{144}Sm and $2\beta^-$ decay of ^{154}Sm. *Eur. Phys. J. A* **2019**, *55*, 201. [CrossRef]
57. Belli, P.; Bernabei, R.; Boiko, R.S.; Cappella, F.; Caracciolo, V.; Cerulli, R.; Danevich, F.A.; di Vacri, M.L.; Incicchitti, A.; Kropivyansky, B.N.; et al. First search for 2ϵ and $\epsilon\beta^+$ processes in ^{168}Yb. *Nucl. Phys. A* **2019**, *990*, 64–78. [CrossRef]
58. Belli, P.; Bernabei, R.; Borovlev, Y.A.; Cappella, F.; Caracciolo, V.; Cerulli, R.; Danevich, F.A.; Incicchitti, A.; Kasperovych, D.V.; Polischuk, O.G.; et al. New development of radiopure $ZnWO_4$ crystal scintillators. *Nucl. Instrum. Methods A* **2019**, *935*, 89–94. [CrossRef]
59. Di Marco, A.; Barabash, A.S.; Belli, P.; Bernabei, R.; Boiko, R.S.; Brudanin, V.B.; Cappella, F.; Caracciolo, V.; Cerulli, R.; Chernyak, D.M.; et al. Recent Developments and Results on Double Beta Decays with Crystal Scintillators and HPGe Spectrometry. *Universe* **2018**, *4*, 147. [CrossRef]
60. Barabash, A.S.; Belli, P.; Bernabei, R.; Boiko, R.S.; Brudanin, V.B.; Cappella, F.; Caracciolo, V.; Cerulli, R.; Chernyak, D.M.; Dai, C.J.; et al. Search for rare processes with DAMA experimental set-ups. *EPJ Web Conf.* **2018**, *182*, 02027. [CrossRef]
61. Barabash, A.S.; Belli, P.; Bernabei, R.; Boiko, R.S.; Cappella, F.; Caracciolo, V.; Cerulli, R.; Danevich, F.A.; Di Marco, A.; Incicchitti, A.; et al. Double beta decay of ^{150}Nd to the first excited 0^+ level of ^{150}Sm: Preliminary results. *Nucl. Phys. Atom. Energy* **2018**, *19*, 95–102. [CrossRef]
62. Belli, P.; Bernabei, R.; Boiko, R.S.; Cappella, F.; Caracciolo, V.; Cerulli, R.; Danevich, F.A.; Incicchitti, A.; Kropivyansky, B.N.; Laubenstein, M.; et al. First search for 2ϵ and $\epsilon\beta^+$ decay of ^{162}Er and new limit on $2\beta^-$ decay of ^{170}Er to the first excited level of ^{170}Yb. *J. Phys. G* **2018**, *45*, 095101. [CrossRef]
63. Barabash, A.S.; Basharina-Freshville, A.; Blot, S.; Bongrand, M.; Bourgeois, C.; Breton, D.; Brudanin, V.; Burešovà, H.; Busto, J.; Caffrey, A.J.; et al. Calorimeter development for the SuperNEMO double beta decay experiment. *Nucl. Instrum. Methods A* **2017**, *868*, 98–108. [CrossRef]
64. Ejiri, H.; Higa, K.; Kamada, T.; Kobiki, H.; Matsuoka, K.; Okada, K.; Sano, H.; Shibata, T.; Shima, T.; Tanabe, N.; et al. The high sensitivity beta-gamma spectrometer ELEGANTS V for rare β(e) and $\beta\beta$(ee) decays. *Nucl. Instrum. Methods A* **1991**, *302*, 304–314. [CrossRef]
65. Zuber, K. COBRA-double beta decay searches using CdTe detectors. *Phys. Lett. B* **2001**, *519*, 1–7. [CrossRef]

66. Ebert, J.; Fritts, M.; Gehre, D.; Gößling, C.; Göpfert, T.; Hagner, C.; Heidrich, N.; Klingenberg, R.; Köttig, T.; Kröninger, C.; et al. The COBRA demonstrator at the LNGS underground laboratory. *Nucl. Instrum. Methods A* **2016**, *807*, 114–120. [CrossRef]
67. Belli, P.; Bernabei, R.; Cerulli, R.; Danevich, F.A.; d'Angelo, A.; Goriletsky, V.I.; Grinyov, B.V.; Incicchitti, A.; Kobychev, V.V.; Laubenstein, M.; et al. ^{7}Li solar axions: Preliminary results and feasibility studies. *Nucl. Phys. A* **2008**, *806*, 388. [CrossRef]
68. Bernabei, R.; Belli, P.; Montecchia, F.; Nozzoli, F.; d'Angelo, A.; Cappella, F.; Incicchitti, A.; Prosperi, D.; Castellano, S.; Cerulli, R.; et al. Search for possible charge non-conserving decay of ^{139}La into ^{139}Ce with $LaCl_3$(Ce) scintillator. *Ukr. J. Phys.* **2006**, *51*, *1037*.
69. Belli, P.; Bernabei, R.; Dai, C.J.; He, H.L.; Ignesti, G.; Incicchitti, A.; Kuang, H.H.; Ma, J.M.; Montecchia, F.; Ponkratenko, O.A.; et al. New experimental limit on the electron stability and non-paulian transitions in iodine atoms. *Phys. Lett. B* **1999**, *460*, 236. [CrossRef]
70. Belli, P.; Bernabei, R.; Dai, C.J.; He, H.L.; Ignesti, G.; Incicchitti, A.; Kuang, H.H.; Ma, J.M.; Montecchia, F.; Ponkratenko, O.A.; et al. New limits on the nuclear levels excitation of ^{127}I and ^{23}Na during charge nonconservation. *Phys. Rev. C* **1999**, *60*, 065501. [CrossRef]
71. Bernabei, R.; Belli, P.; Cerulli, R.; Montecchia, F.; Nozzoli, F.; Incicchitti, A.; Prosperi, D.; Dai, C.J.; He, H.L.; Kuang, H.H.; et al. Search for solar axions by Primakoff effect in NaI crystals. *Phys. Lett. B* **2001**, *515*, 6. [CrossRef]
72. Cappella, F.; Cerulli, R.; Incicchitti, A. A preliminary search for Q-balls by delayed coincidences in NaI(Tl). *Eur. Phys. J. C* **2002**, *14*, 1. [CrossRef]
73. Bernabei, R.; Belli, P.; Cappella, F.; Montecchia, F.; Nozzoli, F.; d'Angelo, A.; Incicchitti, A.; Prosperi, D.; Cerulli, R.; Dai, C.J.; et al. Search for spontaneous transition of nuclei to a superdense stat. *Eur. Phys. J. A* **2005**, *23*, 7. [CrossRef]
74. Bernabei, R.; Belli, P.; Cappella, F.; Montecchia, F.; Nozzoli, F.; d'Angelo, A.; Incicchitti, A.; Prosperi, D.; Cerulli, R.; Dai, C.J.; et al. A search for spontaneous emission of heavy clusters in the ^{127}I nuclide. *Eur. Phys. J. A* **2005**, *24*, 51. [CrossRef]
75. Bernabei, R.; Belli, P.; Cappella, F.; Cerulli, R.; Dai, C.J.; d'Angelo, A.; He, H.L.; Incicchitti, A.; Kuang, H.H.; Ma, X.H.; et al. New search for processes violating the Pauli-Exclusion-Principle in Sodium and in Iodine. *Eur. Phys. J. C* **2009**, *62*, 327. [CrossRef]
76. Bernabei, R.; Belli, P.; Montecchia, F.; De Sanctis, M.; Di Nicolantonio, W.; Incicchitti, A.; Prosperi, D.; Bacci, C.; Dai, C.J.; Ding, L.K.; et al. Search for non-paulian transitions in ^{23}Na and ^{127}I. *Phys. Lett. B* **1997**, *408*, 439. [CrossRef]
77. Bernabei, R.; Belli, P.; Cerulli, R.; Montecchia, F.; Amato, M.; Ignesti, G.; Incicchitti, A.; Prosperi, D.; Dai, C.J.; He, H.L.; et al. Extended limits on neutral strongly interacting massive particles and nuclearites from NaI(Tl) scintillators. *Phys. Rev. Lett.* **1999**, *83*, 4918. [CrossRef]
78. Belli, P.; Bernabei, R.; Danevich, F.A.; Incicchitti, A.; Tretyak, V.I. Experimental searches for rare alpha and beta decays. *Eur. Phys. J. A* **2019**, *55*, 140. [CrossRef]
79. Barabash, A.S. Average and recommended half-life values for two-neutrino double beta decay: Upgrade-2019. *AIP Conf. Proc.* **2019**, *2165*, 020002.
80. Belli, P.; Bernabei, R.; Boiko, R.A.; Brudanin, V.B.; Cappella, F.; Caracciolo, V.; Cerulli, R.; Chernyak, D.M.; Danevich, F.A.; d'Angelo, S.; et al. Search for double-β decay processes in ^{106}Cd with the help of a $^{106}CdWO_4$ crystal scintillator. *Phys. Rev. C* **2012**, *85*, 044610. [CrossRef]
81. Polischuk, O.G.; Belli, P.; Bernabei, R.; Brudanin, V.D.; Cappella, F.; Caracciolo, V.; Cerulli, R.; Chernyak, D.M.; Danevich, F.A.; d'Angelo, S.; et al. Search for 2β processes in ^{106}Cd with $^{106}CdWO_4$ crystal scintillator. *Funct. Mater.* **2005**, *22*, 135. [CrossRef]
82. Belli, P.; Bernabei, R.A.; Brudanin, V.B.; Cappella, F.; Caracciolo, V.; Cerulli, R.; Danevich, F.A.; Incicchitti, A.; Kasperovych, V.D.; Klavdiienko, V.R.; et al. Search for double-β decay in ^{106}Cd with an enriched $^{106}CdWO_4$ crystal scintillator in coincidence with four HPGe detectors. *Phys. Rev. C* **2016**, *93*, 045502. [CrossRef]
83. Polischuk, O.G. Enriched Crystal Scintillators for 2β Experiments. *Physics* **2021**, *3*, 103–119. [CrossRef]
84. Cappella, F.; Incicchitti, A. Techniques for background identification in the search for rare processes with crystal scintillators. *Physics* **2021**, *3*, 187–206. [CrossRef]
85. Belli, P.; Bernabei, R.; Cerulli, R.; Dai, C.J.; Danevich, F.A.; Incicchitti, A.; Kobychev, V.V.; Ponkratenko, O.A.; Prosperi, D.; Tretyak, V.I.; et al. Performances of a CeF_3 crystal scintillator and its application to the search for rare processes. *Nucl. Instrum. Methods A* **2003**, *498*, 352. [CrossRef]
86. Belli, P.; Bernabei, R.; Cappella, F.; Cerulli, R.; Danevich, F.A.; d'Angelo, A.; Di Marco, A.; Incicchitti, A.; Nozzoli, F.; Tretyak, V.I. Search for 2β decay of cerium isotopes with $CeCl_3$ scintillator. *J. Phys. G Nucl. Part. Phys.* **2011**, *38*, 015103. [CrossRef]
87. Belli, P.; Bernabei, R.; d'Angelo, S.; Cappella, F.; Cerulli, R.; Incicchitti, A.; Laubenstein, M.; Prosperi, D.; Tretyak, V.I. First limits on neutrinoless resonant 2ϵ captures in ^{136}Ce and new limits for other 2β processes in ^{136}Ce and ^{138}Ce isotopes. *Nucl. Phys. A* **2009**, *824*, 101. [CrossRef]
88. Bernabei, R.; Belli, P.; Incicchitti, A.; Prosperi, D.; Bacci, C.; De Notaristefani, F.; Davies, G.J.; Dai, C.J. Feasibility of 2β decay searches with Ce isotopes using CeF_3 scintillators. *Nuovo Cimento A***1997**, *110*, 189.
89. Belli, P.; Bernabei, R.; Cerulli, R.; Danevich, F.A.; Galenin, E.; Gektin, A.; Incicchitti, A.; Isaienko, V.; Kobychev, V.V.; Laubenstein, D.; et al. Radioactive contamination of SrI_2(Eu) crystal scintillator. *Nucl. Instrum. Methods A* **2012**, *670*, 10. [CrossRef]
90. Danevich, F.A.; Chernyak, D.M.; Dubovik, A.M.; Grinyov, B.V.; Henry, S.; Kraus, H.; Kudovbenko, V.M.; Mikhailik, V.B.; Nagornay, L.L.; Podviyanuk, R.B.; et al. $MgWO_4$ a new crystal scintillator. *Nucl. Instrum. Methods A* **2009**, *608*, 107. [CrossRef]

91. Belli, P.; Bernabei, R.; Boiko, R.S.; Brudanin, V.B.; Bukilic, N.; Cerulli, R.; Chernyak, D.M.; Danevich, F.A.; d'Angelo, S.; Degoda, V.Y.; et al. Development of enriched $^{106}CdWO_4$ crystal scintillators to search for double beta decay processes in ^{106}Cd. *Nucl. Instrum. Methods A* **2010**, *615*, 301. [CrossRef]
92. Belli, P.; Bernabei, R.; Cappella, F.; Cerulli, R.; Danevich, F.A.; d'Angelo, S.; Incicchitti, A.; Kobychev, V.V.; Nagorny, S.S.; Nozzoli, F.; et al. Search for double beta decay processes in ^{108}Cd and ^{114}Cd with the help of low background $CdWO_4$ crystal scintillator. *Eur. Phys. J. A* **2008**, *36*, 167. [CrossRef]
93. Cerulli, R.; Belli, P.; Bernabei, R.; Cappella, F.; Nozzoli, F.; Montecchia, F.; d'Angelo, A.; Incicchitti, A.; Prosperi, D.; Dai, C.J. Performances of a BaF_2 detector and its application to the search for 2β decay modes in ^{130}Ba. *Nucl. Instrum. Methods A* **2004**, *525*, 535. [CrossRef]
94. Belli, P.; Bernabei, R.; Cappella, F.; Caracciolo, V.; Cerulli, R.; Danevich, F.A.; Di Marco, A.; Incicchitti, A.; Poda, D.V.; Polischuk, O.G.; et al. Investigation of rare nuclear decays with BaF_2 crystal scintillator contaminated by radium. *Eur. Phys. J. A* **2014**, *50*, 134. [CrossRef]
95. Caracciolo, V.; Cappella, F.; Cerulli, R.; Di Marco, A.; Laubenstein, M.; Nagorny, S.S.; Safonova, O.E.; Shlegel, V.N. Limits and Performances of a $BaWO_4$ Single Crystal. *Nucl. Instrum. Methods A* **2018**, *901*, 150. [CrossRef]
96. Belli, P.; Bernabei, R.; Cappella, F.; Cerulli, R.; Danevich, F.A.; Dubovik, A.M.; d'Angelo, S.; Galashov, E.N.; Grinyov, B.V.; Incicchitti, A.; et al. Radioactive contamination of $ZnWO_4$ crystal scintillators. *Nucl. Instrum. Methods A* **2011**, *626*, 31. [CrossRef]
97. Belli, P.; Bernabei, R.; Cappella, F.; Cerulli, R.; Danevich, F.A.; Dubovik, A.M.; d'Angelo, S.; Galashov, E.N.; Grinyov, B.V.; Incicchitti, A.; et al. Radiopurity of $ZnWO_4$ crystal scintillators. *Acta Phys. Polonica A* **2010**, *117*, 139. [CrossRef]
98. Belli, P.; Bernabei, R.; Cappella, F.; Cerulli, R.; Danevich, F.A.; Grinyov, B.V.; Incicchitti, A.; Kobychev, V.V.; Mokina, V.M.; Nagorny, S.S.; et al. Search for double beta decay of zinc and tungsten with low background $ZnWO_4$ crystal scintillators. *Nucl. Phys. A* **2009**, *826*, 256. [CrossRef]
99. Belli, P.; Bernabei, R.; Cappella, F.; Cerulli, R.; Danevich, F.A.; Grinyov, B.V.; Incicchitti, A.; Kobychev, V.V.; Nagornaya, L.L.; Nagorny, S.S.; et al. Search for 2β processes in ^{64}Zn with the help of $ZnWO_4$ crystal scintillator. *Phys. Lett. B* **2008**, *658*, 193. [CrossRef]
100. Belli, P.; Bernabei, R.; Cappella, F.; Cerulli, R.; Dai, C.J.; Danevich, F.A.; d'Angelo, S.; Incicchitti, A.; Kobychev, V.V.; Poda, D.V.; et al. Final results of experiment to search for 2β processes in zinc and tungsten with the help of radiopure $ZnWO_4$ crystal scintillators. *J. Phys. G Nucl. Part. Phys.* **2011**, *38*, 115107. [CrossRef]
101. Belli, P.; Bernabei, R.; Cappella, F.; Danevich, F.A.; Denisov, V.Y.; d'Angelo, S.; Incicchitti, A.; Kobychev, V.V.; Poda, D.V.; Polischuk, O.G.; et al. Search for long-lived superheavy eka-tungsten with radiopure $ZnWO_4$ crystal scintillator. *Phys. Scr.* **2015**, *90*, 085301. [CrossRef]
102. Belli, P.; Bernabei, R.; Cappella, F.; Caracciolo, V.; Cerulli, R.; Cherubini, N.; Danevich, F.A.; Incicchitti, A.; Kasperovych, D.V.; Piccinelli, E.; et al. Measurements of $ZnWO_4$ anisotropic response to nuclear recoils for the ADAMO project. *Eur. Phys. J. A* **2020**, *56*, 83. [CrossRef]
103. Danevich, F.A.; Barabash, A.S.; Belli, P.; Bernabei, R.; Boiko, R.S.; Brudanin, V.B.; Cappella, F.; Caracciolo, V.; Cerulli, R.; Chernyak, D.M.; et al. Development of radiopure cadmium tungstate crystal scintillators from enriched ^{106}Cd and ^{116}Cd to search for double beta decay. *AIP Conf. Proc.* **2013**, *1549*, 201.
104. Ejiri, H. Double Beta Decays and Neutrino Masses. *J. Phys. Soc. Jpn.* **2005**, *74*, 2101–2127. [CrossRef]
105. Belli, P.; Bernabei, R.; Bukilic, N.; Cappella, F.; Cerulli, R.; Dai, C.J.; Danevich, F.A.; de Laeter, J.R.; Incicchitti, A.; Kobychev, V.V.; et al. Investigation of beta decay of ^{113}Cd. *Phys. Rev. C* **2007**, *76*, 064603.
106. Danevich, F.A.; Georgadze, A.S.; Kobychev, V.V.; Nagorny, S.S.; Nikolaiko, A.S.; Ponkratenko, O.A.; Tretyak, V.I.; Zdesenko, S.Y.; Zdesenko, Y.G.; Bizzeti, P.G.; et al. Alpha activity of natural tungsten isotopes. *Phys. Rev. C* **2003**, *67*, 014310. [CrossRef]
107. Belli, P.; Bernabei, R.; Cappella, F.; Cerulli, R.; Dai, C.J.; Danevich, F.A.; d'Angelo, A.; Incicchitti, A.; Kobychev, V.V.; Nagorny, S.S.; et al. Search for alpha decay of natural Europium. *Nucl. Phys. A* **2007**, *789*, 15. [CrossRef]
108. Zdesenko, Y.G.; Avignone, F.T.; Brudanin, V.B.; Danevich, F.A.; Nagorny, S.S.; Solsky, I.M.; Tretyak, V.I. Scintillation properties and radioactive contamination of $CaWO_4$ crystal scintillators. *Nucl. Instrum. Methods A* **2005**, *538*, 657. [CrossRef]
109. Belli, P.; Bernabei, R.; Boiko, R.S.; Cappella, F.; Cerulli, R.; Danevich, F.A.; d'Angelo, S.; Incicchitti, A.; Kobychev, V.V.; Kropivyansky, B.N.; et al. New observation of $2\beta2\nu$ decay of ^{100}Mo to the 0_1^+ level of ^{100}Ru in the ARMONIA experiment. *Nucl. Phys. A* **2010**, *846*, 143–156. [CrossRef]
110. Polischuk, O.G.; Barabash, A.S.; Belli, P.; Bernabei, R.; Cappella, F.; Caracciolo, V.; Cerulli, R.; Chernyak, D.M.; Danevich, F.A.; d'Angelo, S.; et al. Investigation of 2β decay of ^{116}Cd with the help of enriched $^{116}CdWO_4$ crystal scintillators. *AIP Conf. Proc.* **2017**, *1894*, 020018.
111. Bernabei, R.; Belli, P.; Cappella, F.; Cerulli, R.; Montecchia, F.; Nozzoli, F.; Incicchitti, A.; Prosperi, D.; Tretyak, V.I.; Zdesenko, Y.G.; et al. Search for β and $\beta\beta$ decays in ^{48}Ca. *Nucl. Phys. A* **2002**, *705*, 29–39. [CrossRef]
112. Belli, P.; Bernabei, R.; Cappella, F.; Cerulli, R.; Danevich, F.A.; d'Angelo, A.; Incicchitti, A.; Kobychev, V.V.; Laubenstein, M.; Polischuk, O.G.; et al. Search for 7Li solar axions using resonant absorption in LiF crystal: Final results. *Phys. Lett. B* **2012**, *711*, 41–45. [CrossRef]
113. Bernabei, R.; Belli, P.; Montecchia, F.; Nozzoli, F.; d'Angelo, A.; Cappella, F.; Incicchitti, A.; Prosperi, D.; Castellano, S.; Cerulli, R.; et al. Performances and potentialities of a $LaCl_3$:Ce scintillator. *Nucl. Instrum. Methods A* **2005**, *555*, 270–281. [CrossRef]
114. Elwell, D.; Scheel, H.J. *Crystal Growth from High-Temperature Solutions*; Academic Press: London, UK, 2003.

115. Scheel, H.J. *Historical Introduction, Chapter 1 in Handbook of Crystal Growth*; Hurle, D.T.J., Ed.; Elsevier: Amsterdam, The Netherlands, 1993; Volume 1.
116. Scheel, H.J.; Fukuda, T. *Crystal Growth Technology*; Wiley: Hoboken, NJ, USA, 2003.
117. Feigelson, R.S. *50 Years Progress in Crystal Growth*; Elsevier: Amsterdam, The Netherlands, 2004.
118. Lecoq, P.; Gektin, A.; Korzhik, M. *Inorganic Scintillators for Detector Systems*; Springer: Berlin/Heidelberg, Germany, 2006.
119. Dhanaraj, G.; Byrappa, K.; Prasad, V.; Dudley, M. *Handbook of Crystal Growth*; Springer: Berlin/Heidelberg, Germany, 2010.
120. Kubota, S.; Hishida, M.; Suzuki, M.; Ruan, J.Z. Dynamical behavior of free electrons in the recombination process in liquid argon, krypton, and xenon. *Phys. Rev. B* **1979**, *20*, 3486. [CrossRef]
121. Barabanov, I.R.; Gavrin, V.N.; Pshukov, A.M. Liquid xenon scintillation spectrometer. *Nucl. Instrum. Methods* A **1987**, *254*, 355–360. [CrossRef]
122. Incicchitti, A.; Belli, P.; Scafi, M. Liquid Xenon as a detector medium. *Nucl. Instrum. Methods A* **1990**, *289*, 236–242. [CrossRef]
123. Belli, P.; Bernabei, R.; d'Angelo, S.; Andreanelli, L.; Bronzini, F.; Buccheri, A.; Incicchitti, A.; Prosperi, D. Liquid Xenon detectors and their applications. *Nucl. Instrum. Methods A* **1990**, *299*, 191–194. [CrossRef]
124. Belli, P.; Bernabei, R.; d'Angelo, S.; Incicchitti, A.; Prosperi, D. Detecting 'dark matter' using a liquid xenon scintillation detector. *Nuovo Cimento A* **1990**, *103*, 767–771. [CrossRef]
125. Belli, P.; Bernabei, R.; d'Angelo, S.; Incicchitti, A.; Prosperi, D. Liquid xenon scintillators. *Nucl. Instrum. Methods A* **1991**, *310*, 150–153. [CrossRef]
126. Belli, P.; Bernabei, R.; Bacci, C.; Incicchitti, A.; Marcovaldi, R.; Prosperi, D. Liquid xenon detectors for dark matter experiments. *Nucl. Instrum. Methods A* **1992**, *316*, 55–57. [CrossRef]
127. Belli, P.; Bernabei, R.; Di Nicolantonio, W.; Landoni, V.; Montecchia, F.; Incicchitti, A.; Prosperi, D.; Bacci, C.; Besida, O.; Dai C.J. Search for WIMPs with enriched xenon at Gran Sasso. *Nuovo Cim. C* **1996**, *19*, 537–544. [CrossRef]
128. Belli, P.; Bernabei, R.; Di Nicolantonio, W.; Landoni, V.; Incicchitti, A.; Prosperi, D.; Dai, C.J.; Bacci, C. Charge conservation and electron lifetime: Limits from a liquid xenon scintillator. *Astropart. Phys.* **1996**, *5*, 217–219. [CrossRef]
129. Belli, P.; Bernabei, R.; Di Nicolantonio, W.; Landoni, V.; Montecchia, F.; Incicchitti, A.; Prosperi, D.; Bacci, C.; Dai C.J. Limits on WIMP–^{129}Xe inelastic scattering. *Phys. Lett. B* **1996**, *387*, 222–226. [CrossRef]
130. Bernabei, R.; Belli, P.; Montecchia, F.; Incicchitti, A.; Prosperi, D.; Dai, C.J.; Angelone, M.; Batistoni, P.; Pillon, M. New limits on particle dark matter search with a liquid Xenon target-scintillator. *Phys. Lett. B* **1998**, *436*, 379–388. [CrossRef]
131. Belli, P.; Bernabei, R.; Dai, C.J.; Ignesti, G.; Incicchitti, A.; Montecchia, F.; Ponkratenko, O.A.; Prosperi, D.; Tretyak, V.I.; Zdesenko, Y.G. Charge non–conservation restrictions from the nuclear levels excitation of Xe–129 induced by the electron's decay on the atomic shell. *Phys. Lett. B* **1999**, *465*, 315–322. [CrossRef]
132. Belli, P.; Bernabei, R.; Dai, C.J.; Ignesti, G.; Incicchitti, A.; Montecchia, F.; Ponkratenko, O.A.; Prosperi, D.; Tretyak, V.I.; Zdesenko, Y.G. Quest for electron decay $e^- \to \nu_e\gamma$ with a liquid xenon scintillator. *Phys. Rev. D* **2000**, *61*, 117301 [CrossRef]
133. Bernabei, R.; Amato, M.; Belli, P.; Cerulli, R.; Dai, C.J.; Denisov, V.Y.; He, H.L.; Incicchitti, A.; Kuang, H.H.; Ma, J.M.; et al. Search for the nucleon and di-nucleon decay into invisible channels. *Phys. Lett. B* **2000**, *493*, 12–18. [CrossRef]
134. Bernabei, R.; Belli, P.; Cerulli, R.; Montecchia, F.; Incicchitti, A.; Prosperi, D.; Dai, C.J.; Angelone, M.; Batistoni, P.; Pillon, M. Light response of a pure liquid xenon scintillator irradiated with 2.5 MeV neutrons. *Eur. Phys. J.* **2001**, *3*, 1–11. [CrossRef]
135. Bernabei, R.; Belli, P.; Cappella, F.; Cerulli, R.; Montecchia, F.; Incicchitti, A.; Prosperi, D.; Dai, C.J. Search for neutrinoless beta beta decay in ^{134}Xe. *Phys. Lett. B* **2002**, *527*, 182–186. [CrossRef]
136. Bernabei, R.; Belli, P.; Cappella, F.; Cerulli, R.; Montecchia, F.; Incicchitti, A.; Prosperi, D.; Dai, C.J. Investigation of beta beta decay modes in ^{134}Xe and ^{136}Xe. *Phys. Lett. B* **2002**, *546*, 23–28 [CrossRef]
137. Bernabei, R.; Belli, P.; Bussolotti, A.; Cappella, F.; Cerulli, R.; Montecchia, F.; Dai, C.J.; Incicchitti, A.; Mattei, A.; Prosperi, D. The liquid xenon set-up of the DAMA experiment. *Nucl. Instrum. Methods A* **2002**, *482*, 728–743. [CrossRef]
138. Collar, J.I. A Realistic Assessment of the Sensitivity of XENON10 and XENON100 to Light-Mass WIMPs. *arXiv* **2011**, arXiv:1106.0653.
139. Doke, T. Fundamental properties of liquid argon, krypton and xenon as radiation detector media. *Port. Phys.* **1981**, *12*, 9.
140. Brassard, C. Liquid ionization detectors. *Nucl. Instrum. Methods* **1979**, *162*, 29. [CrossRef]
141. Feltesse, J. Liquid noble gas and warm liquid detectors. *Nucl. Instrum. Methods A* **1989**, *283*, 375. [CrossRef]
142. Davies, G.J.; Davies, J.D.; Lewin, J.D.; Smith, P.F.; Jones, W.G. Liquid xenon as a dark matter detector. Prospects for nuclear recoil discrimination by photon timing. *Phys. Lett. B* **1994**, *320*, 395. [CrossRef]
143. Asakura, K.; Gando, A.; Gando, Y.; Hachiya, T.; Hayashida, S.; Ikeda, H.; Inouea, K.; Ishidoshiro, K.; Ishikawa, T.; Ishio, S.; et al. Search for double-beta decay of ^{136}Xe to excited states of ^{136}Ba with the KamLAND-Zen experiment. *Nucl. Phys. A* **2016**, *946*, 171–181. [CrossRef]
144. Galan, J. Microbulk MicrOMEGAs for the search of $0\nu\beta\beta$ of ^{136}Xe in the PandaX-III experiment. *JINST* **2016**, *11*, P04024. [CrossRef]
145. Albert, J.B.; Auger, M.; Auty, D.J.; Barbeau, P.S.; Beauchamp, E.; Beck, D.; Belov, V.; Benitez-Medina, C.; Bonatt, J.; Breidenbach, M.; et al. Improved measurement of the $2\nu\beta\beta$ half-life of ^{136}Xe with the EXO-200 detector. *Phys. Rev. C* **2014**, *89*, 015502. [CrossRef]
146. Agostini, F.; Ahmed Maouloud, S.E.M.; Althueser, L.; Amaro, F.; Antunovic, B.; Aprile, E.; Baudis, L.; Baur, D.; Biondi, Y.; Bismark, A.; et al. Sensitivity of the DARWIN observatory to the neutrinoless double beta decay of ^{136}Xe. *Eur. Phys. J. C* **2020**, *80*, 808. [CrossRef]

147. Bernabei, R.; Belli, P.; Incicchitti, A.; Prosperi, D. *Liquid Noble Gases for Dark Matter Searches: A Synoptic Survey*; Exorma: Rome, Italy, 2009; ISBN: 978-88-95688-12-1.
148. Bernabei, R.; Belli, P.; Incicchitti, A.; Cappella, F.; Cerulli, R. Liquid Noble gases for Dark Matter searches: An updated survey. *Int. J. Mod. Phys. A* **2015**, *30*, 1530053. [CrossRef]
149. Doke, T.; Hitachi, A.; Kikuchi, J.; Masuda, K.; Okada, H.; Shibamura, E. Absolute Scintillation Yields in Liquid Argon and Xenon for Various Particles. *Jpn. J. Appl. Phys.* **2002**, *41*, 1538. [CrossRef]
150. Shutt, T.; Dahl, C.E.; Kwong, J.; Bolozdynya, A.; Brusov, P. Performance and fundamental processes at low energy in a two-phase liquid xenon dark matter detector. *Nucl. Phys. B* **2007**, 173, 160. [CrossRef]
151. Chepel, V.; Araújo, H. Liquid noble gas detectors for low energy particle physics. *JINST* **2013**, *8*, R04001. [CrossRef]
152. Fiorini, E.; Niinikoski, T.O. Low-temperature calorimetry for rare decays. *Nucl. Instrum. Methods A* **1984**, *224*, 83. [CrossRef]
153. Goulding, F.S.; Landis, D.A. Semiconductor Detector Spectrometer Electronics. *Pure Appl. Phys.* **1974**, *40*, 413–481.
154. Swartz, E.T.; Pohl, R.O. Thermal boundary resistance. *Rev. Mod. Phys.* **1989**, *61*, 605–668. [CrossRef]
155. Pirro, S. Further developments in mechanical decoupling of large thermal detectors. *Nucl. Instrum. Methods A* **2009**, *559*, 672–674. [CrossRef]
156. Barucci, M.; Beeman, J.W.; Caracciolo, V.; Pagnanini, L.; Pattavina, L.; Pessina, G.; Pirro, S.; Rusconi, C.; Schäffner, K. Cryogenic light detectors with enhanced performance for rare event physics. *Nucl. Instrum. Methods A* **2019**, *935*, 150–155. [CrossRef]
157. Razeti, M. Distillation and separation of some rare isotopes and their applications. *Nuovo Cimento C* **2017**, *41*, 84.
158. Agnes, P.; Albergo, S.; Albuquerque, I.F.M.; Alexander, T.; Alici, A.; Alton, A.K.; Amaudruz, P.; Arba, M.; Arpaia, P.; Arcelli, S. Separating ^{39}Ar from ^{40}Ar by cryogenic distillation with Aria for dark matter searches. *arXiv* **2021**, arXiv:2101.08686.
159. Dell'Oro, S.; Marcocci, S.; Vissani,F. New expectations and uncertainties on neutrinoless double beta decay. *Phys. Rev. D* **2014**, *90*, 033005. [CrossRef]
160. Caracciolo, V. Feasibility Study of an Experiment to Investigate the Double Beta Decay Modes in ^{106}Cd. Ph.D. Thesis, University of L'Aquila, L'Aquila, Italy, 2012.
161. Agostinelli, S.; Allison, J.; Amako, K.; Apostolakis, L.; Araujoa, H.; Arce, P.; Asaiga, M.; Axeni, D.; Banerjee, S.; Barrand, G.; et al. GEANT4—A simulation toolkit. *Nucl. Instrum. Methods A* **2003**, *506*, 250. [CrossRef]
162. Allison, J.; Amako, K.; Apostolakis, J.; Araujo, H.; Arce Dubois, P.; Asai, M.; Barrand, G.; Capra, R.; Chauvie, S.; Chytracek, R.; et al. Geant4 developments and applications. *IEEE Trans. Nucl. Sci.* **2006**, *53*, 270. [CrossRef]
163. Ponkratenko, O.A.; Tretyak, V.I.; Zdesenko, Y.G. Event generator DECAY4 for simulating double-beta processes and decays of radioactive nuclei. *Phys. At. Nucl.* **2000**, *63*, 1282. [CrossRef]
164. Tretyak, V.I. (Institute for Nuclear Research of NASU, Kyiv, Ukraine). Private communication, 2007.
165. Wang, M.; Audi, G.; Kondev, F.G.; Huang, W.J.; Naimi, S.; Xu, X. The Ame2016 atomic mass evaluation. *Chin. Phys. C* **2017**, *41*, 030003. [CrossRef]
166. Beck, M.; Bockholt, J.; Echternach, J.; Heusse, G.; Hirsch, M.; Klapdor-Kleingrothaus, H.V.; Piepke, A.; Strecker, H.; Zuber, K.; Bakalyarov, A.; et al. New half life limits for the $\beta\beta_{2\nu+0\nu}$ decay of ^{76}Ge to the excited states of ^{76}Se from the Heidelberg-Moscow $\beta\beta$ experiment. *Z. Phys. A* **1992**, *343*, 397. [CrossRef]
167. Meija, J.; Coplen, T.B.; Berglund, M.; Brand, A.; De Biévre, P.; Gröning, M.; Holden, N.E.; Irrgeher, J.; Loss, R.D.; Walczyk, T.; et al. Isotopic compositions of the elements 2013 (IUPAC Technical Report). *Pure Appl. Chem.* **2016**, *88*, 293. [CrossRef]
168. Gavrilyuk, Y.M.; Gangapshev, A.M.; Kazalov, V.V.; Kuzminov, V.V.; Panasenko, S.I.; Ratkevich, S.S. Indications of 2ν2K capture in ^{78}Kr. *Phys. Rev. C* **2013**, *87*, 035501. [CrossRef]
169. Ratkevich, S.S.; Gangapshev, A.M.; Gavrilyuk, Y.M.; Karpeshin, F.F.; Kazalov, V.V.; Kuzminov, V.V.; Panasenko, S.I.; Trzhaskovskaya, M.B.; Yakimenko, S.P. Comparative study of the double-K-shell-vacancy production in single- and double-electron-capture decay. *Phys. Rev. C* **2017**, *96*, 065502. [CrossRef]
170. Sáenz, C.; Cerezo, E.; García, E.; Morales, A.; Morales, J.; Núñez-Lagos, R.; Ortiz de Solórzano, A.; Puimedón, J.; Salinas, A.; Sarsa, M.L.; et al. Results of a search for double positron decay and electron-positron conversion of ^{78}Kr. *Phys. Rev. C* **1994**, *50*, 1170. [CrossRef]
171. Aprile, E.; Aalbers, J.; Agostini, F.; Alfonsi, M.; Althueser, L.; Amaro, F.D.; Anthony, M.; Antochi, V.C.; Arneodo, F.; Baudis, L.; et al. Observation of two-neutrino double electron capture in ^{124}Xe with XENON1T. *Nature* **2019**, *568*, 532–535.
172. Abe, K.; Hiraide, K.; Ichimura, K.; Kishimoto, Y.; Kobayashi, K.; Kobayashi, M.; Moriyama, S.; Nakahata, M.; Norita, T.; Ogawa, H.; et al. Improved search for two-neutrino double electron capture on ^{124}Xe and ^{126}Xe using particle identification in XMASS-I. *Prog. Theor. Exp. Phys.* **2018**, *5*, 053D03.
173. Barabash, A.S.; Kuzminov, V.V.; Lobashev, V.M.; Movikov, V.M.; Ovchinnikov, B.M.; Pomansky, A.A. Results of the experiment on the search for double beta decay of ^{136}Xe, ^{134}Xe and ^{124}Xe. *Phys. Lett. B* **1989**, *223*, 273–276. [CrossRef]
174. Meshik, A.P.; Hohenberg, C.M.; Pravdivtseva, O.V.; Kapusta, Y.S. Weak decay of ^{130}Ba and ^{132}Ba: Geochemical measurements. *Phys. Rev. C* **2001**, *64*, 035205. [CrossRef]
175. Pujol, M.; Marty, B.; Burnard, P.; Philippot, P. Xenon in Archean barite: Weak decay of ^{130}Ba, mass-dependent isotopic fractionation and implication for barite formation. *Geochim. Cosmochim. Acta* **2009**, **73**, 6834–6846. [CrossRef]
176. Barabash, A.S.; Saakyan, R.R. Experimental limits on $2\beta^+$, $K\beta^+$, and 2K processes for ^{130}Ba and on 2K capture for ^{132}Ba. *Phys. At. Nucl.* **1996**, *59*, 179–184.

177. Srinivasan, B. Barite: Anomalous xenon from spallation and neutron-induced reactions. *Earth Planet. Sci. Lett.* **1976**, *31*, 129–141. [CrossRef]
178. Aunola, M.; Suhonen, J. Systematic study of beta and double beta decay to excited final states. *Nucl. Phys. A* **1996**, *602*, 133. [CrossRef]
179. Rumyantsev, O.A.; Urin, M.H. The strength of the analog and Gamow-Teller giant resonances and hindrance of the $2\nu\beta^+\beta^+$ decay rate. *Phys. Lett. B* **1998**, *51*, 443.
180. Staudt, A.; Muto, K.; Klapdor-Kleingrothaus, H.V. Nuclear matrix elements for double positron emission. *Phys. Let. B* **1991**, 268, 312–316. [CrossRef]
181. Mishra, S.; Shukla, A.; Sahu, R.; Kota, V.K.B. Deformed shell model calculations of half lives for β^+/EC decay and 2ν $\beta^+\beta^+/\beta^+$EC/ECEC decay in medium-heavy N Z nuclei. *Phys. Rev. C* **2008**, *78*, 024307. [CrossRef]
182. Domir, P.; Kovalenko, S.; Šimkovic, F.; Semeno, S.V. Neutrino accompanied $\beta^p m\beta^p m$, β^+/EC and EC/EC processes within single state dominance hypothesis. *Nucl. Phys. A* **2005**, *753*, 337–363.
183. Sahu, R.; Kota, V.K.B. Deformed shell model studies of spectroscopic properties of ^{64}Zn and ^{64}Ni and the positron double beta decay of ^{64}Zn. *Pramana* **2014**, *82*, 757. [CrossRef]
184. Gavriljuk, J.M.; Kuzminov, V.V.; Osetrova, N.Y.; Ratkevich, S.S. New limit on the half-life of ^{78}Kr with respect to the 2K(2ν)-capture decay mode. *Phys. At. Nucl.* **2000**, *63*, 2201–2204. [CrossRef]
185. Gavrilyuk, Y.M.; Gangapshev, A.M.; Kazalov, V.V.; Kuzminov, V.V.; Panasenko, S.I.; Ratkevich, S.S.; Yakimenko, S.P. Investigating 2K capture in ^{78}Kr with a large-volume copper proportional counter. *Bull. Russ. Ac. Sci. Phys.* **2011**, *75*, 526. [CrossRef]
186. Ameenah, R.F.; Balraj, S. Nuclear Data Sheets for A = 78. *Nucl. Data Sheets* **2009**, *110*, 1917–2080.
187. Hirsch, M.; Muto, K.; Oda, T.; Klapdor-Kleingrothaus, H.V. Nuclear structure calculation of $\beta^+\beta^+$, β^+/EC and EC/EC decay matrix elements. *Z. Phys. A* **1994**, *347*, 151. [CrossRef]
188. Suhonen, J. Double beta decays of ^{124}Xe investigated in the QRPA framework. *J. Phys. G* **2013**, *40*, 075102. [CrossRef]
189. Singh, S.; Chandra, R.; Rath, P.K.; Raina, P.K.; Hirsch, J.G. Nuclear deformation and the two-neutrino double-β decay in ^{124,126}Xe, ^{128,130}Te, ^{130,132}Ba and ^{150}Nd isotopes. *Eur. Phys. J. A* **2007**, *33*, 375. [CrossRef]
190. Shukla, A.; Raina, P.K.; Rath, P.K. Study of two neutrino $\beta^+\beta^+/\beta^+EC/ECEC$ decay of ^{124,126}Xe and ^{130,132}Ba for $0^+ \rightarrow 0^+$ transition in PHFB model. *J. Phys. G Nucl. Part. Phys.* **2007**, *34*, 549. [CrossRef]
191. Nesterenko, D.A.; Blaum, K.; Block, M.; Droese, C.; Eliseev, S.; Herfurth, F.; Minaya Ramirez, E.; Novikov, Y.N.; Schweikhard, L.; Shabaev, V.M.; et al. Double-β transformations in isobaric triplets with mass numbers A = 124, 130 and 136. *Phys. Rev. C* **2012**, *86*, 044313. [CrossRef]
192. Barabash, A. Precise Half-Life Values for Two-Neutrino Double-β Decay: 2020 review. *Universe* **2020**, *6*, 159. [CrossRef]
193. Gavrilyuk, Y.M.; Gangapshev, A.M.; Kazalov, V.V.; Kuzminov, V.V.;Panasenko, S.I.; Ratkevich, S.S.; Tekueva, D.A.; Yakimenko, S.P. Search for 2K(2ν)-capture of ^{124}Xe. *Phys. Part. Nucl.* **2017**, *48*, 38. [CrossRef]
194. Abe, K.; Hiraide, K.; Ichimura, K.; Kishimoto, Y.; Kobayashi, K.; Kobayashi, M.; Moriyama, S.; Nakagawa, K.; Nakahata, M.; Norita, T. Search for two-neutrino double electron capture on ^{124}Xe with the XMASS-I detector. *Phys. Lett. B* **2016**, *759*, 64. [CrossRef]
195. Aprile, E.; Aalbers, J.; Agostini, F.; Alfonsi, M.; Amaro, F.D.; Anthony, M.; Arneodo, F.; Barrow, P.; Baudis, L.; Bauermeister, B. Search for two-neutrino double electron capture of ^{124}Xe with XENON100. *Phys. Rev. C* **2017**, *95*, 024605. [CrossRef]
196. Katakura, J.; Wu, Z.D. Nuclear Data Sheets for A = 124. *Nucl. Data Sheets* **2008**, *109*, 1655–1877. [CrossRef]
197. Barabash, A.S. How to detect two-neutrino double K capture in a direct (counter) experiment. *JETP Lett.* **1994**, *59*, 644.
198. Meshik, A.; Pravdivtseva, O. Weak Decay of Tellurium and Barium Isotopes in Geological Samples: Current Status. *JPS Conf. Proc.* **2017**, *14*, 020702.
199. Balraj, S. Nuclear Data Sheets for A = 130. *Nucl. Data Sheets* **2001**, *93*, 33–242.
200. Angloher, G.; Bauer, M.; Bauer, P.; Bavykina, I.; Bento, A.; Bucci, C.; Canonica, L.; Ciemniak, C.; Defay, X.; Deuter, G.; et al. New limits on double electron capture of ^{40}Ca and ^{180}W. *Nucl. Phys. G* **2016**, *43*, 095202. [CrossRef]
201. Latest COBRA Annual Report. Available online: https://www.cobra-experiment.org/ (accessed on 1 January 2021).
202. Joachim, E.; Fritts, M.; Gehre, D.; Gößling, C.; Hagner, C.; Heidrich, N.; Klingenberg, R.; Kröninger, K.; Nitsch, K.; Oldorf, C.; et al. Results of a search for neutrinoless double-β decay using the COBRA demonstrator. *Phys. Rev. C* **2016**, *94*, 024603.
203. Alduino, C.; Alfonso, K.; Artusa, D.R.; Avignone, F.T., III; Azzolini, O.; Bari, G.; Bellini, F.; Benato, G.; Bersani, A.; Biassoni, M.; et al. Search for neutrinoless β^+EC decay of ^{120}Te with CUORE-0. *Phys. Rev. C* **2018**, *97*, 055502. [CrossRef]
204. Alduino, C.; Alfonso, K.; Artusa, D.R.; Avignone, F.T., III; Azzolini, O.; Bari, G.; Bellini, F.; Benato, G.; Bersani, A.; Biassoni, M.; et al. CUORE-0 detector: Design, construction and operation. *J. Instrum.* **2016**, *11*, P07009. [CrossRef]
205. Alfonso, K.; Artusa, D.R.; Avignone, F.T., III; Azzolini, O.; Balata, M.; Banks, T.I.; Bari, G.; Beeman, J.W.; Bellini, F.; Bersani, A.; et al. Search for Neutrinoless Double-Beta Decay of ^{130}Te with CUORE-0. *Phys. Rev. Lett.* **2015**, *115*, 102502. [CrossRef] [PubMed]
206. Armstrong, W.R.; Chang, C.; Hafidi, K.; Lisovenko, M.; Novosad, V.; Pearson, J.; Polakovic, T.; Wang, G.; Yefremenko, V.; Zhang, J.; et al. CUPID pre-CDR. *arXiv* **2019**, arXiv:1907.09376.
207. Ching, C.; Ho, T.; Zhao, W. Is ^{40}Ca A Stable Isotope? *Commun. Theor. Phys.* **1984**, *3*, 517–520. [CrossRef]
208. Belli, P.; Bernabei, R.; Dai, C.J.; Grianti, F.; He, H.L.; Ignesti, G.; Incicchitti, A.; .Kuang, H.H.; Ma, J.M.; Montecchia, F.; et al. New limits on spin-dependent coupled WIMPs and on 2β processes in ^{40}Ca and ^{46}Ca by using low radioactive CaF_2(Eu) crystal scintillators. *Nucl. Phys. B* **1999**, *563*, 97–106. [CrossRef]

209. Bellini, F.; Beretta, M.; Cardani, L.; Carniti, P.; Casali, N.; Celi, E.; Chiesa, D.; Clemenza, M.; Dafinei, I.; Di Domizio, S.; et al. Search for double β-decay modes of ^{64}Zn using purified zinc. *Eur. Phys. J. C* **2021**, *81*, 106. [CrossRef]
210. Azzolini, O.; Beeman, J.W.; Bellini, F.; Beretta, M.; Biassoni, M.; Brofferio, C.; Bucci, C.; Capelli, S.; Cardani, L.; Celi, C. Search for neutrinoless double beta decay of 64Zn and 70Zn with CUPID-0. *Eur. Phys. J. C* **2020**, *80*, 702. [CrossRef]
211. Kiel, H.; Münstermann, D.; Zuber, K. A search for various double beta decay modes of Cd, Te, and Zn isotopes. *Nucl. Phys. A* **2003**, *723*, 499–514. [CrossRef]
212. Barabash, A.S.; Hubert, F.; Hubert, P.; Umatov, V. New limits on the β^+EC and ECEC processes in ^{120}Te. *J. Phys. G* **2007**, *34*, 1721–1728. [CrossRef]
213. Dawson, J.V.; Goessling, C.; Janutta, B.; Junker, M.; Koettig, M.; Muenstermann, D.; Rajek, S.; Reeve, C.; Schulz, O.; Wilson, J.R.; et al. Experimental study of double-β decay modes using a CdZnTe detector array. *Phys. Rev. C* **2009**, *80*, 025502. [CrossRef]
214. Andreotti, E.; Arnaboldi, C.; Avignone, F.T., III; Balata, M.; Bandac, I.; Barucci, M.; Beeman, J.W.; Bellini, F.; Broferio, C.; Bryant, A.; et al. Search for β^+/EC double beta decay of ^{120}Te. *Astropart. Phys.* **2011**, *34*, 643–648. [CrossRef]
215. Bikit, I.; Slivka, J.; Anicin, I.; Veskovic, M.; Conkic, L. Electron-positron conversion decay of ^{64}Zn. *Appl. Radiat. Isot.* **1995**, *46*, 455. [CrossRef]
216. Pirinen, P.; Suhonen, J. Systematic approach to β and $2\nu\beta\beta$ decays of mass A$= 100 - 136$ nuclei. *Phys. Rev. C* **2015**, *91*, 054309. [CrossRef]
217. Danevich, F.A.; Georgadze, A.S.; Kobychev, V.V.; Nikolaiko, A.S.; Ponkratenko, O.A.; Tretyak, V.I.; Zdesenko, S.Y.; Zdesenko, Y.G.; Bizzeti, P.G.; Fazzini, T.F.; et al. Two-neutrino 2βdecay of ^{116}Cd and new half-lifelimits on 2β decay of ^{180}W and ^{186}W. *Nucl. Phys. A* **2003**, *717*, 129–145. [CrossRef]
218. Kang, W.G.; Choi, J.H.; Jeon, E.J.; Lee, J.I.; Kim, H.J.; Kim, S.K.; Kim, Y.D.; Lee, J.H.; Maa, K.J.; Myung, S.S.; et al. Ultra-low gamma-ray measurement system for neutrinoless double beta decay. *Appl. Rad. Isot.* **2013**, *81*, 290–293. [CrossRef]
219. Barabash, A.S.; Gurrianin, R.; Hubert, F.; Hubert, P.; Umatov, V.I. Improved limits on double beta processes in ^{92}Mo. *Z. Phys. A* **1997**, *357*, 351–352. [CrossRef]
220. Bellotti, E.; Fiorini, E.; Liguori, C.; Pullia, A.; Sarbacino, A.; Zanotti, L. An experimental investigation on lepton number conservation in double-beta processes. *Lett. Nuovo Cim.* **1982**, *33*, 273. [CrossRef]
221. Lee, J.I.; Bhang, H.C.; Choi, J.H.; Jeon, E.J.; Kang, W.G.; Kim, H.J.; Kim, S.C.; Kim, S.K.; Kim, Y.D.; Leeet, J.H.; et al. Experimental study on neutrinoless double beta decay of ^{92}Mo. *Nucl. Instrum. Met. A* **2011**, *654*, 157–161. [CrossRef]
222. Rukhadze, N.I.; Briancon, C.; Brudanin, B.B.; Egorov, V.G.; Klimenko, A.A.; Kovalik, A.; Timkin, V.V.; Čhermák, P.; Shitov, Y.A.; Šimkovic, F.; et al. Search for double-β decay of ^{106}Cd. *Bull. Russ. Acad. Sci. Phys.* **2011**, *75*, 879. [CrossRef]
223. Belli, P.; Bernabei, R.; Boiko, R.S.; Cappella, R.; Cerulli, R.; Danevich, F.A.; Incicchitti, A.; Kropivyansky, B.N.; Laubenstein, M.; Poda, D.V.; et al. Search for double beta decay of ^{136}Ce and ^{138}Ce with HPGe gamma detector. *Nulc. Phys. A* **2014**, *930*, 195–208. [CrossRef]
224. Belli, P.; Bernabei, R.; Boiko, R.S.; Cappella, F.; Cerulli, R.; Danevich, F.A.; Incicchitti, A.; Kropivyansky, B.N.; Laubenstein, M.; Mokina, V.M.; et al. New limits on 2ϵ, $\epsilon\beta^+$ and 2ϵ decay of ^{136}Ce and ^{138}Ce with deeply purified cerium sample. *Eur. Phys. J. A* **2017**, *53*, 172. [CrossRef]
225. De Frenne, D.; Negret, A. Nuclear data sheets for A = 106. *Nucl. Data Sheets* **2008**, *109*, 943–1102. [CrossRef]
226. Tretyak, V.I.; Belli, P.; Bernabei, R.; Brudanin, V.B.; Cappella, F.; Caracciolo, V.; Cerulli, R.; Chernyak, D.M.; Danevich, D.F.; d'Angelo, S.; et al. First results of the experiment to search for 2β decay of ^{106}Cd with $^{106}CdWO_4$ crystal scintillator in coincidence with four crystals HPGe detector. *EPJ Web Conf.* **2014**, *65*, 01003. [CrossRef]
227. Danevich, F.A.; Belli, P.; Bernabei, R.; Brudanin, V.B.; Cappella, F.; Caracciolo, V.; Cerulli, R.; Chernyak, D.M.; d'Angelo, S.; Incicchitti, A.; et al. Search for double beta processes in ^{106}Cd with enriched $^{106}CdWO_4$ crystal scintillator in coincidence with four crystals HPGe detector. *AIP Conf. Proc.* **2015**, *1686*, 020006.
228. Tretyak, V.I.; Belli, P.; Bernabei, R.; Brudanin, V.B.; Cappella, F.; Caracciolo, V.; Cerulli, R.; Chernyak, D.M.; Danevich, D.F.; d'Angelo, S.; et al. New limits on 2β processes in ^{106}Cd. *J. Phys. Conf. Ser.* **2016**, *718*, 062062. [CrossRef]
229. Nozzoli, F. ^{146}Nd, ^{144}Sm, and other unexplored 2β-decay isotopes. *Phys. Rev. C* **2018**, *97*, 015501. [CrossRef]
230. Belli, P.; Bernabei, R.; Cappella, F.; Cerulli, R.; Danevich, F.A.; d'Angelo, S.; Di Vacri, M.L.; Incicchitti, A.; Laubenstein, M.; Nagaorny, S.S. First search for double β decay of dysprosium. *Nucl. Phys. A* **2011**, *859*, 126–139. [CrossRef]
231. Finch, S.W.; Tornow, W. Search for neutrinoless double-electron capture of ^{156}Dy. *Phys. Rev. C* **2015**, *92*, 065503. [CrossRef]
232. Laubenstein, M. Screening of materials with high purity germanium detectors at the Laboratori Nazionali del Gran Sasso. *Int. J. Mod. Phys. A* **2017**, *32*, 1743002. [CrossRef]
233. Agostini, M.; Allardt, M.; Bakalyarov, A.M.; Balata, M.; Barabanov, I.; Barros, N.; Baudis, L.; Bauer, C.; Bellotti, E.; Belogurov, S.; et al. Limit on the radiative neutrinoless double electron capture of ^{36}Ar from GERDA Phase I. *Eur. Phys. J. C* **2016**, *76*, 652. [CrossRef]
234. Bikit, I.; Zikić-Todorović, N.; Slivka, J.; Vesković, M.; Krmar, M.; Čonkić, L.J.; Puzović, J.; Aničin, I.V. Double β decay of ^{50} Cr. *Phys. Rev. C* **2003**, *67*, 065801. [CrossRef]
235. Norman, E.B. Improved limits on the double beta decay half-lives of ^{50}Cr, ^{64}Zn, ^{92}Mo and ^{96}Ru. *Phys. Rev. C* **1973**, *31*, 1937. [CrossRef] [PubMed]
236. Bikit, I.; Krmat, M.; Slivka, J.; Vesković, M.; Čonkić, L.J.; Aničin, I.V. New results on the double β decay of Iron. *Phys. Rev. C* **1998**, *58*, 2566. [CrossRef]

237. Rukhadze, N.I.; Brudanin, V.B.; Klimenko, A.A.; Piquemal, F.; Rukhadze, E.N.; Shitov, Y.A.; Štekl, I.; Warot, G. Investigating the Double Beta Decay of ^{58}Ni. *Bull. Rus. Ac. Sci. Phys.* **2018**, *82*, 708–711. [CrossRef]
238. Jeskovsky, M.; Frekers, D.; Kovacik, A.; Povinec, P.P.; Puppe, P.; Stanicek, J.; Sykora, I.; Simkovic, F.; Thies, J.H. A search for double-electron capture in ^{74}Se using coincidence/anticoincidence gamma-ray spectrometry. *arXiv* **2015**, arXiv:1507.02200.
239. Barabash, A.S.; Brudanin, V.B.; Klimenko, A.A.; Konovalov, S.I.; Rakhimov, A.V.; Rukhadze, E.N.; Rukhadze, N.I.; Shitov, Y.A.; Stekl, I.; Warot, G.; et al. Improved limits on β^+EC and ECEC processes in ^{74}Se. *Nucl. Phys. A* **2020**, *996*, 121697. [CrossRef]
240. Frekers, D.; Puppe, P.; Thies, J.H.; Povinec, P.P.; Šimkovic, F.; Staniček, J.; Sýkora, I. Double-electron capture of ^{74}Se and the search for neutrinoless decay. *Nucl. Phys. A* **2011**, *860*, 1–7. [CrossRef]
241. Belli, P.; Bernabei, R.; Cappella, F.; Cerulli, R.; Danevich, F.A.; d'Angelo, S.; Incicchitti, A.; Kovtun, G.P.; Kovtun, N.G.; Laubenstein, M.; et al. Search for 2β decays of ^{96}Ru and ^{104}Ru by ultralow-background HPGe γ spectrometry at LNGS: Final results. *Phys. Rev. C* **2013**, *87*, 034607. [CrossRef]
242. Lehnert, B.; Andreotti, E.; Degering, D.; Hult, M.; Laubenstein, M.; Wester, T.; Zuber, K. Double beta decays into excited states in ^{110}Pd and ^{102}Pd. *J. Phys. G* **2016**, *43*, 115201. [CrossRef]
243. Barabash, A.S.; Hubert, P.; Nachab, A.; Konovalov, S.I.; Umatov, V. Improved limits on β^+EC and ECEC processes in ^{112}Sn. *Phys. Rev. C* **2011**, *83*, 045503. [CrossRef]
244. Ješkovský, M.D.; Fekers, D.; Kováčik, A.; Povinec, P.P.; Puppe, P.; Staníček, J.; Sýcora, I.; Šimkovic, F.; Thies, J.H. A search for double-electron capture of ^{74}Se to excited levels using coincidence/anticoincidence gamma-ray spectrometry. *Nucl. Instrum. Methods A* **2015**, *795*, 268–275. [CrossRef]
245. Lehnert, B.; Wester, T.; Degering, D.; Somme, D.; Wagner, L.; Zuber, K. Double electron capture searches in ^{74}Se. *J. Phys. G* **2016**, *43*, 085201. [CrossRef]
246. Boiko, R.S. Chemical purification of lanthanides for low-background experiments. *Int. J. Mod. Phys. A* **2017**, *32*, 1743005. [CrossRef]
247. Marchegiani, F.; Ferella, F.; Nisi, S. Material screening with mass spectrometry. *Physics* **2021**, *3*, 71–84. [CrossRef]
248. Polischuk, O.G.; Barabash, A.S.; Belli, P.; Bernabei, R.; Boiko, R.S.; Cappella, F.; Cerulli, R.; Danevich, F.A.; Incicchitti, A.; Laubenstein, M.; et al. Purification of Lanthanides for Double Beta Decay Experiments. *AIP Conf. Proc.* **2013**, *1549*, 124.
249. Boiko, R.S.; Barabash, A.S.; Belli, P.; Bernabei, R.; Cappella, F.; Cerulli, R.; Danevich, F.A.; Incicchitti, A.; Laubenstein, M.; Mokina, V.M.; et al. Purification of cerium, neodymium and gadolinium for low background experiments. *EPJ Web Conf.* **2014**, *65*, 04001. [CrossRef]
250. Danevich, F.A.; Hult, M.; Kasperovych, D.V.; Kovtunc, G.P.; Kovtun, K.V.; Lutter, G.; Marissens, G.; Polischuk, O.G.; Stetsenko, S.P.; Tretyak, V.I. First search for 2ϵ and $\epsilon\beta^+$ decay of ^{174}Hf. *Nucl. Phys. A* **2020**, *996*, 121703. [CrossRef]
251. Belli, P.; Bernabei, R.; Cappella, F.; Caracciolo, V.; Cerulli, R.; Danevich, F.A.; Incicchitti, A.; Kasperovych, D.V.; Kobychev, V.V.; Kovtun, G.G.; et al. New experimental limits on double-beta decay of osmium. Accepted for publication in *J. Phys. G Nucl. Part. Phys.* **2021**. [CrossRef]
252. Belli, P.; Bernabei, R.; Cappella, F.; Cerulli, R.; Danevich, F.A.; d'Angelo, S.; Di Marco, A.; Incicchitti, A.; Kovtun, G.P.; Kovtun, N.G.; et al. First search for double-β decay of ^{184}Os and ^{192}Os. *Eur. Phys. J. A* **2013**, *49*, 24. [CrossRef]
253. Belli, P.; Bernabei, R.; Cappella, F.; Cerulli, R.; Danevich, F.A.; Di Marco, A.; Incicchitti, A.; Laubenstein, M.; Nagorny, S.S.; Nisi, S. First search for double-β decay of platinum by ultra-low background HPGe γ spectrometry. *Eur. Phys. J. A* **2011** *47*, 91. [CrossRef]
254. Bukhner, E.; Vishnevskij, I.N.; Danevich, F.A. Rare decays of mercury nuclei. *Sov. J. Nucl. Phys.* **1990**, *52*, 193–197.
255. Kawrakow, I.; Rogers, D.W.O. *The EGSnrc Code System: Monte Carlo Simulation of Electron and Photon Transport*; NRCC Rep. (National Research Council Canada) Report PIRS-701; NRCC: Ottawa, ON, Canada, 2003.